REPUBLIC OF TÜRKİYE

ALTINBAŞ UNIVERSITY

Institute of Graduate Studies

Electrical and Computer Engineering

COMPLEXITY REDUCTION OF FILTERED-OFDM SYSTEMS FOR HIGH-SPEED VISIBLE LIGHT COMMUNICATIONS

Hayder Saeed Rashid HUJIJO

Doctor of Philosophy

Supervisor

Asst. Prof. Dr. Muhammad ILYAS

Istanbul, 2025

COMPLEXITY REDUCTION OF FILTERED-OFDM SYSTEMS FOR HIGH-SPEED VISIBLE LIGHT COMMUNICATIONS

Hayder Saeed Rashid HUJIJO

Electrical and Computer Engineering

Doctor of Philosophy

ALTINBAŞ UNIVERSITY

2025

The dissertation titled COMPLEXITY REDUCTION OF FILTERED-OFDM SYSTEMS FOR HIGH-SPEED VISIBLE LIGHT COMMUNICATIONS prepared by HAYDER SAEED RASHID HUJIJO and submitted on 16/06/2025 has been **accepted unanimously** for the degree of PhD in Electrical and Computer Engineering.

____

Asst. Prof. Dr. Muhammad ILYAS

Supervisor

Thesis Defense Committee Members:

Asst. Prof. Dr. Muhammad ILYAS	Department of Computer Engineering, Altınbaş University	__________________
Assoc. Prof. Dr. Oğuz ATA	Department of Software Engineering, Altınbaş University	__________________
Assoc. Prof. Dr. Hakan KOYUNCU	Department of Computer Engineering, Altınbaş University	__________________
Assoc. Prof. Dr. Jawad RASHEED	Department of Computer Engineering, Istanbul Sabahattin Zaim University	__________________
Assoc. Prof. Dr. Alaa HAMITOGLU	Department of Computer Engineering, Istinye University	__________________

I hereby declare that this dissertation meets all format and submission requirements for a PhD dissertation.

I hereby declare that all information/data presented in this graduation project has been obtained in full accordance with academic rules and ethical conduct. I also declare all unoriginal materials and conclusions have been cited in the text and all references mentioned in the Reference List have been cited in the text, and vice versa as required by the abovementioned rules and conduct.

Hayder Saeed Rashid HUJIJO

Signature

DEDICATION

To my family, and friends,

I dedicate this thesis to my esteemed advisor, Asst. Prof. Dr. Muhammad ILYAS, whose unwavering guidance, encouragement, and support have been invaluable throughout my academic journey. I also express my heartfelt gratitude to the members of the Thesis Defense Committee. This work stands as a testament to the wisdom and support of my mentors, for which I am profoundly thankful.

ABSTRACT

COMPLEXITY REDUCTION OF FILTERED-OFDM SYSTEMS FOR HIGH-SPEED VISIBLE LIGHT COMMUNICATIONS

HUJIJO, Hayder Saeed Rashid

PhD., Electrical and Computer Engineering, Altınbaş University,

Supervisor: Asst. Prof. Dr. Muhammad ILYAS

Date: 06/2025

Pages: 135

Contemporary wireless communication infrastructures face inherent limitations in radio frequency (RF) bandwidth allocation. As global requirements for enhanced data throughput intensify, systemic challenges, such as spectral congestion and diminished data transmission efficiency, assume critical importance. Within the framework of emerging 5G and 6G architectures, scholarly and industrial focus has pivoted toward leveraging the optical spectrum as a viable alternative to circumvent these constraints. Notably, visible light communication (VLC) systems have recently emerged as an innovative paradigm for augmenting traditional RF-dependent wireless networks. Among these advancements, the Filtered-Orthogonal Frequency Division Multiplexing (F-OFDM) modulation scheme has positioned itself as a promising solution for mitigating OFDM's inherent limitations of excessive out-of-band radiation and consequent spectral inefficiency.

In direct detection and intensity modulation (DD/IM), LEDs require real-valued and non-negative signals, achieved through the inverse fast Fourier transform (IFFT) with Hermitian symmetry (HS). While this enables noncomplex-valued signals, it halves the electrical bandwidth. Larger IFFT/FFT sizes increase processing demands, chip area, energy consumption, and hardware costs. The HS constraint complicates the design by requiring duplicate FFT/IFFT blocks, raising computational complexity. Additionally, increasing subcarriers worsens the peak-to-average power ratio (PAPR), adding further challenges.

Legacy optical OFDM methods employed to transform bipolar OFDM signals into unipolar formats include DC-biased (DCO-OFDM) and asymmetrically clipped (ACO-OFDM) techniques. However, these adaptations entail compromises: DCO-OFDM elevates power requirements, whereas ACO-OFDM diminishes spectral efficiency. This thesis primarily concentrates on optimizing spectral efficiency and reducing the complexity of VLC systems. Therefore, the effort offered in this thesis introduces a different methodology to eliminating the reliance on HS.

Two methods, NHS-DCO-F-OFDM and NHS-Flip-F-OFDM, are proposed to generate real F-OFDM signals by rearranging the real and imaginary components of complex F-OFDM signals in the time domain. These methods reduce system complexity by 50%, avoid PAPR issues, and enhance power efficiency contrasted to established HS-based F-OFDM. The NHS-filtered OFDM approach also improves bandwidth efficacy and cuts out-of-band emission power by 115 dB, offering better spectral localization than conventional OFDM.

Keywords: Complexity Reduction, Flip-Filtered-OFDM, NHS-DCO-F-OFDM, PAPR, Spectral Efficiency, Visible Light Communication

TABLE OF CONTENTS

Pages

LIST OF TABLES

Pages

LIST OF FIGURES

Pages

ABBREVIATIONS

5G	:	Fifth Generation
6G	:	Sixth Generation
A/D	:	Analogy-to-Digital
ACI	:	Adjacent Channel Interference
ACO-OFDM	:	Asymmetrically Clipped Optical OFDM
ADO-OFDM	:	Asymmetrically Clipped DC-Biased Optical OFDM
ASCO-OFDM	:	Asymmetrically and Symmetrically Clipped Optical OFDM
AWGN	:	Additive White Gaussian Noise
BER	:	Bit Error Rate
CCDF	:	Complementary Cumulative Distribution Function
CP	:	Cyclic Prefix
CSK	:	Colour Shift Keying
D/A	:	Digital-to-Analogy
DAC	:	Digital-to-Analogy Converters
dB	:	Decibel
DC	:	Direct Current
DCO-OFDM	:	Direct Current-Biased Optical OFDM
DMT	:	Discrete Multitone Modulation
DPPM	:	Differential Pulse Position Modulation
EPPM	:	Expurgated Pulse Position Modulation
eUF-OFDM	:	Improved Universal Filtered OFDM
EVM	:	Error Vector Magnitude
FFT	:	Fast Fourier Transform

FIR	:	Finite Impulse Response
Flip-WPM	:	Flip-Wavelet Packet Modulation
FOFDM	:	Filtered OFDM
F-OFDM	:	Flip-OFDM
FOOFDM	:	Fast Optical OFDM
FSO	:	Free-Space Optical
Gbps	:	Gigabits per Second
GHz	:	Gigahertz
HS	:	Hermitian symmetry
ICI	:	Inter-Carrier-Interference
IEEE	:	Institute of Electrical and Electronics Engineers
IFFT	:	Inverse Fast Fourier Transform
IM	:	Intensity Modulation
IM/DD	:	Intensity Modulation and Direct Detection
IoT	:	Internet of Thing
IQ	:	In-phase/Quadrature
IR	:	Infrared
ISI	:	Inter-Symbol Interference
JM-F-OFDM	:	Juxtapose Method Filtered OFDM
kHz	:	Kilohertz
L	:	Filter Length
LD	:	Laser Diode
LED	:	Light-Emitting Diodes
LiFi	:	Light-Fidelity
Mbps	:	Megabits per Second

MHz	:	Megahertz
MWC	:	Mobile World Congress
N	:	FFT/IFFT size
NHS	:	Non-Hermitian Symmetry
NHS-DCO-F-OFDM	:	Non-Hermitian Symmetry-Direct Current-Biased Optical-Filtered-OFDM
NHS-Flip-F-OFDM	:	Non-Hermitian Symmetry Flip-Filtered-OFDM
OFDM	:	Orthogonal Frequency Division Multiplexing
OOB	:	Out-of-Band Emission
OOFDM	:	Optical OFDM
OOK	:	On-Off Keying
OPPM	:	Overlapping PPM
OWC	:	Optical Wireless Communication
PA	:	Power Amplifier
PADO-OFDM	:	Pre-distorted Asymmetrically Clipped DC-Biased Optical OFDM
PAM	:	Pulse Amplitude Modulation
PAPR	:	Peak-to-Average Power Ratio
PD	:	Photo Diode
PPM	:	Pulse Position Modulation
PWM	:	Pulse Width Modulation
QAM	:	Quadrature Amplitude Modulation
RF	:	Radio Frequency
RGB	:	Red-Green-Blue
RMS	:	Root Mean Square

SCO-OFDM	:	Symmetrically Clipped Optical OFDM
SNR	:	Signal-to-Noise Ratio
THz	:	Terahertz
UF-OFDM	:	Universal Filtered OFDM
U-OFDM	:	Unipolar OFDM
VLC	:	Visible Light Communication
VPPM	:	Variable PPM
WDM	:	Wavelength-Division Multiplexing
Wi-Fi	:	Wireless-Fidelity
WiGig	:	Wireless Gigabit

LIST OF SYMBOLS

*	:	Convolution Process
∂W	:	Tone Offset
B	:	Bandwidth
E	:	Signal Energy
error fc (.)	:	Complementary Error Function
$f_B(n)$	:	Prototype Filter
h(n)	:	Optical Channel Impulse Response
J, j	:	Square Root -1
K	:	Clipping Factor
K_b	:	DC Bias
$\log_2$	:	Logarithm Base 2 Process
M	:	QAM Order
$n_{clipping}$	:	Clipping Noise
$O_{FFT\ Add}$	:	Fast Fourier Transform Additions Complexity
$O_{FFT\ Multip.}$	:	Fast Fourier Transform Multiplications Complexity
P_{elec}	:	Electrical Power
P_r	:	Probability
P_S	:	Signal Power
$P\mu$	:	Noise Power
W	:	Number of Subcarriers
W(n)	:	Window Function
X(k)	:	Transmitted Frequency Symbol
x_{ACO}	:	Asymmetrically Clipped Optical
x_{DC}	:	DC Bias of the Signal
$x_{DCO\text{-}OFDM}$	:	Direct Current-Biased Optical OFDM Signal

X_H : Real Signal after Hermitian Symmetry

$x_I(k)$: Imaginary Part of the Signal the Transmitter

X_k : Subcarrier Symbols

$x_R(k)$: Real Part of the Signal at the Transmitter

x_{sub} : Subband Transmitted Signal

$Y(k)$: Received Frequency Symbol

$y_I(n)$: Imaginary Part of the Signal at the Receiver

$y_R(n)$: Real Part of the Signal at the Receiver

$\rho_B(n)$: Sinc Impulse Response

$\sigma^2_{x,NHS}$: Non-Hermitian Symmetry Transmitted Signal Power

$\sigma^2_{\mu,NHS}$: Non-Hermitian Symmetry Received Signal Power

$\mu(n)$: Channel Noise

1. INTRODUCTION

1.1 BACKGROUND

The emergence of 5G and subsequent advancements in 6G technology have catalysed transformative innovations across industries, such as self-operating transportation systems, seamless inter-device communication, and sophisticated automation in manufacturing and production. These advancements are made possible by providing high data rates, low latency, and ultra-reliable communication. Consequently, the demand for such capabilities is anticipated to intensify in the near future. Moreover, with over 80% of mobile data traffic originating from indoor environments, developing a new technology specifically designed for indoor use is crucial. Such a technology would complement Radio Frequency (RFs), which is increasingly facing congestion and limitations due to electromagnetic interference [1].

Extending the wireless band from lower to higher frequency ranges has become imperative to address the increasing bandwidth requirements, especially for multimedia services. Optical wireless communication (OWC) is categorized according to transceiver characteristics and use-case environments. Notably, visible light communication (VLC), or LiFi, a prominent subset of OWC, has attracted significant research attention over the last two decades. VLC employs light-emitting diodes (LEDs) to simultaneously enable interior lighting and wireless data transfer [2]. Therefore, many researchers have started to explore the unexplored visible range, which holds an enormous potential for high broadcast data-rate. The spectrum of visible light does not have regulatory constraints like traditional wireless frequency bands, offering inherent benefits such as impedance to electromagnetic interference and enhanced communication security [3].

The accelerated transition from conventional incandescent lighting to LED-based indoor illumination has catalyzed the evolution of VLC. Beyond their superior energy efficiency, LEDs possess the capacity to be switched at extremely high speeds (operating within the 430–790 THz spectrum), rendering them optimal for high-speed data transmission. Breakthroughs in foundational technologies have markedly enhanced VLC’s performance, with data rates surging from mere megabits per second (Mbps) to tens of gigabits per second

(Gbps). This capability establishes VLC as an encouraging contender for integration into next-generation wireless communication systems.

A central goal of VLC systems is to achieve high-speed data transfer within indoor settings. This is accomplished by leveraging indoor LED lighting infrastructure, which concurrently serves dual purposes: illumination and data transmission. The fast response features of LED semiconductor substances make intensity modulation and direct detection (IM/DD) methods available for white light signals, which are helpful for wireless communication strength [3]. Most of the presently available LEDs are limited to a modulation bandwidth of under a few megahertz [4], yet undergoing the big data era poses a need for higher transmission speed, this situation has driven researchers to explore new approaches to solve this problem.

Modulation techniques in VLC systems are broadly categorized into multicarrier and single-carrier schemes. Of these, single-carrier modulation, favoured for its simplicity and straightforward implementation, has seen widespread adoption in VLC applications. Established methods in this category include on-off keying (OOK), pulse position modulation (PPM), pulse amplitude modulation (PAM), pulse width modulation (PWM), and colour shift keying (CSK). These techniques, while providing significant benefits in spectral efficiency and/or hardware simplicity, are also limited by a common challenge of increased susceptibility to inter-symbol interference (ISI) at high levels data-rates, which adversely impacts system performance [1], [2].

Unlike single-carrier methods, multicarrier modulation tactics like orthogonal frequency-division multiplexing (OFDM) enhance spectral efficiency and minimize inter-symbol interference (ISI), positioning them as effective solutions for high-level data transfer in VLC procedures. This is achieved by zone-paced input data for orthogonal subcarriers in separate narrowband frequency channels, each assigned a parallel substreams. Subsequently, these combined time-domain substreams are synthesized into a composite, bipolar, complex-valued waveform by means of the IFFT [5]. However, as optical transmission inherently enforces constraints on the signal in the form of intensity-modulation and thus is necessarily real-valued and non-negative, specific adaptations for optical channels exist for OFDM. Such modulations are direct current biased optical OFDM (DCO-OFDM), asymmetrically clipped optical OFDM (ACO-OFDM), unipolar OFDM (U-OFDM), and Flip-OFDM [6] to ensure compatibility with the unipolar nature of light intensity.

DCO-OFDM (Direct Current-Biased Optical OFDM) is a widely adopted modulation procedure that enables high-pace data transformed in LED-based optical wireless communication (OWC) approaches, making it a cornerstone for such applications [3]. It utilizes a DC bias voltage on bipolar OFDM waveform, thus converting the signal to a unipolar form whose dynamic range is commensurate with the non-negative intensity bound of LEDs, which are unable to emit negative light. DCO-OFDM offers high spectral efficiency, so is suitable for high throughput applications. Some, due to the adoption of parallel narrowband subcarriers, whose lower-sided orthogonality naturally counteracts the ISI phenomenon [7], possess an always set upper bound of coherence even in bandwidth-limited scenarios.

Not only that, DCO-OFDM will also delight in the fundamental benefits of OFDM, including multipath fading resistance and compatibility with the currently established wireless technologies. Yet that comes at a cost: For example, the increased DC bias translates to bigger power consumption and, thus, poorer energy efficiency. Therefore, to prevent residue negative values, signal clipping has been implemented, resulting in signal distortion, which in turn leads to mutual quality deterioration of the signal [6].

ACO-OFDM (Asymmetrically Clipped Optical OFDM) serves as a more power-efficient substitute to DCO-OFDM by eliminating the need for DC biasing. This is achieved through a subcarrier allocation strategy that transmits data only on odd-indexed subcarriers, followed by asymmetrically clipping the negative constituents of the time-domain signal at zero to ensure non-negative output [4]. Notably, this method fundamentally reduces clipping related to distortion, as the discarded negative components inherently lack information-bearing content due to the method’s theoretical foundation. By avoiding the energy burden involved in DC biasing, ACO-OFDM is energy-efficient and robust against inter-symbol interference (ISI). Thus, making it particularly advantageous for energy-constrained VLC systems [7].

ACO-OFDM also demonstrates superior optical power efficiency contrasted to DCO-OFDM, making it particularly well-suited for applications where minimizing power consumption is critical. However due to the fact that only half of the available subcarriers are used for data transmission, its spectral efficiency is lower than that of DCO-OFDM, which can limit the resulting data rate. Furthermore, dependency on odd subcarriers makes it susceptible to noise and interference, thereby deteriorating signal quality [6], [7].

The Flip-OFDM benefits from avoiding the need for DC biasing by dividing the dipolar OFDM signal into positive and negative frames, in which the frames with negative values are inverted and transmitted one after the other. This technique improves bit error rate (BER) performance in environments that utilize systems with LED nonlinearity in the signal paths due to minimizing the effect of signal distortion due to LED nonlinearity caused by its dynamic range compression [7]. However, (as with other OFDM-based schemes) Flip-OFDM experiences from the fundamental elevated peak-average power ratio (PAPR) of multicarrier systems. A high PAPR produces multiple significant disadvantages: (1) it speeds up LED degradation by putting light sources into nonlinear saturation domains; (2) it weakens the light-communication compromise by reducing luminous efficiency when transmitting with a high peak; (3) it intensifies the clipping distortion when signals exceed the LED's linear dynamic range.

Moreover, OFDM requires long cyclic prefixes (CPs) to mitigate multipath dispersion, resulting in unnecessary data overhead that limits spectral efficiency and effective bandwidth utilization. Due to these constraints, rectangular pulse shaping is often employed in conventional OFDM systems, which produces a considerable amount of out-of-band (OOB) spectral leakage. Not only this leakage results in loss of optical power, but it also increases inter-channel interference in wavelength-division multiplexing (WDM) systems, further reducing the total power efficiency of the LED [7], [8].

Filtered orthogonal frequency-division multiplexing (F-OFDM) has appeared as a progressive enhancement to conventional OFDM, addressing key limitations through sub-band partitioning and adaptive filtering. In F-OFDM, the signal bandwidth is divided into discrete sub-bands, each independently optimized with application-specific parameters (e.g., numerology, modulation order). Tailored finite impulse response (FIR) filters are then applied to these sub-bands, enabling precise spectral shaping [8]. This architecture demonstrates multiple performance enhancements:

i. Superior OOB suppression: Filtering minimizes spectral leakage, reducing interference in adjacent channels and improving compatibility with heterogeneous networks.
ii. Asynchronous multi-service support: Sub-band isolation relaxes synchronization requirements across diverse services (e.g., IoT, high-speed data), enabling flexible resource allocation.
iii. PAPR mitigation: Sub-band-specific filtering attenuates high-amplitude peaks, enhancing power amplifier efficiency and LED operational longevity [9].
iv. Enhanced spectral efficiency: Flexible guard-band reduction and overlapping sub-band configurations optimize bandwidth utilization.
v. Design simplification: Cross-band interference mitigation via filtering reduces coordination complexity in multi-user environments.

By striking the right trade-offs between these diverse benefits, F-OFDM provides a scalable framework for next-generation optical wireless systems, especially in scenarios requiring the co-existence of heterogeneous services under stringent spectral and energy constraints [8], [9].

1.2 PROBLEM STATEMENT

Intensity modulation is the prevailing emission mode in visible light communication systems to encode information onto light-emitting diodes (LEDs), thus demanding transmitted signals to be purely real and nonnegative in order to adhere to the unipolar nature of optical intensity modulation. Traditional optical OFDM systems utilize the Hermitian symmetry (HS) property to satisfy the aforementioned constraint, i.e., they symmetrically construct frequency-domain data symbols before IFFT operation. Although this guarantees a real-amounted time-domain signal, it also introduces a severe limitation, as the enforced symmetry forces half of the effective bandwidth to be wasted, which drastically restricts spectral efficiency. In the context of VLC, this trade-off between signal unipolarity and bandwidth efficiency presents challenges to the design of high-throughput systems and thus demands the exploration of new approaches to balance these competing demands without negating signal integrity or complexity of the underlying system.

Although Hermitian symmetry (HS)-based optical OFDM solves the unipolarity needs for VLC systems, the required implementation introduces escalating hardware inefficiencies that compound the spectral limitations. Enforcing HS necessitates duplicating FFT/IFFT processing blocks (e.g., 2N-point IFFT modulation and N-point FFT demodulation), which directly amplifies computational complexity, chip area utilization, and energy consumption [10], [11]. Moreover, scaling the FFT size to mitigate bandwidth inefficiency—a logical countermeasure to the inherent 50% subcarrier redundancy—paradoxically exacerbates system costs and power demands. Hence, this limitation results in relatively larger FFT sizes that, although theoretically beneficial for spectral bandwidth, leads to chip area inflation and hardware scalability restrictions, as well as an growth in the PAPR [12], thus compromising the feasibility of high-throughput VLC deployments. Resolving this multidimensional trade-off—balancing spectral efficiency, computational overhead, and energy-footprint constraints—remains an open challenge in realizing cost-effective, large-scale optical OFDM architectures.

While optical OFDM techniques like DCO-OFDM and ACO-OFDM address the unipolarity requirements of VLC systems by converting bipolar signals into intensity-modulated waveforms, they introduce compounding inefficiencies that exacerbate the spectral and hardware limitations discussed earlier. DCO-OFDM applies a DC bias to shift the signal into nonnegative values, but this incurs significant power overheads due to bias-induced losses and clipping distortions [12], [13]. ACO-OFDM circumvents DC biasing by exploiting asymmetric subcarrier allocation, yet it sacrifices 75% of the usable bandwidth, further diminishing spectral efficiency [14]. Even advanced formats like Flip-OFDM, which leverage Hermitian symmetry (HS) to optimize signal recovery, remain constrained by the inherent HS subcarrier redundancy—only half of the subcarriers carry information, necessitating doubled IFFT sizes at the transmitter and compounding hardware complexity [12]. These trade-offs create a trilemma among power efficiency, spectral utilization, and computational scalability, leaving unresolved the core challenge of achieving high-throughput VLC without prohibitive energy costs or hardware overheads.

1.3 AIMS AND OBJECTIVES

The preceding analysis highlights the critical trade-offs inherent in conventional optical OFDM schemes for direct detection and intensity-modulated (DD/IM)-based VLC systems. These include the power inefficiency of DC-biased OFDM (DCO-OFDM), the spectral limitations of asymmetrically clipped OFDM (ACO-OFDM), and the hardware complexity imposed by Hermitian symmetry (HS)-based subcarrier redundancy. To address these interrelated challenges, this work proposes a non-Hermitian symmetry (NHS) Filtered-OFDM (NHS-F-OFDM) framework with the following aims and objectives:

Aim: To design a novel NHS-F-OFDM modulation scheme that eliminates the spectral and computational inefficiencies of HS-based optical OFDM, thereby enabling high-performance VLC systems with minimal power consumption, reduced hardware complexity, and enhanced bandwidth utilization. The complete objectives are outlined as follows:

i. *Evaluate the Efficacy of Filtered-OFDM in VLC Systems*: Investigate the role of filtered subcarrier processing in mitigating inter-symbol interference (ISI) and improving bit error rate (BER) performance.
ii. *Enhance Spectral Efficiency via Non-Hermitian Symmetry*: Develop a non-HS subcarrier mapping strategy to eliminate the 50% spectral redundancy inherent in HS-based OFDM, thereby doubling usable bandwidth while preserving unipolar signal generation.
iii. *Minimize Hardware and Power Overheads*: Propose an NHS-F-OFDM architecture that avoids redundant FFT/IFFT block duplication (e.g., 2N-point IFFT at the transmitter), reducing chip area utilization, computational complexity, and energy consumption.
iv. *Analyze PAPR Performance*: Characterize the PAPR of the proposed NHS-F-OFDM system and benchmark it against conventional HS-based F-OFDM to assess robustness against nonlinear distortions.
v. *Experimental Validation of System Performance*: Simulate an NHS-F-OFDM system and measure key performance indicators, including spectral efficiency, SNR, and BER.
vi. *Theoretical and Numerical Demonstration*: Derive mathematical models to quantify the spectral efficiency gains and hardware complexity reduction achieved by NHS-F-OFDM and then compare the outcomes to DCO-OFDM, ACO-OFDM, and HS-F-OFDM. Validate these models via MATLAB R2023a simulations.

1.4 ORIGINAL CONTRIBUTIONS

This thesis makes contributions to the advancement of VLC systems by addressing the inherent limitations of conventional optical OFDM schemes. In Chapter 3, the Non-Hermitian Symmetry DC-Biased Filtered-OFDM (NHS-DCO-F-OFDM) framework is introduced as a transformative solution to decrease computational complication while preserving compatibility with direct detection and intensity modulation systems. By eliminating the Hermitian symmetry (HS) constraint, the suggested technique accomplishes 66.5% stenography in multiplicative operations and 57% in additive operations across the VLCs system compared to conventional F-OFDM.

This advancement is done by introducing a novel signal-generation process that merges the imaginary and real elements of the complex OFDM signal at the output of the inverse fast Fourier transform (IFFT). An N/2-sample IFFT can also be realized through this integration to produce an N-sample real-amounted signal. The design not only enlarges spectral efficiency by achieving better utilization of available subcarriers but also delivers reduced hardware complexity, lower power consumption, and better chip area utilization. Simulation results show a noticeable improvement in the bit error rate functioning in the indoor VLC scheme, proving the feasibility of this approach for energy-limited systems.

Using these developments as a basis, Chapter 4 introduces a new concept, NHS-Flip-F-OFDM, which optimizes bandwidth and power efficiencies. This technique yields an N-sample real-valued signal by replacing HS by placing both parts of the signal (real and complex) beside each other, therefore shrinking the dimension of IFFT to N/4-point. Moreover, this approach maintains a lower computational complexity contrasted to the standard Flip-F-OFDM, with almost no need for duplicate processing of subcarriers. More importantly, by achieving a PAPR close to that of the traditional Flip-F-OFDM, the proposed technique ensures that configurations of the method do not induce the nonlinear distortion of the DCO-F-OFDM. Furthermore, NHS-Flip-F-OFDM not only surpasses NHS-DCO-F-OFDM in spectral efficacy and bit error rate (BER) functioning—particularly under low SNR conditions—but also achieves additional reductions in chip area and power consumption. Theoretical contributions comprise a mathematical framework quantifying the relation between NHS subcarrier mapping, FFT/IFFT sizing, and spectral efficiency. This framework unveils the reason behind the trilemma where the HS redundancy elimination frees optical OFDM from power efficiency, spectral efficiency, and computational scalability trade-off, backed up by MATLAB R2023a simulations that corroborate the complexity reduction as well as the improved BER performance. These contributions together allow low-cost, high-efficiency VLC systems via hardware simplicity and spectrum efficiency.

1.5 THESIS OUTLINE

This thesis is structured as follows:

Chapter 2 provides a comprehensive overview of visible light communication (VLC) systems, encompassing a comparative analysis of VLC and radio frequency (RF) communication paradigms. It further examines the core components and modulation techniques fundamental to VLC, alongside a critical evaluation of unipolar OFDM and modified OFDM methodologies employed within direct detection/intensity modulation frameworks.

Chapter 3 is organized into three sequential phases. It first explains the realization of a conventional direct-current-biased filtered OFDM (DCO-F-OFDM) approach based on Hermitian symmetry (HS) simulation. Based on this foundation, a theoretical and analytical exposition of the proposed non-Hermitian symmetry (NHS) DCO-F-OFDM technique is presented, which can mitigate the spectral inefficiencies of HS-based systems. The chapter ends by comparing the simulation results of both methods based on performance measures such as computational complexity, bit error rate, peak-average power ratio (PAPR), and signal-to-noise ratio.

The evaluation of the effectiveness of the propounded NHS-Flip-F-OFDM technique through the systematic exploration of its advantages over the conventional Flip-F-OFDM system has been done in Chapter 4. The chapter started with testing a conventional Hermitian symmetry-based Flip-F-OFDM scheme, showing its potential to produce real-valued signals for intensity modulation and direct detection (IM/DD) systems. Next, the chapter depicts the configuration, principles of operation, and the theory of the propositioned NHS-Flip-F-OFDM technique, stressing that it would remove spectral redundancies, in respect of that within HS-based systems. Subsequently, a comparison of both techniques is made, and the results of the simulation are examined regarding performance measures, such as computational complexity, SNR, BER, and peak-average power ratio.

In Chapter 5, we describe how NHS Filtered-OFDM architecture stands in comparison with traditional HS-based and benchmark OFDM architectures. To show the performance advantages of our strategy, we set up a logical system for analysis. A series of comparisons and computer simulations illustrate the enhancement of the NHS design in terms of computational efficacy, spectrum utilization, bit rate robustness, and PAPR properties. Our evaluations, based as they are on a combination of simulated results and theory, demonstrate just how attractive the NHS-Filtered-OFDM framework is when faced with the restricted resources characterizing VLC environments.

Chapter 6 synthesizes the core contributions of this thesis, presenting conclusions derived from the simulation and theoretical investigations of NHS-based Filtered-OFDM techniques. It critically appraises the trade-offs and restrictions of the propositioned methodologies while contextualizing their significance within the broader landscape of energy- and spectrally efficient communication systems.

2. VISIBLE LIGHT COMMUNICATION SYSTEMS: A BRIEF HISTORY

2.1 INTRODUCTION

In particular, VLC systems have recently attracted scholarly interest as a promising technology to enrich wireless connectivity beyond the limitations found in classical radio frequency (RF)-based systems. The growing need for wireless connectivity at higher speeds has included the limitations of RF systems, such as spectral limitations, congestion on unlicensed frequency bands, and uncontrolled signal propagation. In this regard, the Filtered-Orthogonal Frequency Division Multiplexing (F-OFDM) scheme has become a promising modulation option within VLC structures to mitigate these issues. This chapter traces the chronological trajectory of VLC systems, compares the operating and spectral efficiencies of VLC and RF communication paradigms for fundamental applications, and evaluates VLC components and associated state-of-the-art modulation methodologies. Additionally, it assesses unipolar OFDM and its modified versions emphasizing on IM/DD systems. The chapter concludes with a synthesis of key insights by highlighting major insights and emphasizing the importance of F-OFDM in facilitating next-generation wireless communication infrastructures.

2.2 A BRIEF HISTORY OF VLC SYSTEM

While the VLC system has only recently been studied in contemporary scholarly research, systems that utilize light as a communication medium stretch back century. Light has always been a fundamental medium for communication; many different civilizations have used optical techniques to transmit information. Other historical examples range from the sending of coded messages over distance using smoke signals, beacon fires, and systems of marine lanterns. Of particular note, operational optical communication frameworks were already in use during antiquity, as evidenced by documented systems in Ancient Greece [15]. Therefore, these early innovations underscore the enduring role of light in bridging communicative gaps, long preceding modern advancements in VLC technology.

Charles Chappe created the optical telegraph at the end of the 18th century during the Napoleonic era. Chappe’s optical telegraph system consisted of a mechanical set-up with two movable side arms or indicators attached to a central regulator bar [16] through which discrete symbolic configurations could be produced by means of rotation. These structures were even strategically deployed at networks of towers 10–15 kilometers apart. The system was capable of generating as many as 98 distinct combinations of signals through an optimized encoding protocol that could be identified by the receiver even at great distances. Other inventions followed, such as the experimental demonstration by Alexander Graham Bell and Charles Tainter of the photophone toward the close of the 19th century, which was able to transmit modulated light waves that could successfully transmit a voice message over 213 m [17].

Bell's photophone was a primitive optical communication device consisting of a transmitter-receiver system, as demonstrated in Figure 2.1. Functionally, the system took solar radiation directed via a mirrored array to a thin glass plate, which would vibrate in accordance with the acoustic vibrations of the speaker's voice. The modulated light was then collimated by a secondary lens aimed at the receiver unit, where a parabolic reflector focused the beam into a selenium-based photoconductive cell. Fluctuations in incident light intensity generated corresponding variations in the electrical resistance of the cell, thus encoding the signal transmitted. It was overshadowed commercially by the contemporaneous telephone invented by Bell but was considered by its inventor to be the pinnacle of scientific achievement and illustrative of the potential of light-wave communication [17].

Communication over optical links began to attract interest in the 1970s. At that time, studies revealed the potential of OWC, specifically infrared, in indoor environments where THz-measure electromagnetic spectrum bands could be utilized [18]. These systems initially achieved data rates of up to 1 Mbps. By the late 1990s, advancements in infrared technology-enabled data rates to reach up to 50 Mbps [19].

In the early 2000s, LED lamps were first explored for experimentations engaging VLC. Tanaka et al. demonstrated a dual-purpose application of a white LED bulb in indoor settings, utilizing it simultaneously for illumination and visible light communication (VLC) while attaining data rates as high as 400 Mbps [20]. This breakthrough ushered in widespread VLC research in the 21st century, inspiring subsequent innovations such as advanced modulation methods and LED technology improvements. The academic community clearly responded to this innovation, leading to a significant increase in research in the field.

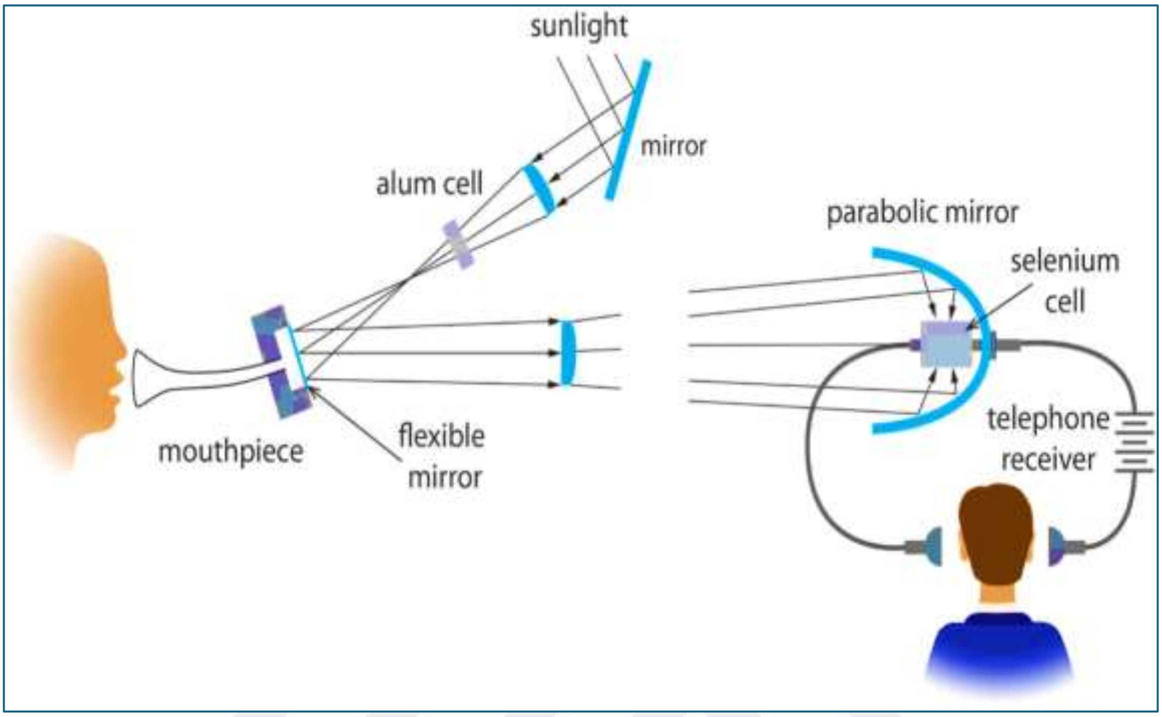

Figure 2.1: Photophone Components by Alexander G. Bell and Charles S. Tainter [17].

Visible light is a robust framework for interdisciplinary research in visible light communication. In contrast to the regulated radio frequency bands that necessitate licensing, the optical spectrum is utilized as a license-exempt resource that allows the free allocation of frequencies for signal transmission [21]. One main difference in the operational bandwidth: radio waves share bands in scales from kHz to GHz, whereas visible light operates within THz by a magnitude higher in spectral space.

In addition, visible light is free from any biological risks which have been reported with ultraviolet or infrared light, associated with photobiological hazards. Radio-based systems, from a security perspective, have fundamental vulnerabilities stemming from their characteristic of passing through opaque physical objects, which makes the standard wireless networking unsafe from being eavesdropped without being noticed [22]. In contrast, VLC systems exploit different photonic properties of light, leading to line-of-sight transmissions, which improves data security, especially in indoor scenarios. Contemporary VLC research integrates diverse fields ranging from applied realizations (i.e., Li-Fi ecosystems) to theoretical developments of new modulation at the level of the wave-particle duality of light and spectral efficiency [22].

2.3 VISIBLE LIGHT COMMUNICATION VERSES RADIO FREQUENCY

In recent years, communication technologies have advanced significantly, with Wi-Fi becoming the dominant method for wireless Internet access. However, challenges like the calamity of the RF spectrum and the increasing need for wireless communication have spurred the development of new technologies and research efforts. Within this context, VLC is being explored primarily as a harmonizing solution to Wi-Fi to converge the expanding bandwidth requirements of wireless networks [23]. Some researchers also propose that VLC could replace RF in specific scenarios [24]. Regardless, it is vital to assess the strengths and restrictions of VLC associated with RF communication. Table 2.1 specifies a general indication of the dissimilarities between these two technologies [25].

Table 2.1: Visible Light Communications and Radio Frequency Comparison.

Property	**VLC**	**RF**
Bandwidth size	From 380 to 780 THz	From 3 to 3000 GHz
Electromagnetic interference	No	Yes
Penetration	Walls (line-of-sight required)	Wall penetrations and other obstacles
Distance coverage	Short	Wide
Modulation procedures	Real and unipolar	Complex and bipolar
Security level	High-level	Medium-level
Noise sources	Sunlight and other lights	Electrical and electronic signals and devices
Mobility	Short distance	Long distance
Power consumption	Low	Medium

A key advantage of VLC is its ability to utilize existing infrastructure for communication facilities. The LEDs system, normally used for illumination can be used as a vided source of data transmission. Traditional VLC infrastructures serve as a way to transmit data in addition to their primary function of luminescence, and therefore, any energy used for communication imposes no additional operating costs. This dual-mode operation concept harnesses existing illumination energy, effectively decoupling data transmission at the avoidable expense of regular wireless communication overhead. [26]. Additionally, recent research has increasingly focused on using low-cost devices for VLC system implementation. For instance, in [26], the researchers developed an open-source podium for VLC explores using microcomputers (Beaglebone) and inexpensive LEDs. Another notable example is the effort by scientists at the Disney Research Centre, who created a VLC system utilizing commercial LEDs [27].

A further advantage of visible light lies in its expansive spectrum, which dwarfs the capacity of regulated radio frequencies. While radio bands are tightly controlled and allocated by global telecommunications authorities, the visible light spectrum remains unlicensed and freely accessible, enabling diverse academic and commercial innovations [26]. Light has distinct security benefits over radio waves due to its unique propagation properties. When a Wi-Fi access point is deployed, radio waves are emitted based on the coverage area associated with the antenna, which can easily extend for several hundred meters. This property enables the waves to pass through walls and other solid barriers, which creates security loopholes since such signals can be subject to interception and eavesdropping [28].

In addition, an important feature of using light as a medium for communication is its very high wave frequency (terahertz (THz)) range, which enables very high data rate transmission. Today's highest Wi-Fi specification, the WiGig concept, achieves up to 1 Gbps data transmission speed. Conversely, as a result of the higher frequency of light waves, the research on visible light communication has achieved impressive transmission speeds of up to 100 Gbps [29]–[31].

2.4 VLC COMPONENTS

Visible light communication employs light as a mode for data broadcast. The primary principle of VLC functions is to grant both illumination and communication capabilities concurrently. Consequently, VLC systems are designed to incorporate both light transmission and reception components. In the majority of existing research, light-emitting diodes (LEDs) are engaged as the primary transmitters. However, laser diodes (LDs) have also been used for this purpose, owing to their capacity to achieve data rates exceeding 40 Gbps. These LEDs modulate light intensity to encode and transmit information. On the receiving end, photosensors directly capture the light and convert it into a digital data stream [32]. In VLC systems, it is critical to ensure that the modulation techniques employed for data transmission do not compromise the inherent brightness of the light source. Thus, the selection of the LED type is critical to the overall performance of a VLC approach.

Figure 2.2 outlines the architecture of a VLC scheme. The process begins with encoding and modulating input data, which is then converted into real, unipolar signals. These signals drive LEDs to transmit information via light intensity modulation. Reception needs a direct line of sight between the receiver and LED to detect the modulated optical signals.

However, light signals can degrade during transmission due to scattering effects and ambient light interference. Optical filters help address this by reducing unwanted ambient light noise. At the receiver, the incident light modulates the photocurrent in the photosensor. Equalizers then amplify and stabilize the signal, minimizing its vulnerability to noise [27]. The signal is then demodulated to reconstruct the original data. The following section delves into the functional roles of individual components in a VLC system.

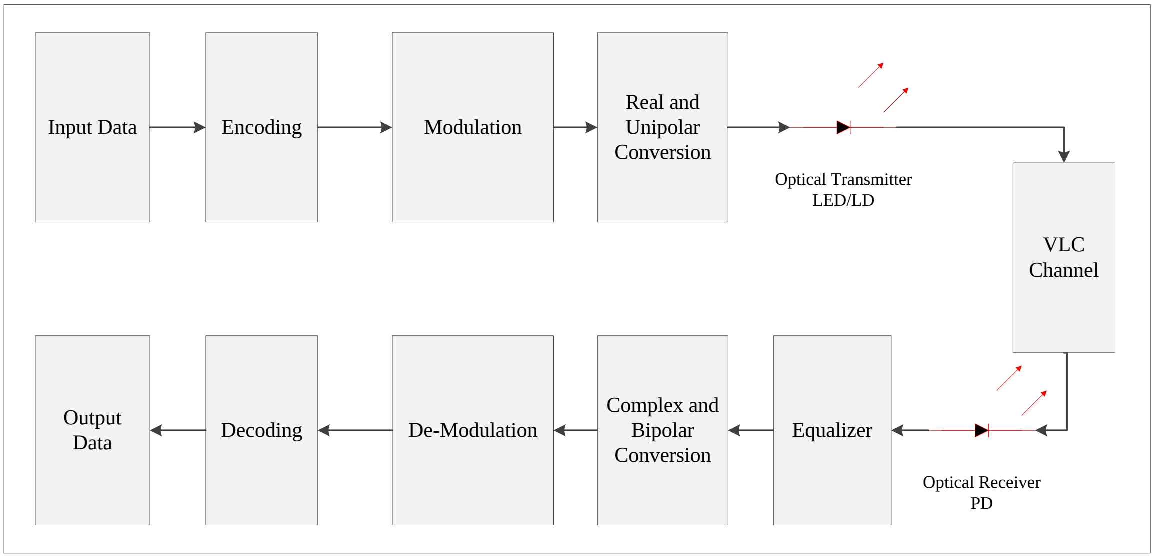

Figure 2.2: Typical VLC Architecture System.

2.4.1 VLC Transmitter

Light-emitting diodes (LEDs) are the predominant transmitters in VLC approaches. Commercial LED-based lighting fixtures typically incorporate arrays of LEDs coupled with a driver circuit, which regulates the electrical current supplied to the diodes and thereby governs their luminous output. This driver circuit employs transistor-based mechanisms to modulate the intensity of emitted light at frequencies exceeding the temporal resolution of human vision, rendering the data transmission imperceptible. To enable communication, LED luminaires are engineered to reconfigure the driver circuit for encoding information through optical intensity modulation [33]. Consequently, the architectural and electrical design of these luminaires critically influences the bandwidth, reliability, and overall efficacy of VLC implementations. White light is the preferred choice for illumination in both indoor and outdoor settings because it closely resembles natural sunlight and accurately reflects the colors of objects. In solid-state lighting, white light generation primarily relies on two methods.

2.4.1.1 Blue LEDs with phosphor

A prevalent methodology in solid-state illumination systems employs blue LEDs encapsulated within a phosphor coating to generate white illumination. In this configuration, the blue spectral output from the LED excites the adjacent phosphor layer, inducing a photoluminescent emission in the yellow wavelength range. The additive mixing of these discrete spectral components (blue and yellow) synthesizes broadband white light. Precise control over the phosphor layer's thickness enables tunability of the correlated color temperature, thereby facilitating the production of white light across a spectrum of chromaticity values [33].

2.4.1.2 RGB combination

White light synthesis can alternatively be realized through an additive combination of discrete red, green, and blue (RGB) emission spectra. This method requires monolithic integration of three distinct semiconductor emitters, thereby increasing component complexity and manufacturing costs relative to phosphor-converted blue LED architectures. Phosphor-based systems remain predominant in commercial illumination due to their simplified optoelectronic design and economic viability. However, the Stokes shift-induced spectral broadening inherent in phosphor down conversion imposes intrinsic limitations on modulation bandwidth, restricting operational frequencies to the low-megahertz regime [33]. In contrast, RGB-based systems support high-frequency data transmission through advanced multiplexing techniques such as Colour Shift Keying (CSK), which exploits wavelength diversity to encode information across multiple parallel optical channels. The spectral dimension advantage inherent in RGB configurations, coupled with their enhanced temporal response characteristics, renders them particularly suitable for visible light communication systems demanding high-speed modulation capabilities.

2.4.2 VLC Receiver

Receivers in VLC systems are engineered to transduce incident optical radiation into demodulated electrical signals. Within such architectures, two primary receiver typologies are employed to detect transmissions from LED luminaires: photodetectors (non-imaging receivers, typically implemented as photodiodes) and imaging sensors (e.g., camera-based systems) [15], [33]. Photodiodes (PDs) remain the predominant choice for VLC implementations owing to their high quantum efficiency, rapid temporal response, and stable operational characteristics under diverse illumination conditions [27]. Non-imaging receivers operate via direct detection of intensity-modulated light, enabling robust signal recovery even in multipath environments. Conversely, imaging sensors leverage spatial resolution to decode spatially encoded data streams, albeit with trade-offs in bandwidth and latency. Consequently, the superior modulation bandwidth and cost-effectiveness of photodiodes solidify their status as the default solution for high-space, low-intricacy VLC deployments. On the other side, photodiodes have high sensitivity and can measure wavelengths from the visible (e.g., ultraviolet) and infrared light [34].

Photodiodes are also prone to saturation in external environments, such as when exposed to sunlight, which can cause them to fail in receiving data due to high levels of interference. Consequently, alternative components are often employed to capture light in such situations. In addition, LEDs themselves can be utilized as receivers due to their inherent photo sensing properties [35]. In contrast to photodetectors, LEDs exhibit unique properties, making them highly efficient in specific scenarios. LEDs detect a narrower frequency range than photodiodes, which helps minimize interference and noise. Additionally, LEDs sensitivity remains permanent over time. One key advantage of LEDs in VLC systems is their ability to function as both transmitters and receivers. This merit enables the creation of systems with a single LED at each point, simplifying the design and installation process. Furthermore, their widespread availability and popularity make LEDs accessible components, simplifying the implementation of VLC applications.

2.5 MODULATION TECHNIQUES IN VLC

Contrasting RF communications, VLC differs fundamentally in how data is encoded and transmitted. Unlike RF, which can encode information in the phase and amplitude of the signal, VLC relies on variations in light intensity for data transmission, with reception achieved through direct detection. This method is known as Direct Detection Intensity-Modulated (DD-IM). In VLC systems, the modulation scheme must strike a balance between achieving high data rates and maintaining adequate lighting quality, as LEDs are often used simultaneously for both communication and illumination [36].

This section examines modulation techniques at the physical layer commonly implemented in VLC, alongside strategies to enhance high-capacity system performance. These methods are split into two primary categorizations: single-carrier and multi-carrier modulation schemes. Each involves distinct advantages and trade-offs, governed by system parameters such as data throughput, channel robustness, and integration with illumination requirements.

2.5.1 Single-Carrier Modulation (SCM) Schemes

Due to its straightforward implementation and efficiency, single-carrier modulation is broadly operated in VLC systems. By reason of the single-frequency carrier data transmission, such schemes are best suited for low-cost and low-energy VLC systems. This popularity is partly due to their inherent simplicity and robustness, which is especially valuable when hardware and power consumption are critical criteria for hardware design.

2.5.1.1 On–off keying (OOK)

OOK is an elementary procedure wherein information is transmitted by turning LEDs on and off for binary numbers (0 and 1) values, or by modifying the light intensity of the signal in two levels [36]. VLC approaches have been presented to accomplish a wide variety of data rates using OOK and white LEDs [37], [38]. For example, an OOK-based VLC system reported in reference [39] reported a distance of 2 meters and 40 Mbps, with the ability to go higher. However, all these OOK-based systems encountered several challenges in increasing the data rate. One critical issue is its sensitivity to ambient light interference, where external sources such as sunlight or indoor lighting introduce noise, significantly degrading performance.

Moreover, due to its binary nature, OOK is less spectrally efficient than advanced modulation schemes and does not support high data rate environments. Furthermore, the frequency with which LEDs can switch on and off can lead to visible flicker if the frequency of switching is not taken into account, compromising their function as sources of illumination. Further, OOK has limited robustness against multipath effects and inter-symbol interference (ISI) in highly dynamical VLC environments, resulting in high bit error rate [37], [39].

2.5.1.2 Pulse amplitude modulation (PAM)

Even though a substantial performance is achieved via PAM, which can simply be stated as a more elegant version of data modulation than OOK-based methods [40]. This information is encrypted in the amplitude of the lightwave produced by the transmitter, which we call PAM. This represents the amplitude of a binary or multi-level symbol associated with each wave. In the VLC system, PAM faces many challenges which impose performance and practicality.

Sensitivity to ambient light noise is a significant issue. External light peaking from sunlight and blow-up lighting pumps noise and boosts the detectors' SNR. LED conducting nonlinearity is another challenge, where the LEDs cannot accurately modulate the light intensity at very high transmitted data rates or intensity levels, resulting in significantly distorted signals.

In addition, as higher level PAM (e.g., 4-PAM, 8-PAM) allows higher data transmission rates, it can only be used where SNR is sufficiently high and advanced errors correction is used to provide a better accuracy for retaining transmitted signals, resulting in a more complex design at the receiver side. Another technical challenge is to ensure that PAM-based modulation does not produce flicker at frequencies that are sensed by the human eye, which necessitates high-frequency switching [41], [42].

2.5.1.3 Pulse position modulation (PPM)

Pulse Position Modulation (PPM) serves as an energy-competent modulation procedure in VLC approaches, encoding data through the temporal displacement of a single optical pulse within a predetermined symbol period [43]. PPM achieves a high energy efficiency as only a single pulse is transmitted in a frame, causing less power consumption than other solutions such as On-Off Keying. Due to it being immune to amplitude distortions such as LED nonlinearity or channel fading, it is well-suited for VLC systems. On the downside, PPM has low spectral efficiency because more symbols in a frame result in longer frame sizes, ultimately restricting data rates.

Also, accurate synchronization between receiver and transmitter is fundamental to ensure accurate detection of pulse positions, introducing significant complexity into system implementation [44], [45]. Ambient light interference can also affect PPM's performance in VLC, causing pulses to be masked and requiring several complex noise mitigation strategies. In spite of these challenges, sophisticated versions of PPM have also been proposed [44]-[48], which include differential PPM (DPPM), expurgated PPM (EPPM), overlapping PPM (OPPM) and variable PPM (VPPM) respectively. These changes are intended to improve efficacy in certain applications.

2.5.1.4 Pulse width modulation (PWM)

Pulse Width Modulation is another transmitter modulation procedure for VLC. Data is encrypted in the width or duration of the light pulses emitted by LEDs. By controlling the pulse width for each symbol, PWM allows encoding information while keeping a constant average light intensity, thus making it suitable for dual-simultaneous lighting and communication systems. PWM can resist some amplitude-related distortions. The most notable example is the nonlinearity of LEDs, which causes amplitude-dependent distortion [33].

However, there are challenges like the need for precise timing to decode the different pulse widths and susceptibility to interference from ambient light sources, which can impact the width of the perceived pulse at the receiver. Moreover, the narrow spectral competence of the PWM requires more bandwidth to differentiate the various widths, which can limit its use in high data rate applications. However, these limitations make PWM less practical for the large-scale realization of LED devices with a high degree of antilog; the dimension of the LED lighting is still limited to indoor light and low-cost IoT (Internet of Things) applications, which is the priority direction in next generation of VLC systems.

2.5.1.5 Color shift keying (CSK)

To address the limitations of traditional modulation schemes, including restricted data throughput and reduced dimming flexibility, the IEEE 802.15.7 standard established Color Shift Keying (CSK) in 2011 as a spectrally efficient technique [49]. CSK modulation uses several optical sources of diverse colors (wavelengths). RGB visible light communication transmitters emit light of a specific color to transfer data [50]. Nevertheless, CSK modulation is incompatible with VLC systems employing phosphor-based white LED sources, as its operation relies on independent control of multiple narrowband emitters. Consequently, RGB LED configurations (featuring discrete red, green, and blue wavelengths) become mandatory to enable the spectral agility required for chromatic coordinate manipulation in CSK-based schemes.

CSK is especially effective in using the available spectrum, which is much more spectrally efficient than an amplitude-based modulation scheme. Nevertheless, it has been difficult to implement and requires accurate color calibration and compensation for chromatic distortions due to channel conditions like different distances or interference from ambient light. Moreover, it is worth mentioning that CSK demands complex receivers that can decode chromatic evasions accurately, which also raises the cost of the system [51].

2.5.2 Multi-Carrier Modulation (MCM) Schemes

Multi-carrier modulation schemes are developed techniques in VLC systems applied to improve spectral and data rate efficiencies and guarantee resilience to channel impairments. These schemes split the transmission bandwidth into numerous sub-carriers, enabling simultaneous transmission of multiple data streams. Orthogonal Frequency Division Multiplexing (OFDM) and its modifications are the most common multi-carrier modulation scheme implemented in VLC.

A key limitation of traditional single-carrier modulation techniques is the significant escalation of inter-symbol interference (ISI) at higher data paces, driven by the nonlinear frequency-selective characteristics of VLC transmitters, which constrain achievable performance. This causes the problem of complex equalization on the receiving side [52]. Multiple multi-carrier modulation procedures have been investigated to improve the performance and data rates of spectrally constrained VLC systems, with Orthogonal Frequency Division Multiplexing (OFDM) emerging as a widely adopted approach for addressing these challenges. OFDM modulation-a technique allows high data rate transmission with minimal interference. It does so by mapping the data stream into several orthogonal sub-carriers to mitigate problems such as Inter-Symbol Interference (ISI) [53].

This approach enables the distribution of parallel data streams across multiple orthogonal narrowband subcarriers. These frequency-domain subcarriers are synthesized into a unified time-domain signal via an IFFT, generating a nonunipolar, complex- amounted waveform [54]. However, a fundamental incompatibility arises in optical systems, as IM/DD mechanisms require strictly real and non-negative signals to encode information via light intensity variations. There are many adaptations of optical OFDM to satisfy these needs, and supporting research is examining alternative methods to improve its performance. Moreover, [36] proposed some multi-carrier options for VLC systems.

2.6 PRINCIPLES OF OFDM FOR OPTICAL COMMUNICATIONS

Orthogonal Frequency Division Multiplexing (OFDM) is a multi-carrier modulation approach optimized for optical communication systems to accommodate the unique features of optical channels, such as unipolarity and diverse impairments. In contrast, for optical settings, the signals are modulated based on their intensity and directly observed, so non-negative values are required (i.e., light intensity cannot be negative). Some variants of this concept, incorporating Asymmetrically Clipped Optical OFDM (ACO-OFDM) and Direct Current-biased Optical OFDM (DCO-OFDM), are proposed to meet this requirement [54].

OFDM partitions the available optical spectrum into multiple orthogonal subcarriers, facilitating simultaneous data transmission. This approach increases spectral efficiency and strengthens resistance to channel distortions such as chromatic dispersion and multipath effects. At the transmitter, the IFFT is exploited to maintain subcarrier orthogonality, while the receiver employs the FFT for signal reconstruction. To address ISI—a key limitation in dispersive optical environments [53], [54] —each OFDM symbol incorporates a cyclic prefix, effectively reducing ISI impact.

Besides, the OFDM technique is adapted to the optical communication field to mitigate the nonlinearities arising from LEDs for the VLC system and the laser sources in the fiber optics, and hence the channel noise. Dynamic optimization through techniques such as adaptive modulation and coding for each subcarrier according to the channel conditions improves the system performance. This makes OFDM a strong and widely applicable method for the accomplishment of high data rates, high spectral efficiency, and reliability over extensive optical communication systems such as, but not limited to, fiber optics, free-space optics (FSO), and VLC [55].

2.7 UNIPOLAR OFDM SCHEMES FOR IM/DD SYSTEMS

Towards this end, optical OFDM signals can be adapted for visible light communication procedures, which count on intensity modulation (IM) combined with direct detection (DD). Here, the OFDM signal directly modulates the intensity of the light source itself. This adaptation, termed optical OFDM for VLC, was initially introduced in [55]. In conventional radio frequency (RF) systems, OFDM is transmitted as an electrical signal that assumes both nonpositive and nonnegative voltage values and RF receivers employ local oscillators to enable coherent detection of the transmitted complex waveforms. In contrast, VLC procedures employ only direct detection schemes without coherent signal recovery methods, as detailed in [37].

A key change arises because the generated OFDM symbol is always a bipolar complex waveform. Hence, it needs to be transformed into a real-valued unipolar signal. This conversion means that the subcarriers need to be subject to Hermitian symmetry constraint, which means that the complex signal can be turned into a real-valued with bipolarity signal [56]. Moreover, a number of methods have been widely studied in the literature to produce a nondipolar signal. The section below describes in further detail the pros and cons of these approaches.

2.7.1 Direct Current-Biased Optical OFDM (DCO-OFDM)

Among the earliest and amplest straightforward techniques to produce real-valued, unipolar OFDM waveforms well-matched with optical IM/DD approaches is Direct Current-Biased Optical OFDM (DCO-OFDM). This procedure acquaints with a fixed DC bias to the bipolar IFFT-generated signal, shifting it into the positive domain to ensure non-negativity—a critical requirement for IM/DD-based optical transmission. This bias is generally quantified as double the input signal's standard deviation [36], [57]. However, the inherent high PAPR of OFDM necessitates applying a noteworthy DC bias to shift the nonunipolar signal into the nonnegative domain, ensuring the signal remains non-negative for intensity modulation (IM) compatibility. This requirement often results in elevated optical power consumption. Alternatively, avoid a large DC bias (and therefore the inconveniences of high optical power required) by using a DC-bias K_b proportionally to the RMS (Root Mean Square) electrical power level P_{elec} instead.

$$K_b = k\, P_{elec} \tag{2.1}$$

where k stands for the cutting component and P_{elec} represents the variance of *x(n)* which defined as,

$${P_{elec}}^2 = E[x^2(n)] \tag{2.2}$$

As established in the work [58] the scale of DC bias is expressed as $10\ log_{10}[k^2 + 1]$dB. Consequently, the DC bias of the signal $x_{DC}(n)$ is assigned by:

$$x_{DC}(n) = x(n) + K_b \tag{2.3}$$

Residual negative amplitudes are truncated at zero to enforce the nonnegativity of the optical transmitter's input signal. This hard cutting process, however, inherently introduces clipping distortion (noise), as earlier discussed. Consequently, the unipolar signal of DCO-OFDM is assigned by:

$$x_{DCO-OFDM}(n) = x(n) + K_b + n_{clipping} \tag{2.4}$$

Where $n_{clipping}$ represents the clipping noise. For OFDM approaches, the PAPR scales linearly with the number of subcarriers. As demonstrated in previous work [58], [59], this sets a requirement for higher DC bias levels to prevent clipping noise, which in turn becomes coupled to the applied DC level. In Figure 2.3, the amplitude characteristics of a real OFDM signal under the DC offset of 0 dB, 5 dB, and 10 dB are contrasted to analyze the influence of bias adjustments. The findings show gradually vanishing residual negative signal peaks with increasing DC bias. This characteristic suggests that higher DC bias in bipolar OFDM signal would lower its clipping-induced distortion and further reduce the distortion area.

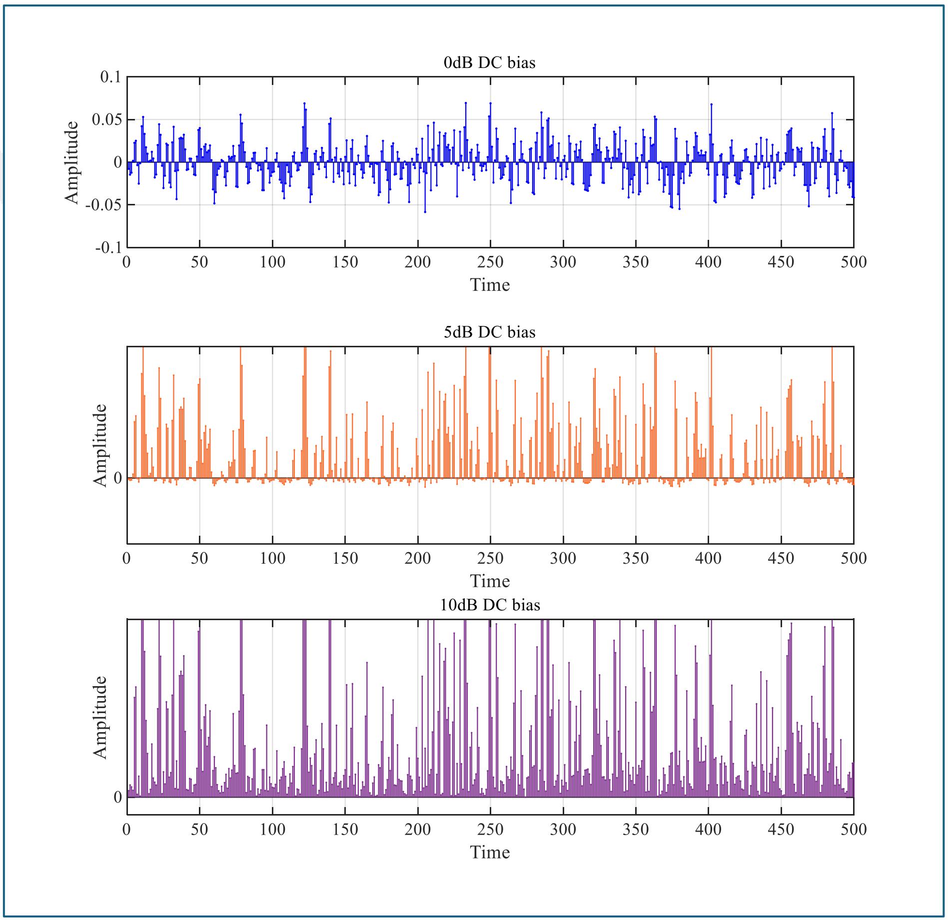

Figure 2.3: Time Domain Signals with Different K_b.

In DCO-OFDM systems, the Hermitian symmetry constraint restricts the transmission to $N/2-1$ independent complex symbols for an IFFT of size N. In this scheme, the electrical OFDM signal drives the optical intensity modulation (rather than field amplitude) of the transmitter. Since the necessitated optical power scales linearly with the OFDM signal amplitude, the imposition of a DC bias—essential for ensuring non-negativity—creates an inherent trade-off in optical power efficiency, as established in prior studies [58].

Specifically, the DC bias boosts the mean optical power but does not contribute to information-bearing signal components, thereby reducing the effective power utilization for data transmission. More specifically, the added DC bias elevates the system's baseline optical power consumption, creating a performance penalty unique to DCO-OFDM implementations.

2.7.2 Asymmetrically Clipped Optical OFDM (ACO-OFDM)

In previous works, a novel method was introduced that can boost power efficacy in optical OFDM approaches by replacing DCO-OFDM [60]. This process, termed asymmetrically clipped optical OFDM (ACO-OFDM), creates unipolar signals aimed at IM/DD procedures by smartly assigning subcarriers to pass along data so that no DC biasing is needed. For ACO-OFDM, odd-indexed subcarriers are modulated with respect to the remaining even-indexed subcarriers, such that Hermitian symmetry properties are maintained, and, therefore, real-valued time-domain signals can be guaranteed [61]. This selective modulation scheme inherently suppresses the negative amplitude signals through asymmetric clipping, facilitating the direct generation of unipolar waveforms. Consequently,

$$X(N-k)=\begin{cases} X^{*}(k), & k\ odd \\ 0\ , & k\ even \end{cases} \tag{2.5}$$

As demonstrated in [60], the discrete-time domain signal at the output of IFFT exhibits an anti-symmetric property,

$$x\left(n+\frac{N}{2}\right)=-x(n), \quad n=0,1,\ldots\ldots,\frac{N}{2}-1 \tag{2.6}$$

Nonlinear hard clipping gives unipolar time-domain signals in ACO-OFDM as it simply clamps all negative excursions of the bipolar waveform. This asymmetrical signal processing guarantees that only amplitude components of a positive nature are transferred, which meets the specifications of intensity-modulated optical systems. Mathematically, the respective discrete-time signal is represented as:

$$x_{ACO}(n)=\begin{cases} x(n), & if\ x(n)>0 \\ 0\ , & if\ x(n)\leq 0 \end{cases} \tag{2.7}$$

Lastly, ACO-OFDM inherently uses an anti-symmetric mechanism in the time domain of its optical waveform for distortion-less signal recovery that withstands nonlinear clipping.

Essentially, by removing the negative excursions of its bipolar counterpart, a DC biasing is eliminated while the positive signals can be retained, increasing optical power efficiency over DCO-OFDM. Importantly, because of the anti-symmetry, the original data symbols *X(k)*, transmitted only over the odd-indexed subcarriers, can be perfectly recaptured from the clipped unipolar signal at the receiver.

Yet this efficiency comes at a spectral cost: Hermitian symmetry constraints (to ensure real-valued transmission) combined with the restriction to odd subcarriers reduce the usable subcarriers to $N/4$ for an N-point IFFT. This results in a 50% lower spectral efficiency compared to DCO-OFDM, which utilizes $N/2-1$ subcarriers [58]. Overall, ACO-OFDM represents a unique compromise between power usage and spectrum efficiency in optical OFDM systems.

2.7.3 Flip-OFDM

In contrast to traditional ACO-OFDM systems, Flip-OFDM modulates all subcarriers to produce Hermitian symmetric real-valued bipolar OFDM signals. While ACO-OFDM can only transmit data on odd-indexed subcarriers, Flip-OFDM modulates all available subcarriers and has been discussed in the literature with comparable power efficiency as the former but with an orthogonal trade-off in transceiver hardware complexity [62]. The technique maintains the anti-symmetric features of the time-domain signal, allowing for asymmetric clipping of the negative segments of the waveform—similar to ACO-OFDM—while bypassing the spectral efficiency loss associated with odd-subcarrier restrictions.

This structural difference simplifies some features of signal efforts but requires an adjusted transmitter and collector design, for example, as seen in Figure 2.4. Flip-OFDM preserves the same inherent benefit of DC bias-free signal transmission, making ACO-OFDM an attractive candidate for optical OFDM. However, its hardware implementation requires more synchronization and frame handling processes than ACO-OFDM, illustrating optical OFDM systems' performance vs complexity balance.

The real non-unipolar time-domain signal can be decayed into two dissimilar constituents: positive component $x^{+}(n)$, representing all non-negative amplitudes, and negative component $x^{-}(n)$, capturing the inverted absolute values of negative excursions. Mathematically, this decomposition is expressed as:

$$x(n) = x^{+}(n) + x^{-}(n) \tag{2.8}$$

where

$$x^{+}(n) = \begin{cases} x(n) & if \quad x(n) \geq 0 \\ 0, & \quad otherwise \end{cases} \tag{2.9}$$

and

$$x^{-}(n) = \begin{cases} x(n) & if \quad x(n) < 0 \\ 0, & \quad otherwise \end{cases} \tag{2.10}$$

The non-unipolar signal *x(n)* is adapted for non-dipolar transmission by allocating its positive component to the first OFDM subframe and its inverted negative counterpart to the following subframe, as illustrated in the following:

$$x_{2N}(n) = \begin{cases} x^{+}(n), & n = 0, 1, .., \ N-1 \\ -x^{-}(n-N), & n = N, ..., 2N-1 \end{cases} \tag{2.11}$$

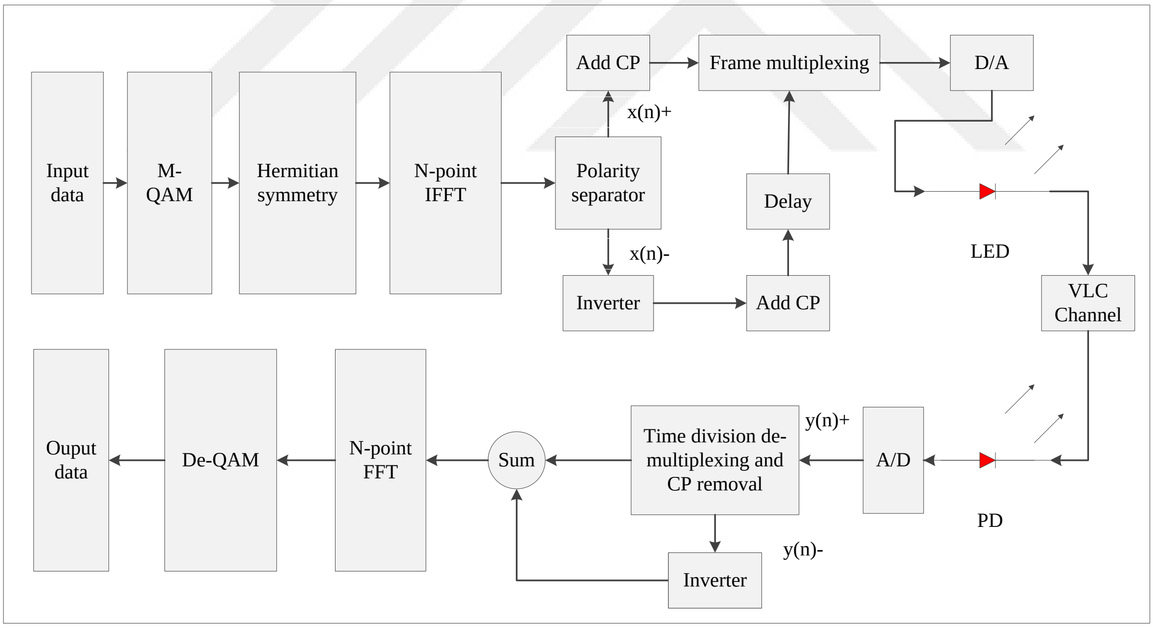

Figure 2.4: Flip-OFDM Transceiver.

The original bipolar waveform is rebuilt at the receiver by subtracting the second subframe (flipped negative component), $y^{-}(n)$, from the first subframe (positive component), $y^{+}(n)$, as illustrated in the following equation:

$$y(n) = y^{+}(n) - y^{-}(n) \tag{2.12}$$

The transmitted frequency domain signal is then reconstructed by standard OFDM demodulation. As demonstrated in [58], Flip-OFDM and ACO-OFDM achieve identical functioning across key metrics, including SE (spectral efficiency), SNR (signal-to-noise ratio), and BER (bit error rate). Moreover, due to the N-point IFFT process, Flip-OFDM theoretically provides a transmission rate through the usage of complex N-point IFFT/FFT processing, which is twice the data transmission rate of ACO-OFDM. This indicates that the throughput of ACO-OFDM is lower than that of Flip-OFDM under the same computational complexity [63].

While Flip-OFDM achieves a 50 percent reduction in receiver hardware intricacy contrasted to ACO-OFDM, it introduces two significant limitations; Hermitian symmetry dependency: The mandatory Hermitian symmetry constraint for generating real-valued OFDM signals increases power dissipation and requires larger integrated circuit (IC) footprint, and Compatibility limitations: Flip-OFDM is restricted to ACO-OFDM signal generation and lacks compatibility with modern DCO-OFDM-based approaches [64], [65], which are critical for high-efficiency optical power modulation schemes.

2.7.4 Asymmetrically Clipped DC-Biased Optical OFDM (ADO-OFDM)

Asymmetrically Clipped DC-Biased Optical OFDM is a mixed technique that integrates information prearrangement across odd and even sub-carriers. This method mirrors ACO-OFDM by utilizing odd subcarriers but extends its functionality by incorporating even subcarriers, aligning it more closely with the principles of DCO-OFDM. This combination enables ADO-OFDM to leverage both approaches' benefits, balancing spectral and energy efficiency while addressing the unipolar signal requirements of optical communication systems [66].

Despite the better spectral efficiency and energy saving of ADO-OFDM, there are some drawbacks which can hinder its practical realization. ADO-OFDM has a hybrid nature, which increases the complication of the receiver and transmitter designs, since the odd and the even subcarriers should be processed separately [67]. The introduction of a DC bias in the even subcarriers accounts for increased power consumption and subsequently eliminates the energy efficiency advantage in the system. Asymmetric clipping of signals produces clipping noise that can destroy signal quality and rise the BER in scenarios with high modulation.

In addition, the non-uniform power allocation of the odd and even subcarriers causes the SNR asymmetry that may affect the reliability of the system in adverse channel conditions [68]. These trade-offs and additional computational requirements create obstacles to the scalability and adaptability of ADO-OFDM over future high-speed VLC applications.

2.7.5 Asymmetrically and Symmetrically Clipped Optical OFDM (ASCO-OFDM)

ASCO-OFDM is a specially designed modulation method aimed at IM/DD approaches in VLC. This is an advanced version of OFDM that utilizes the principles of Asymmetrically Clipped Optical OFDM (ACO-OFDM) and Symmetrically Clipped Optical OFDM (SCO-OFDM) to improve performance in VLC approaches. To take benefit of both odd and even subcarriers, ASCO-OFDM overcomes the difficulty of transmitting unipolar signals necessary for optical systems [69].

In ASCO-OFDM odd subcarriers are asymmetrically clipped like in ACO-OFDM, and energy-efficient transmission is possible with no DC bias being needed. The even subcarriers, however, are clipped spectrally symmetrically, similar to SCO-OFDM for adding supplemental data. This dual approach advances the system's spectral efficacy relative to ACO-OFDM solitarily and makes this a candidate for high-level data rate applications. In addition, ASCO-OFDM preserves the subcarriers' orthogonality to avoid ICI while dealing with the multipath effect which is generally shown in VLC environments [70].

Asymmetric clipping has been proposed for this purpose yet causes higher computational complexity at the receiver to recapture the transmitted signal with respect to symmetric clipping as well as higher clipping noise. In spite of these challenges, ASCO-OFDM proves to be especially beneficial in scenarios where spectral and energy efficiency is significant, which includes indoor VLC approaches, vehicular communication, and hybrid VLC-RF networks.

2.8 FILTERED-OFDM: A MODIFIED SCHEME OF OFDM IN VLC SYSTEMS

OFDM is broadly regarded as a transformative advancement in wireless communication, utilizing orthogonal subcarriers for high-speed data communication. Notable advantages—like greater spectral efficiency and improved resilience to multipath fading—establish it as a pillar of contemporary broadband technology. However, the present OFDM-based systems have a major issue, which is called adjacent channel interference (ACI) due to significant out-of-band emissions (OOBE). To increase spectral efficiency, mitigation of OOBE has become a concern for 5G and next-generation networks [71].

In recent studies, UF-OFDM as well as its improved version eUF-OFDM have been underscored as promising solutions to OOB emissions [72], [73]. In addition to conventional filtering techniques, complementary methodologies, including pulse-shaping approaches, have been proposed relaxation of spectral leakage with further reductions of OOB radiation [74], [75]. On the other hand, filtered OFDM (F-OFDM) is shown to be a more efficient way of addressing OOBE without the penalty of BER metrics, providing a good trade-off for spectral occupancy and signal quality [76].

Optical-OFDM system also presents a superior peak-average-power ratio [77]. Notably, PAPR increases proportionally with the number of subcarriers. Consequently, this necessitates a larger backoff in the transmitter's power amplifier (PA) and amplifies quantization noise in the analogy-to-digital (A/D) converters at the receiver [77]. In direct detection and intensity modulation systems, the impact of PAPR is more pronounced due to the limited lifespan of LED emitters, where a high PAPR can significantly impair the overall interior lighting functionality [78], [79].

Filtered-OFDM was reintroduced by Huawei at the MWC (Mobile World Congress) in 2015 [80]. F-OFDM represents an adaptive modulation scheme incorporating flexible subcarrier bandwidth, aiming to enhance the traditional OFDM technique [81]. This method applies digital filters to the OFDM signal, which do not distort the passband signal while filtering out the out-of-band components. By doing so, OOB emissions are reduced, leading to lower ISI typically present in the OFDM waveform [37]. The primary modifications between F-OFDM and OFDM can be reviewed in Table 2.2.

Table 2.2: The Primary Differences between F-OFDM and OFDM.

Aspect	OFDM	F-OFDM
Filtering	A single, wideband filter for the entire spectrum.	Individual filters applied to each sub-band.
Spectral Leakage	High spectral leakage due to limited filtering at the edges.	Significantly reduced leakage with tailored sub-band filters.
Numerology Support	Limited to uniform numerology across all subcarriers.	Supports mixed numerologies for diverse use cases.
Efficiency	Less efficient in scenarios with diverse bandwidth needs.	Enhanced spectral efficiency through flexible allocation.
Out-of-Band Emissions	Higher emissions due to weaker edge control.	Strong suppression of out-of-band emissions.
Complexity	Lower computational complexity.	Higher complexity due to the need for multiple filters.

2.8.1 Why Filtered-OFDM For VLC System?

Filtered-OFDM is particularly suitable for use in visible light communication approaches, as it has the potential to solve key challenges encountered in this field. As VLC is within the visible light spectrum, it requires accurate emission to avoid interfering with adjacent channels, and also spectral efficacy. Although conventional OFDM has still very good performance, but it experiences from high OOBE and cross-talk interference, which greatly impact the performance in high-density VLC systems [82].

F-OFDM addresses these concerns with subband specific filter, which reduces spectrum leakage and maximizes signal separation. In addition, VLC systems are subject to nonlinear constraints that emerge from LED features and are required to achieve a broad diversity of applications, from IoT and indoor navigation to high-speed data transmission. The adjustable filtering capabilities of F-OFDM permit the optimization of performance for these varying signal requirements is also another benefit to making it a flexible and intuitive solution for advanced VLC systems [81].

2.8.2 Technical Advantages of F-OFDM in VLC Systems

There are multiple technical advantages of using the filtered-OFDM system in VLC systems. One major benefit of this technique is the improvement of signal integrity, owing to the fact that each subband has intermodulation distortions filtered out enabling increases in the related signal-to-noise ratio. This attribute is especially important for VLC since the quality of the light signal can be affected by environmental factors. In addition, F-OFDM sustains hybrid communication models, facilitating seamless synchronization with other technologies such as RF systems, which improves its adaptability in environments needing various connectivity options. Additionally, this one adds the dynamic ability to adapt according to the nonlinear behavior of VLC channels, precisely by LEDs, improving the performance of the system. With these functionalities, F-OFDM can provide more robust, higher-rate communication, making it a highly applicable solution for VLC systems that need to accommodate futuristic, high-speed, and interference-sensitive applications [82], [83].

2.8.3 Implementation Considerations in VLC Systems

Numerous technical challenges plague the practical implementation of filtered orthogonal frequency-division multiplexing (F-OFDM) in VLC approaches, despite its unparalleled increases in spectral efficiency: [83], [84]:

i. Increased Computational Overhead: The necessity to create separate filters for each subband leads to significant processing overhead. All this complexity needs to be enabled using algorithmic optimizations or hardware acceleration following the literals of real-time operational limits as significant to the VLC applications.
ii. Strict latency constraints: VLC systems, especially those that cater to real-time services (e.g., AR, industrial automation, or ultra-high-definition streaming) require ultra-low latency. The multi-stage filtering operations inherent to F-OFDM come at the possible disadvantage of processing delays, requiring parallelized architectures or reduced-complexity filter designs to avoid temporal distortion.

iii. Backward Compatibility Requirements: Nobility of F-OFDM must be retained often with legacy VLC infrastructure covering commercial off-the-shelf LEDs and photodetectors. Along with these challenges, the non-linear electro-optical characteristics of conventional components (which can add noise that degrades the integrity of the filtered signal) and the inherent necessity of adaptive equalization techniques for mitigating the discrepancy between reconfigurable F-OFDM and legacy heterogeneous modulation schemes make it difficult to integrate F-OFDM into a practical system.

2.8.4 Filtered-OFDM Filter Design

For a filter to be suitable for use in filtered-OFDM (F-OFDM), it must adhere to the following requirements [85]:

i. The filter's passband should maintain minimal amplitude variation across subcarriers within the designated subband. This design consideration is critical for mitigating distortion effects, particularly for edge-located data subcarriers in the subband. Such optimization ensures signal integrity by reducing nonlinear phase and amplitude distortions that disproportionately impact subcarriers near subband boundaries.
ii. The filter's frequency roll-off must initiate precisely at the passband edges and exhibit a narrow transition bandwidth. This characteristic is essential for optimal bandwidth utilization, as it reduces spectral inefficiency by minimizing guard band allocation. Furthermore, the sharp spectral confinement enables the coexistence of adjacent subband signals employing heterogeneous numerologies, allowing their frequency-domain placement near minimal guard subcarriers. Such spectral compactness supports flexible multi-numerology systems while preserving inter-subband isolation.
iii. The filter must provide adequate stopband attenuation to guarantee negligible interference leak between adjacent subband.

The optimal prototype filter that satisfies the previously mentioned requirements is the sinc impulse response, $\rho_B(n)$, characterized by a bandwidth of B. However, this filter is inherently non-causal and impractical for real-world implementation. To address this matter, the desired filter is constructed by convolving the sinc impulse response, $\rho_B(n)$, with a window function, $w(n)$, as represented by the following expression:

$$f_B(n) \triangleq \rho_B(n).w(n) \tag{2.13}$$

A raised-cosine window was applied to ensure soft transitions and prevent frequency spillover in the truncated filter. The raised-cosine window provides smooth roll-off characteristics and helps reduce spectral leakage. The expression for the raised-cosine window is as follows [85]-[87]:

$$\rho_B(n) = sinc\left((W + 2\partial W)\frac{n}{N}\right) \quad for - \frac{L}{2} \le n \le \frac{L}{2} \tag{2.14}$$

In which *L* signifies the filter size, and *N* symbolizes the FFT size, the number of subcarriers signifies W, and ∂W indicates the tone offset. By normalizing the filter coefficients, we ensure that the filter response is properly scaled and aligned with the desired frequency range. The normalization process helps achieve optimal performance and maintain the desired characteristics of the filter as follows [84]:

$$f_B(n) \triangleq \frac{\rho_B(n)\,.\,w(n)}{\sum_n \rho_B(n)\,.\,w(n)} \tag{2.15}$$

Where $w(n)$ is assigned as:

$$w(n) = \left(\frac{1}{2} + \frac{1}{2}\cos\frac{2\pi n}{L-1}\right)^{0.6} \quad , \quad -\frac{L}{2} \le n \le \frac{L}{2} \tag{2.16}$$

Ensuring minimal out-of-band emissions is a critical aspect of the filter's design [86]. Consequently, the guard interval through sub-bands can be very small, allowing for efficient utilization of the spectrum.

2.9 SUMMARY

The chapter started with a general description of visible light communication systems including evolution history, differences with radio frequency (RF) communication paradigms, and architectures. The subsequent analysis explored various modulation approaches suitable for VLC, highlighting their compatibility with IM/DD systems. As VLC transmission is based on optical signals, the modulation schemes must intrinsically produce real and unipolar waveforms. In order to fulfil this necessity, a variety of unipolar signal generation strategies including DC-biased optical OFDM (DCO-OFDM), asymmetrically clipped optical OFDM (ACO-OFDM), Flip-OFDM asymmetrically, clipped DC-biased optical OFDM (ADO-OFDM) and asymmetrically shaped clipping optical OFDM (ASCO-OFDM) were discussed. Finally, a new modulation framework, which is F-OFDM, was introduced as an engaging nominee to progress the spectral effectiveness of VLC approaches via optimized subcarrier filtering.

3. FILTERED-OFDM IN VISIBLE LIGHT COMMUNICATION SYSTEMS: COMPLEXITY REDUCTION AND IMPROVED SPECTRAL EFFICIENCY

3.1 INTRODUCTION

Filtered Orthogonal Frequency-Division Multiplexing (F-OFDM) is an evolution of conventional OFDM developed to tackle increasing demands on spectral efficiency and dynamic flexibility in future communication systems. As a promising modulation framework in visible light communication systems, F-OFDM has unique advantages, particularly its ability to optimize spectrum utilization according to constraints that VLC faces, such as limited modulation bandwidth in the optical wireless channel [11]. The subband-specific filtering mechanism allows for customized spectral shaping, which reduces inter-carrier interference and enables resilient data transmission in limited-bandwidth VLC scenarios.

VLC systems encode and transmit data by changing the modulating intensity of optical radiation from light resources like laser diodes (LDs) or light-emitting diodes (LEDs). This process follows the IM/DD paradigm, commonly applied to embed information into the amplitude of the optical carrier and recover data through photodetection at the receiver. Conventional OFDM and filtered OFDM (F-OFDM) baseband signals are incompatible with VLC systems since their complex-valued and bipolar nature, which violates the unipolar signal constraints imposed by IM/DD-based optical transmission. To make a compromise between this difference, advanced signal conditioning techniques, such as Hermitian symmetry imposition, DC biasing, or clipping operations are required to be employed to obtain F-OFDM waveforms that are strictly real-valued and non-negative, to meet the VLC physical-layer constraints [88].

The two widely used tactics for producing real-valued signals that serve as inputs for the intensity modulation in the OFDM approaches are as follows [88]. The first method is based on generating a complex-valued signal with an IFFT, followed by applying radio-frequency upconversion to obtain a corresponding waveform in the real-time domain. This approach, however, adds extra implementation complexity, requiring additional hardware infrastructure, such as DAC and IQ modulators. Besides, carrier-frequency compensated equalization might also be needed to recover the transmitted signal correctly, complicating system design additional [89].

By contrast, the second approach implements a Hermitian symmetry (HS) constraint in the input subcarriers before applying the IFFT process. This method intrinsically guarantees the generation of a real-amounted signal in the time domain by invoking conjugate symmetry on the frequency-domain data, consequently eliminating the need for additional hardware modules e.g. DACs, and IQ mixers [89]. The HS-based approach provides a low-complexity alternative that aligns with the cost-sensitive and power-limited operation paradigms of the underlying optical wireless communication systems.

The HS approach mandates conjugate symmetry in the frequency-domain symbols prior to their input into the IFFT. This ensures the generation of real-valued OFDM signals, which inherently satisfy the unipolar modulation requirements imposed by intensity-modulated communication systems [90], [91]. IFFT itself is the essential computation process used in an OFDM structure that modulates the data to orthogonal subcarriers while ensuring coherent demodulation at the receiver [92].

However, the IFFT/FFT length acts a crucial direct role in the transaction performing in terms of the qualification of power efficiency and hardware resource allocation. Namely, computational complexity grows quadratically with the transform size, since larger IFFT/FFT operations require exponentially more complex multiplications and additions. This increase in number crunching has a direct impact on power dissipation, especially for systems using high-order modulation schemes, or wide bandwidths. Moreover, longer IFFT/FFT lengths require more arithmetic logic units (ALUs) and memory buffers, thus stretching the footprint of the integrated circuit and increasing its manufacturing cost, which is an important aspect, especially for resource-limited or mass-deployed communication systems [92].

The implementation of the HS limitation in optical OFDM systems inherently requires dual FFT/IFFT processing blocks. This architecture employs asymmetric FFT/IFFT configurations, where a 2N-point subcarrier inverse fast Fourier transform operation in the modulator corresponds to an N-point subcarrier FFT operation in the demodulator [91], [92]. Such asymmetric processing introduces trade-offs in power efficiency and chip area, while simultaneously exacerbating computational overhead and hardware implementation costs. These challenges stem from the quadratic scaling of arithmetic operations and the need for parallelized processing elements to accommodate larger transform sizes. Over the years, various optical OFDM systems have been recommended to achieve signal positivity in IM/DD procedures. In these systems, the transmitted signals are modulated based on light intensity and must be unipolar [91].

In the direction of converting a conventional dipolar OFDM signal, processed with Hermitian symmetry, into a unipolar signal, two widely adopted optical OFDM approaches are employed: DCO-OFDM and ACO-OFDM [90]-[92]. In DCO-OFDM, a direct current (DC) bias is directed, and the negative components of the transmitted signal are clipped to zero [93]. However, this method incurs significant power losses because of the included DC bias. Alternatively, due to ACO-OFDM's asymmetric nature, the output signal is directly clipped to zero without requiring a DC bias or loss of information at the IFFT stage. However, ACO-OFDM can utilize only a quarter of the available bandwidth, which reduces spectral efficiency.

Numerous HS-based OFDM formats have been proposed to decrease system hardware complexity. However, owing to the HS restriction, only 50 percent of the subcarriers are utilized for information broadcast, resulting in a multiplied IFFT volume. The study in [94] introduced a low-complexity receiver for a hybrid ACO-OFDM scheme. The outcomes exposed that the proposed receiver demonstrated error probability performance similar to a conventional receiver. While the researchers in [95] proposed an innovative unipolar transceiver by enhancing a conventional ASCO-OFDM system. This approach improved SNR and reduced the receiver complexity of the system. Additionally, the computational complication of ADO-OFDM can be minimized through the introduction of pre-distorted ADO-OFDM [96]. Based on this work, the authors concluded that PADO-OFDM offers the advantage of low processing latency at the receiver. Furthermore, in [97], a study was conducted to assess the functioning of fast optical OFDM (FOOFDM) in VLC applications, comparing it with DCO-OFDM. The simulation outcomes indicate that FOOFDM exhibits lower computational complexity than DCO-OFDM.

In [98], the authors proposed a size-efficient IFFT/FFT technique that does not require Hermitian symmetry. This method combines two N-points complex- amounted IFFT output segments to generate a real- amounted signal. In [99], the study demonstrated that non-HS-OFDM achieved bit-error-rate and transmission-rate performances similar to those of HS-OFDM but with a smaller IFFT/FFT size, effectively halving the computational difficulty. Specifically, they introduced a technique that utilizes the real and imaginary parts of the N-point complex-amounted IFFT output to construct a noncomplex-amounted signal without applying an HS limitation.

One objective of this thesis is to examine and simulate the implementation of the Filtered-OFDM scheme, which is not covered enough in the literature. This adaptive modulation technique improves OFDM in VLC systems by allowing for a flexible subcarrier bandwidth. The remainder of this chapter is structured as follows: firstly, a conventional F-OFDM scheme based on HS is implemented and tested. Next, the proposed non-Hermitian symmetry (NHS) F-OFDM technique is explained and examined in detail. Finally, the simulation results of the two methods are evaluated based on computational complexity, SNR, BER performance, and PAPR considerations.

3.2 FILTERED- ORTHOGONAL FREQUENCY DIVISION MULTIPLEXING (F-OFDM) BASED ON HERMITIAN PROPERTY

3.2.1 System Model

Filtered-OFDM signals like OFDM signals necessitate to be real and positive to be used for driving light sources like LEDs and LDs to ensure compatibility with the characteristics of these light sources. A widely used method for producing real-time filtered-OFDM signals engages in directing Hermitian symmetry to the frequency samples at the IFFT input. This modulation technique is meant to be Discrete Multitone (DMT) modulation [11], [100].

In typical F-OFDM architectures, as revealed in Figure 3.1, the input data flow is initially segmented into N parallel substreams via a serial-to-parallel (S/P) converter within the processing chain. These streams are then digitally encoded with a constellation mapping scheme and transformed to the frequency-domain using a DFT (discrete Fourier transform) framework. In particular, to guarantee that real-valued F-OFDM signals can be synthesized, the frequency-domain samples fed to the IFFT block should fulfill the Hermitian symmetry restriction. This restriction requires conjugate symmetry for the frequency-domain samples and thus ensures that the obtained time-domain waveform is strictly real-valued, as mathematically formalized in [98]:

$$X_H = (X_0,\ X_1,\ X_2, \dots X_{N-1},\ X_{N-1}^*, X_2^*,\ X_1^*) \tag{3.1}$$

The real signal obtained after applying the Hermitian symmetry is denoted as X_H, is derived from complex frequency samples. The HS constraint is brought by appending original frequency-domain samples with their complex-conjugate counterparts to impose conjugate symmetry on the spectral representation. At the same time, nulling redundant components (e.g. $X_0 = X_N = 0$) suppresses residual complex-valued time-domain signal, thus ensuring the synthesized waveform remains strictly real-valued. The systematic suppression of non-

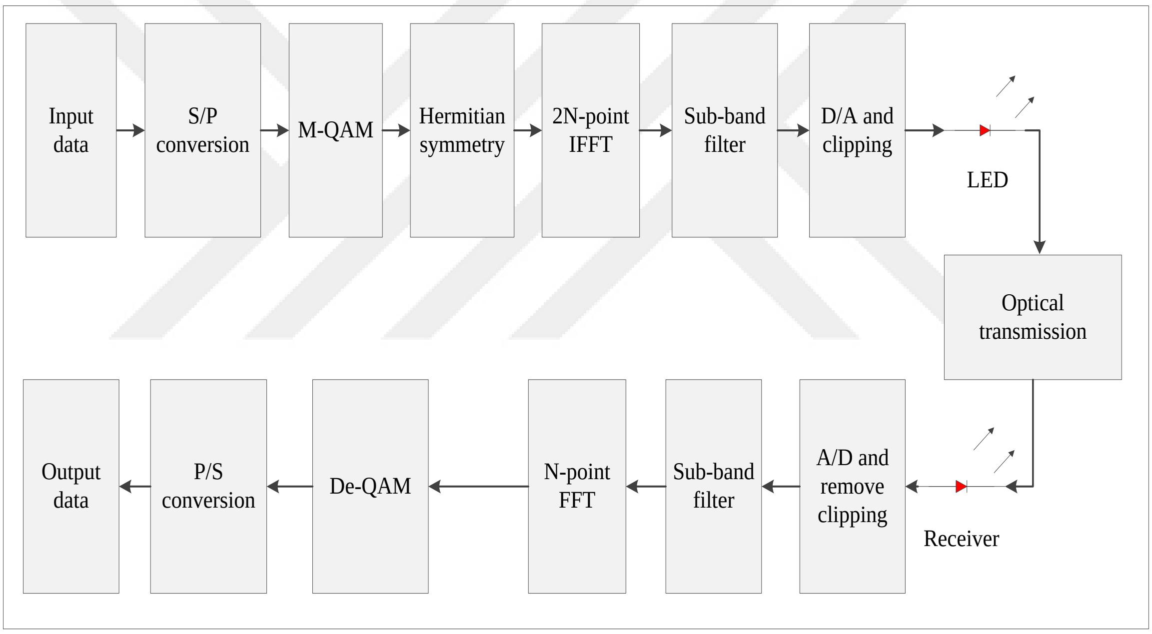

Figure 3.1: Standard F-OFDM Transmitter and Receiver.

symmetric spectral elements ensures compatibility with intensity-modulation systems that necessarily require real and non-negative signals for transmission [101]. The complex signals, represented by X_1 to X_{N-1} after quadrature amplitude modulation (QAM), contribute to creating the final real-amount signal.

The synthesized time-domain signal inherently satisfies the real-valued condition due to the HS limitation, which requires the second half of frequency-domain subcarriers to mirror the complex conjugate of the first half. This symmetrical configuration guarantees a strictly real-amounted output following the IFFT. However, merely fifty percent of the subcarriers transmit independent data, thereby reducing spectral efficiency by 50% relative to standard OFDM. To acquire the discrete time-domain signal $x(n)$, the frequency-domain symbol $X(k)$ is processed via an inverse fast Fourier transform, whose statistical representation is expressed as:

$$x(n) = \frac{1}{N}\sum_{k=0}^{N-1} X_k e^{\frac{2\pi jkn}{N}}, \quad n = 0,1,\ldots,N-1 \tag{3.2}$$

Here N denotes the FFT/IFFT size and X_k represents the moudulation symbols mapped to the k^{th} subcarrier. To satisfy the HS limitation, the IFFT input must be expanded to 2N points, doubling its original size. Consequently, the original formulation in equation (3.2) can be re-arrange as follows [17]:

$$x(n) = \frac{1}{2N}\sum_{k=0}^{2N-1} X_H e^{\frac{j\pi kn}{N}}, \quad n = 0,1,\ldots\ldots,2N-1 \tag{3.3}$$

Enforcing the Hermitian symmetry constraint eliminates the imaginary component of the time-domain signal at the IFFT output, ensuring the signal is strictly real-valued, as illustrated in Figure 3.2. To synthesize the F-OFDM signal, a spectrally constrained sub-band filter for the time-domain waveform is produced by a windowing approach. For IM/DD procedures, a DC bias is applied to compensate for possible clipping distortion due to the signal's non-negativity and strictly real-valued constraints that need to be followed for the transmitted signals [102], [103]. The output, though real, preserves bipolar magnitude information which fails to meet the unipolar needs of an IM/DD approach. A DC offset is then used (move signal to positive domain) and hard-clipped at the DAC stage to force unipolarity.

The F-OFDM receiver design shown in Figure 3.1 operates under the assumptions of Additive White Gaussian Noise (AWGN), idealized equalization, and flat channel resulting in received signal $y(n)$. First, the measured optical signal is translated into an electrical domain using a photodetector. Then, the DC offset is removed after ADC. Followed by the matched subband filter to yield a processed signal, frequency-domain symbols can then be recovered via QAM demodulation with an FFT.

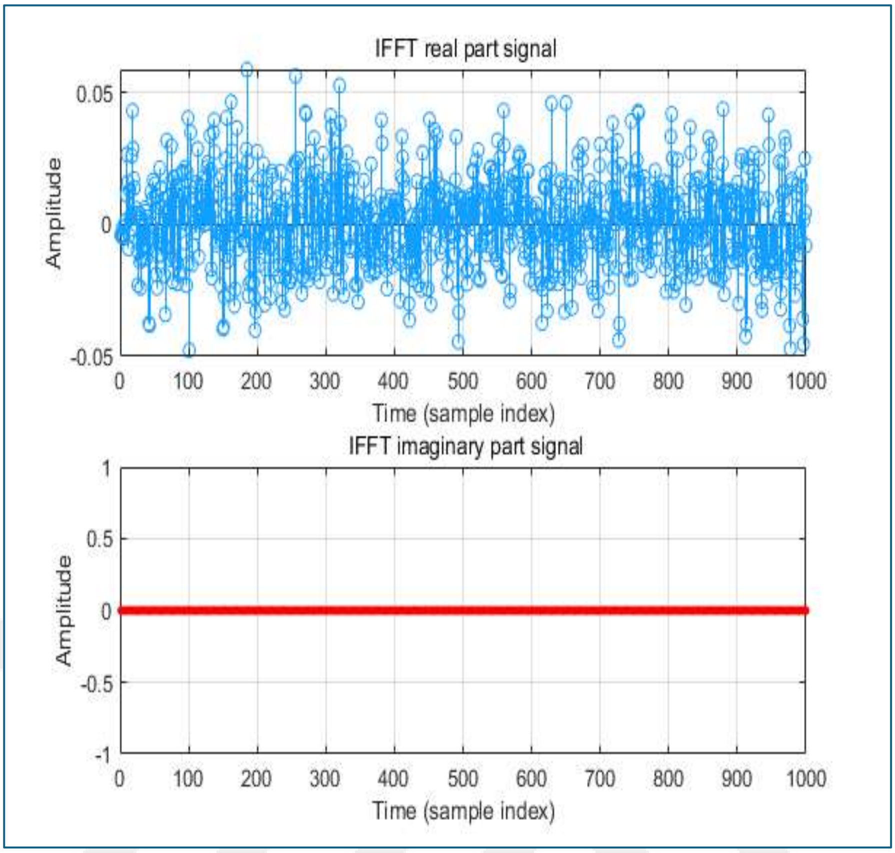

Figure 3.2: The Effect of Hermitian Symmetry on IFFT Output.

3.3 NON-HERMITIAN SYMMETRY FILTERED-OFDM (NHS-F-OFDM)

3.3.1 System Model

To address the limitations of the previously mentioned HS-F-OFDM technique, we propose a new approach that enhances hardware complexity without requiring the frequency-domain symbols to adhere to the Hermitian property constraint. This technique is termed Non-Hermitian Symmetry Filtered-OFDM (NHS-F-OFDM) or Juxtapose Method (JM) F-OFDM. The architectural configurations of the NHS-F-OFDM transmitter and receiver are shown in Figure 3.3.

As illustrated in Figure 3.3, the NHS-F-OFDM architecture removes the necessity for HS limitations by directly processing frequency-domain symbols via the inverse fast Fourier transform. This methodology fabricates a complex- amounted F-OFDM signal at the IFFT output stage. The system employs quadrature amplitude modulation (QAM), a design choice justified by its capacity to suppress noise interference and optimize spectral efficiency, thereby enabling high-speed data transmission [98]. Subsequent to modulation, a specialized signal processing stage transforms the IFFT-generated complex signal into a real-valued output, ensuring compatibility with conventional transmission frameworks.

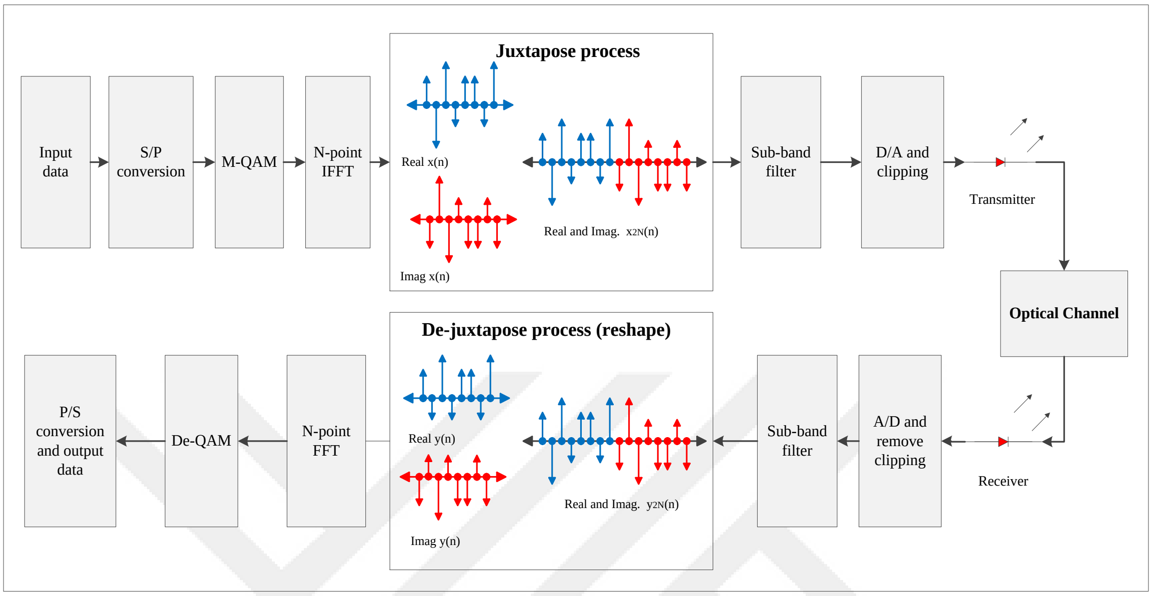

Figure 3.3: The Proposed System of NHS-F-OFDM.

In the NHS-F-OFDM transmitter architecture (Figure 3.3), the input information stream undergoes S/P conversion, partitioning it into *N* parallel streams. These streams are straight entered to an *N*-point IFFT module. Owing to the absence of HS constraints, the IFFT operation gives a non-real-valued time-domain signal, yielding a complex-valued output expressible as [98]:

$$x(n) = \sum_{k=0}^{N-1}[X_R(k) + jX_I(k)]e^{\frac{2\pi jkn}{N}} \tag{3.4}$$

The imaginary and real sections of the complex frequency-domain symbol $X(k)$ are signified by $x_R(k)$, and $x_I(k)$ correspondingly. To eliminate any direct current (DC) change, the DC part of the frequency-domain symbol $x(0)$ is adjusted to zero. Consequently, the time-domain complex signal, $x(n)$, is expressed as follows:

$$x(n) = x_R(n) + jx_I(n) \;\; for\; n = 1, 2, \dots, N-1 \tag{3.5}$$

In which the real and unreal parts of $x(n)$ are symbolized by $x_R(n)$ and $x_I(n)$ correspondingly. To construct a double N-point real F-OFDM signal, $x_{2N}(n)$, the sections of the N-point non-real F-OFDM signal, imaginary and real in the time domain, are combined, resulting in the following juxtaposition:

$$x_{2N}(n) = \begin{cases} x_R(n), & n = 0, 1, \dots, N-1 \\ x_I(n-N), & n = N,\ 2N-1 \end{cases} \tag{3.6}$$

Figure 3.4 demonstrates the two parts of the complex signal, along with the new NHS-F-OFDM signal, which becomes equivalent to a 2N-point IFFT signal.

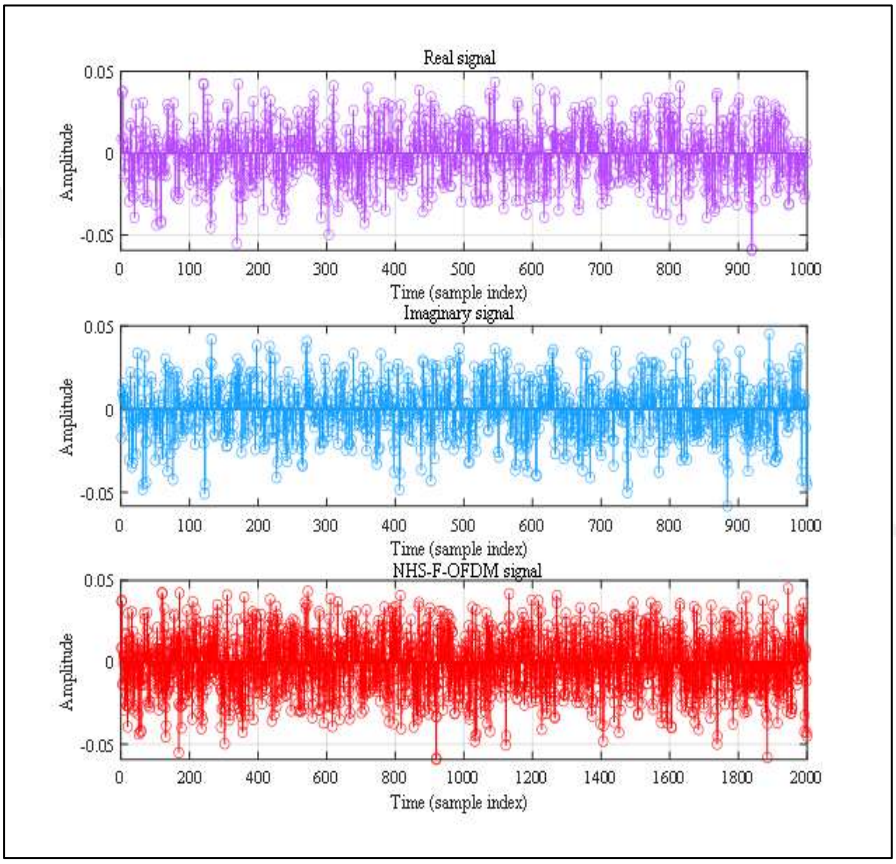

Figure 3.4: Real Part, Imaginary Part, and NHS-F-OFDM Signal.

The F-OFDM signal is filtered through using a subband filter, designed using a window function [87], [105]. The transmitted signal must adhere to strict real-amounted and nonnegative constraints to avoid complex components [106]. However, the subband-filtered output, while real, exhibits bipolarity, violating IM/DD requirements [107]. A digital-to-analog converter operates to operate a DC bias to the signal, permitting the signal to be expressed as unipolar. The minimum bias magnitude must equal the absolute quantity of the signal’s largest negative scale to ensure non-negativity. Owing to the elevated peak-average power ratio inherent in OFDM signals, conventional biasing necessitates disproportionately high DC offsets, increasing optical power demands [87], [105]–[107]. To avoid this, an efficient solution uses an optimized DC bias (K_b), proportionally scaled to P_{elec}, resulting in minimizing bias overhead and minimization of the amount of optical power required, explained in [74], [98]:

$$K_b = k\ P_{elec} \tag{3.7}$$

Here, k stands for the clipping component, and P_{elec} denotes the signal variance $x(n)$. The variance of the time-domain signal states as in the following:

$$P_{elec}{}^2 = E[x^2(n)] \tag{3.8}$$

As derived in [58], the requisite DC bias is quantified as $10\ log_{10}[k^2 + 1]dB$. Accordingly, the DC bias of the signal $x_{DC-F-OFDM}(n)$ is mathematically expressed by:

$$x_{DC-F-OFDM}(n) = x(n) + K_b \tag{3.9}$$

To preserve the non-negativity of the time-domain signal before optical transmission, the negative amplitude peaks of the residual part are clipped to zero. Dropping the negative portion in this clipping operation limits the signal to a positive value so satisfies the constraints of the intensity modulation/direct detection system (See Figure 3.5). This leads to the unipolarity of the DCO-F-OFDM (DC-biased F-OFDM) signal, allowing the signal to be transferred through the optical channel.

On the receiver side, shown in Figure3.3, the optical signal propagates through a flat-fading AWGN channel under idealized equalization conditions, yielding the received signal $y(n)$. Then, A photodetector is applied for optoelectronic transformation, altering the optical signal into an electrical domain representation. Following this, the signal undergoes analogy-to-digital conversion, and the DC bias component is subtracted. The subsequent signal is then processed through a matched subband-filter, matched to the transmitter's spectral shaping. Consequently, the two N-point real signals $y_{2N}(n)$ are transformed into the N-point complex signal, as expressed in the following [98],

$$\begin{cases} y_R(n) = y_{2N}(n) & for \quad n = 0, 1, \dots N - 1 \\ y_I(n) = y_{2N}(N + n) & for \quad n = 0, 1, \dots , N - 1 \end{cases} \tag{3.10}$$

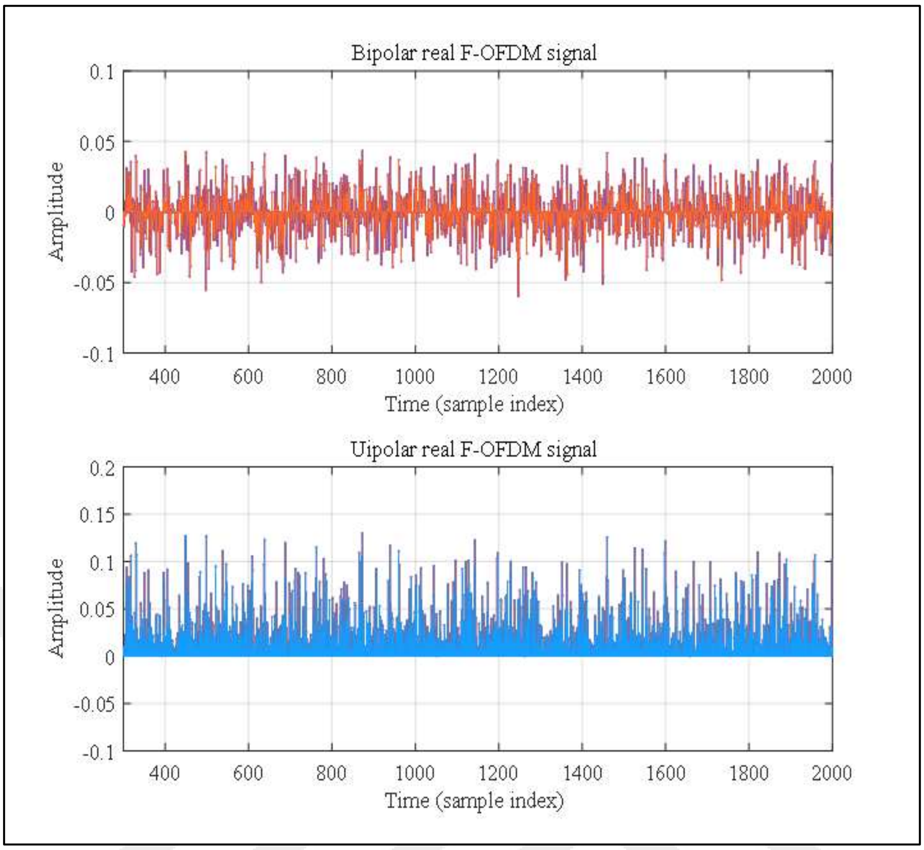

Figure 3.5: Bipolar F-OFDM Signal and Unipolar F-OFDM Signal After Clipping Using 7dB of DC Bias.

Where $y_R(n)$, and $y_I(n)$ represent the real portion and imaginary portion of $y(n)$ correspondingly. Subsequently, the complex-valued signal undergoes demodulation in accordance with the established framework of complex F-OFDM systems. The recovered frequency symbols $Y(k)$ is then expressed as follows:

$$Y(k) = \sum_{n=0}^{N-1} y_n e^{\frac{-2\pi jkn}{N}} \tag{3.11}$$

$$Y(k) = \sum_{n=0}^{N-1} [y_R(k) + jy_I(k)] e^{\frac{-2\pi jkn}{N}} = Y(k) = Y_R(k) + jY_I(k) \tag{3.12}$$

In this context, $y_R(k)$ and $y_I(k)$ signify the real and imaginary portions of the demodulated frequency-domain symbols, correspondingly.

3.4 FILTER DESIGN

Several criteria must be fulfilled during the filter design process for the F-OFDM format to ensure its suitability [87]. One key criterion is to achieve a high degree of flatness in the passband region. This merit ensures minimal distortion of the filter on the sub-carriers. Another important criterion is to design the filter with a sharp transition band. This factor ensures efficient bandwidth utilization, minimizing the need for guard overhead. The sharper the transition band, the more bandwidth can be utilized.

Additionally, the filter must exhibit sufficient attenuation in the stopband. This ensures that the interfering leakage between two sub-bands is insignificant. The filter minimizes the potential interference between adjacent sub-bands by providing adequate attenuation in the stopband, thereby maintaining the signal's integrity [87]. The ideal prototype filter that meets the mentioned criteria is a sinc impulse response $\rho_B(n)$ with a bandwidth of *B*. However, this filter is non-causal and thus not practically realizable. Therefore, the desired filter is obtained by convolving the sinc impulse response $\rho_B(n)$ with a window function $w(n)$, mathematically expressed as follows:

$$f_B(n) \triangleq \rho_B(n).w(n) \tag{3.13}$$

A raised-cosine window ensures soft transitions and prevents frequency-domain spillover in the truncated filter response. The raised-cosine window provides smooth roll-off characteristics and helps reduce spectral leakage. The expression for the raised-cosine window is as follows [22], [26]:

$$\rho_B(n) = sinc\left((W + 2\partial W)\frac{n}{N}\right) for - \frac{L}{2} \leq n \leq \frac{L}{2} \tag{3.14}$$

In which L is the filter dimension, *N* symbolizes the FFT size, the number of subcarriers signifies W, and ∂W indicates the tone offset. Normalizing the filter coefficients ensures that the filter response is properly scaled and aligned with the desired frequency range. The normalization process helps achieve optimal performance and maintain the desired characteristics of the filter as follows:

$$f_B(n) \triangleq \frac{\rho_B(n)\,.\,w(n)}{\sum_n \rho_B(n)\,.\,w(n)} \tag{3.15}$$

Where $w(n)$ mathematically expressed by:

$$w(n) = \left(\frac{1}{2} + \frac{1}{2}\cos\frac{2\pi n}{L-1}\right)^{0.6} \quad , \quad -\frac{L}{2} \leq n \leq \frac{L}{2} \tag{3.16}$$

The filter design parameters are given in Table 1. Minimizing out-of-band emissions is crucial in the filter design process [107]. As a result, the guard interval separating sub-bands can be reduced to a minimum, enabling more efficient spectrum utilization compared to DCO-OFDM. As a result, the transmission signal of each sub-band, denoted as $x_{sub}(n)$, can be signified by the following expression [11], [108]:

$$x_{sub}(n) = x(n).w(n) \tag{3.17}$$

Figure 3.6 compares the spectra of F-OFDM and OFDM signals. The OOBE power for F-OFDM is 178 dB, compared to 63 dB for OFDM. This indicates that F-OFDM achieves an out-of-band emission power gain of 115 dB over OFDM. Consequently, the F-OFDM system demonstrates superior spectral localization.

Table 3.1: Filter Parameters of the Proposed System.

Parameter	**Values**
Filter type	Raised cosine
Subcarrier spacing	15 kHz
Filter order	513
Tone-off set	2.5
Roll-off	3/5

On the other hand, the smooth roll-off characteristic intrinsic to the raised-cosine filter contributes to enhanced spectral efficiency. Adjusting the window transition enables a systematic trade-off between temporal and frequency-domain localization. Figure 3.7 demonstrates the impact of roll-off on out-of-band emissions, showing that increasing the roll-off improves out-of-band emissions and, as a result, enhances spectral localization.

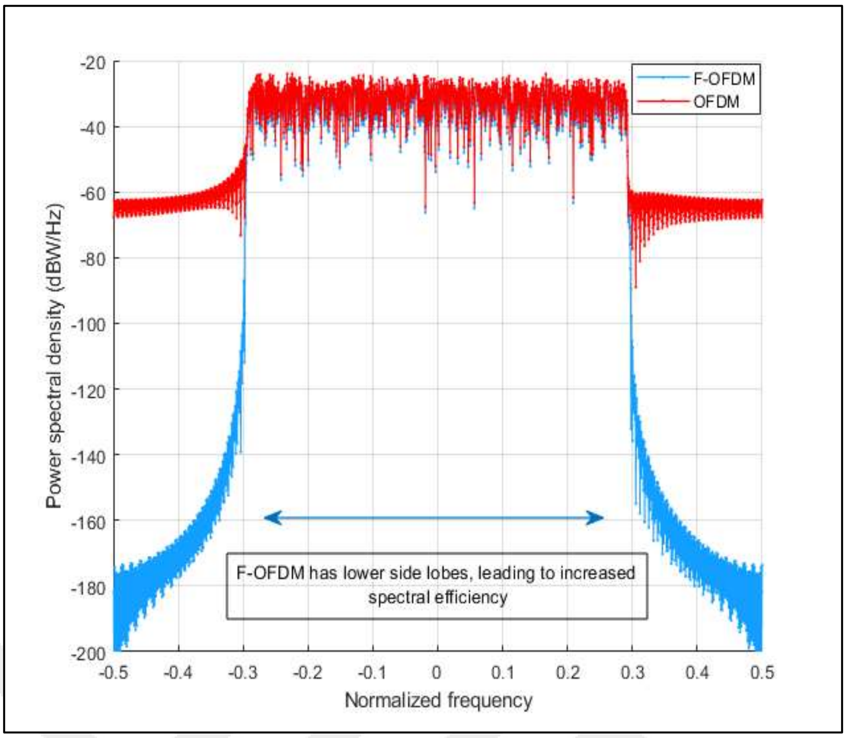

Figure 3.6: Power Spectral Density of Truncated Frequency between F-OFDM and OFDM Signals.

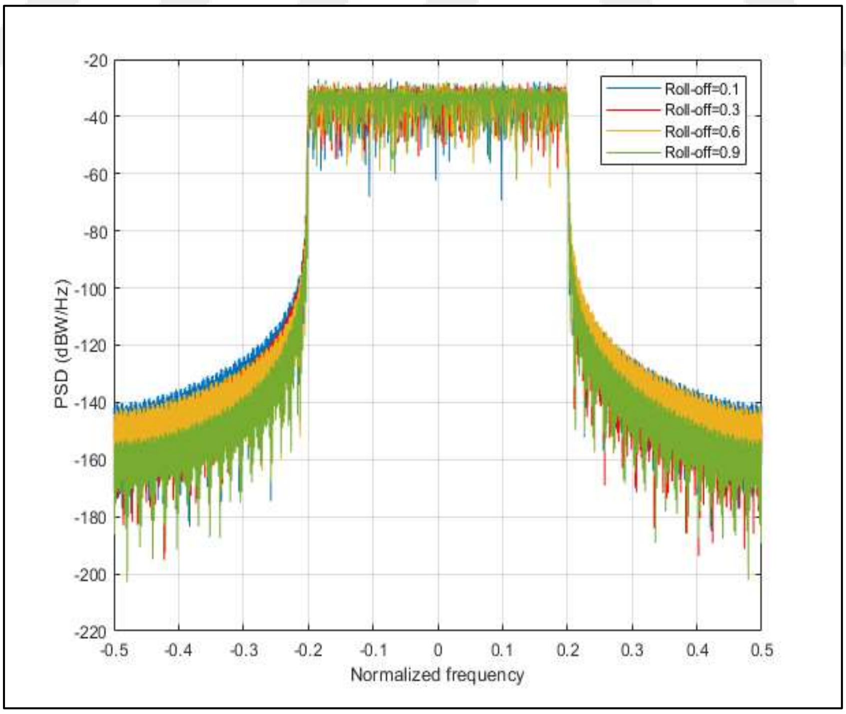

Figure 3.7: Comparison of Power Spectral Density of F-OFDM Based on Different Roll-Off Properties.

3.5 SIMULATION RESULTS AND DISCUSSION

This partition evaluates, examines, and compares the proposed system with the traditional F-OFDM approach. The evaluation focuses on computational complexity, SNR, BER performance, and PAPR. The analysis is conducted using simulation verification and mathematical modeling.

3.5.1 Computational Complexity

A comparative analysis of computational complication was conducted between the proposed Non-Hermitian Symmetric Filtered OFDM (NHS-F-OFDM) framework and established F-OFDM systems. This evaluation quantified operational demands by enumerating the requisite complex multiplications and additions inherent to their respective implementations. This gives a comparative idea of the computations required by each system. NHS-F-OFDM is mainly aimed at reducing complexity solutions at both ends of the transmitter and receiver architectures. The composition of the approach is done in such a way that, by the use of IFFT blocks of size N points enabled by real F-OFDM signal synthesis, can transmit or demodulate 2N-point real F-OFDM signals. This methodology drastically lowers computational overhead, while maintaining the functional performance of the system.

The NHS-F-OFDM framework demonstrates a 50% reduction in computational resource utilization relative to conventional F-OFDM architectures. Leveraging the computational efficiency inherent in the radix-2 FFT algorithm [109], [110], the total arithmetic operations required to generate an N-point real-valued F-OFDM signal under Hermitian symmetry constraints can be systematically derived. This includes quantifying both complex-valued additions and multiplications essential for the signal's computational realization as follows:

$$O_{FFT\ Add} = 3Nlog_2(N) - 3N + 4 \tag{3.18}$$

$$O_{FFT\ Multip.} = Nlog_2(N) - 3N + 4 + N(L-1) \tag{3.19}$$

Where N signifies FFT length, while L corresponds to the filter range. Otherwise, the arithmetic operations (additions and multiplications) directly relate to increases in computation complexity associated with the FFT/IFFT operations in an NHS-F-OFDM receiver, specifically when an N/2-point inverse FFT is being used. This is analytically expressed as follows [62], [110]:

$$O_{FFT\ Add} = 3\frac{N}{2}log_2\left(\frac{N}{2}\right) - 3\frac{N}{2} + 4 \tag{3.20}$$

$$O_{FFT\ Multip.} = \frac{N}{2}log_2\left(\frac{N}{2}\right) - 3\frac{N}{2} + 4 + \frac{N}{2}(L-1) \tag{3.21}$$

Comparative examination of the number of required arithmetic functions for the suggested NHS-F-OFDM framework and standard F-OFDM, for synthesizing real-valued F-OFDM signals, is shown in Figures 3.8 and 3.9. This comparison, grounded in a rigorous mathematical framework, positions NHS-F-OFDM as an efficient operational method for reducing arithmetic operations whilst preserving signal fidelity.

Hence, in order to decline the calculational load at the transmitter segment, the NHS–F–OFDM is presented by performing a fast IFFT operation which can be described by equations (3.21) and (3.22). Conversely, conventional F-OFDM systems lack any such optimizations and are therefore still heavily restricted by their inherent limitations. Specifically, the transmitter of the traditional F-OFDM has an extremely high computational complexity, in that, the full-length IFFT of all subcarriers needs to be performed, and this increases with the required number of subcarriers for signal generation. This inefficiency underscores the practical superiority of the NHS-F-OFDM approach, which strategically minimizes processing overhead without compromising waveform integrity.

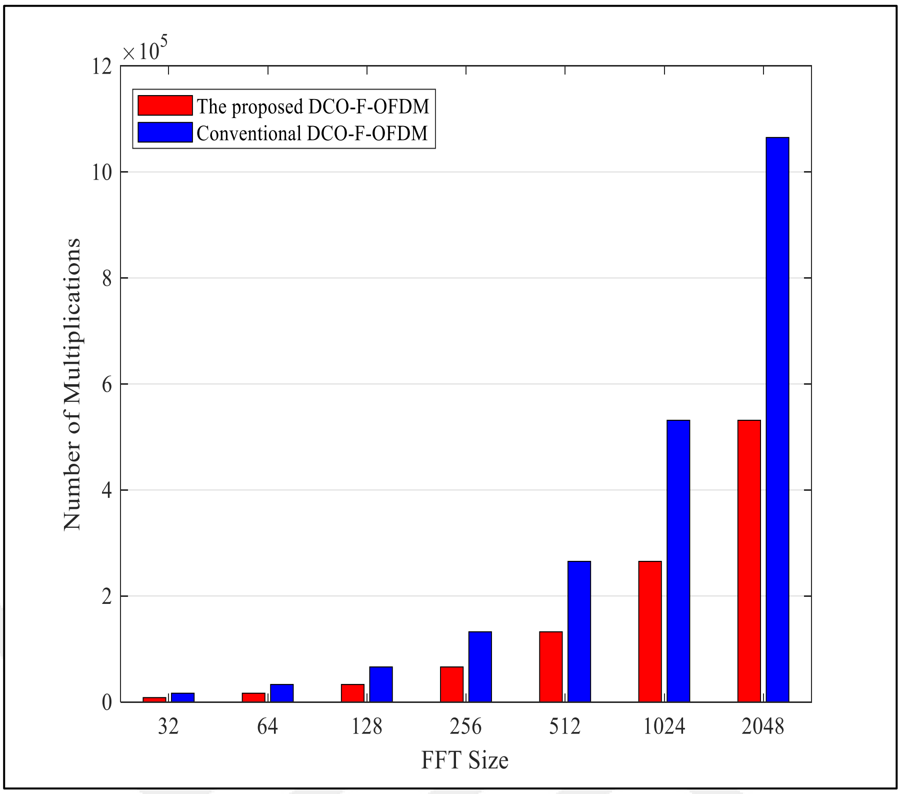

Figure 3.8: F-OFDM Multiplications Complexity.

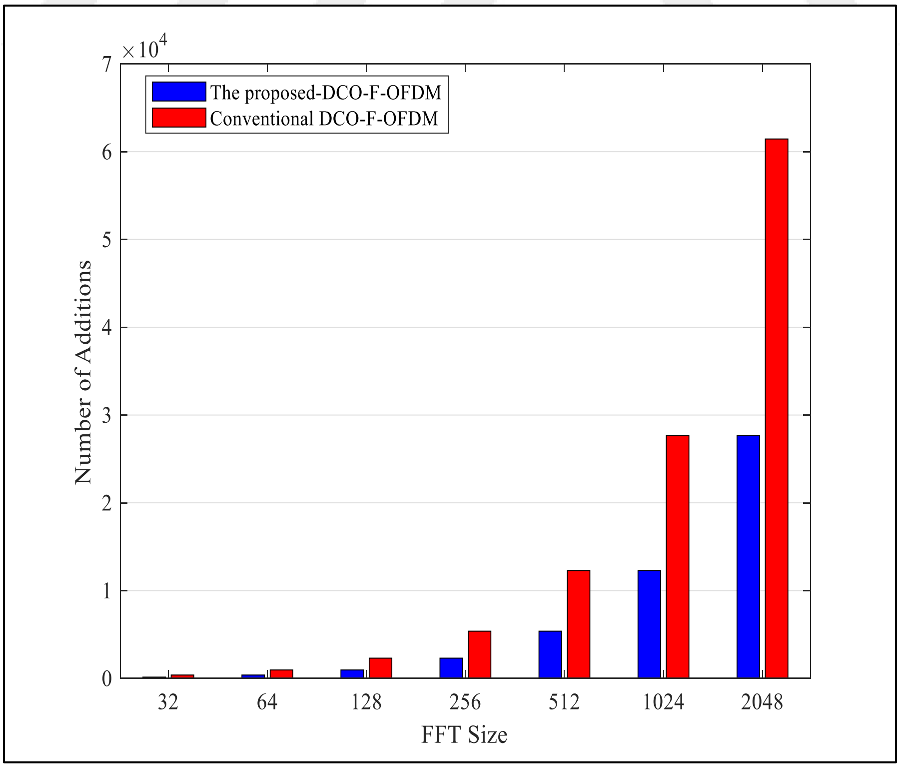

Figure 3.9: F-OFDM Addition Complexity.

3.5.2 Signal-to-Noise Ratio (SNR)

The signal-to-noise ratio quantifies the power ratio between an intended transmission and unwanted noise disturbances; in communication frameworks, it serves as a deterministic parameter governing signal reliability and discriminability. In the optical wireless communication architecture shown in Figure 3.10, the main noise contributions are due to the fluctuations of photons and thermal effects in the receiver circuitry [111]. Photon noise originates from the stochastic temporal distribution of discrete photon detection events, predominantly influenced by extrinsic ambient optical radiation.

Although devices using optical filtering methods are capable of suppressing such unwanted background radiation, residual shot noise will remain in the response of even the best-designed photodetectors, originating from the standard quantum limitations of photon detection processes [112]. This phenomenon illustrates the difficulty of obtaining noise-free signal recovery in real-world optical systems, given the fundamental limitations on SNR behavior from thermal and quantum-mechanical noise mechanisms.

The dominance of background illumination over the transmitted optical signal power results in a negligible contribution of the conveyed optical signal to the aggregate shot noise variance. As a result, shot noise is traditionally treated as a signal-independent stochastic process and is usually guessed as an AWGN source in most analytical scenarios. In this case, the noise generation is dominated by the stochastic arrival of photons, with its statistical properties being largely independent of the signal.

Likewise, in cases where background light is absent, thermal noise due to physical processes in the receiver preamplifier becomes the main source of noise. This thermal contribution, driven by charge carrier fluctuations within electronic circuitry, is also statistically decoupled from the shape of the signal waveform and can be rigorously treated as a Gaussian stochastic process. These assumptions underpin system-level noise analyses, where signal-independent Gaussian noise models simplify theoretical derivations while retaining fidelity to empirical observations. Under both operational scenarios, the noise characteristics are appropriately modeled as Gaussian-distributed and statistically decoupled from the signal waveform [111], [112].

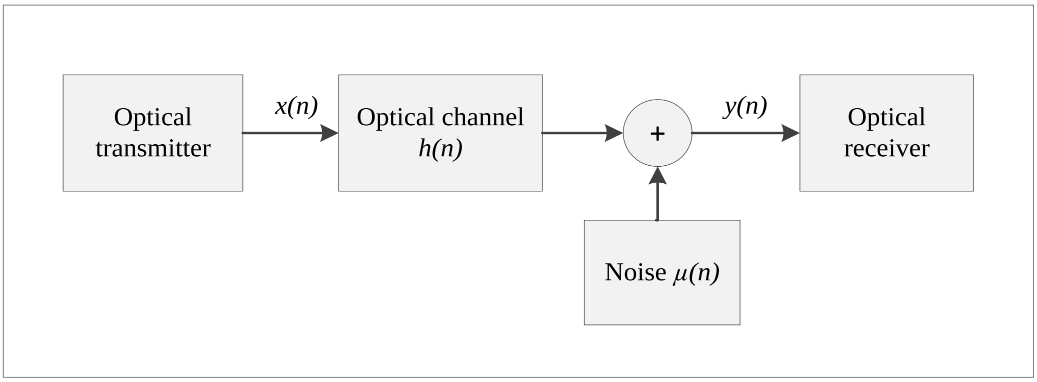

Figure 3.10: Optical Channel Model.

In this investigation, the transmitted signal propagates through an optical transmission medium characterized by a discrete-time impulse response $h(n)$. The system is formulated under an AWGN framework, wherein the detected received signal $y(n)$ is defined by the discrete-time convolution:

$$y(n) = x(n) \ast h(n) + \mu(n) \tag{3.22}$$

Where $\ast$ is the convolving process, $x(n)$ means the signal transmitted, and $\mu(n)$ represents the additive noise process characterized by a zero mean and variance σ_μ^2 [98]. The frequency-domain demonstration of the received symbol, $Y(k)$, arises from the linear convolution process in the time domain, which corresponds to the multiplicative interaction of the channel's frequency response $H(k)$ with the transmitted frequency-domain symbols $X(k)$, combined with the additive Gaussian-distributed noise $\mathrm{M}(k)$. This is mathematically defined as:

$$Y(k) = H(k)X(k) + \mathrm{M}(k) \tag{3.23}$$

Based on (3.24), the SNR at the recipient part is given by:

$$SNR = \frac{P_s}{P_\mu} = \frac{E\{|X(k)|^2\}}{E\{|\mathrm{M}(k)|^2\}} \tag{3.24}$$

Let P_s, and P_μ denote the time-domain signal power and noise power, respectively. By invoking Parseval's theorem, which establishes the equivalence of energy (and thus average power) between time- and frequency-domain representations, the SNR in the time domain is expressed as:

$$SNR = \frac{E\{|x(n)|^2\}}{E\{|\mathrm{M}(n)|^2\}} \tag{3.25}$$

In conventional F-OFDM, the frequency-domain symbols are precisely recaptured from the clipped time-domain signal, circumventing receiver-side signal processing such as equalization [98]. So, let's consider σ_x^2 is the total average power of the transmitted signal, and $H(k) = 1$ for simplicity, then the SNR of F-OFDM is given by:

$$SNR_{F-OFDM} = \frac{\sigma_x^2}{\sigma_\mu^2} \tag{3.26}$$

Now, for the proposed NHS-F-OFDM, the received juxtaposed real and imaginary signals produced by converting the complex time signal is expressed based on (3.11) as:

$$y_R(n) = y_R(n) + \mu_R(n) \tag{3.27}$$

$$y_I(n) = y_I(n) + \mu_I(n) \tag{3.28}$$

Where the channel noise is categorized by $\mu_R(n)$, and $\mu_I(n)$ respectively. Then, the transmitted signal power, $\sigma_{x,NHS}^2$, is given by:

$$\sigma_{x,NHS}^2 = \frac{1}{2N}\{\sum_{n=0}^{N-1}|x_R(n)|^2 \ + \ \sum_{n=N}^{2N-1}|x_I(n)|^2\} \tag{3.29}$$

Following a comparable method, the receiver power noise, $\sigma_{\mu,NHS}^2$, is expressed as:

$$\sigma_{\mu,NHS}^2 = \frac{1}{2N}\{\sum_{n=0}^{N-1}|\mu_R(n)|^2 \ + \ \sum_{n=N}^{2N-1}|\mu_I(n)|^2\} \tag{3.30}$$

Therefore, at the receiver, the N-point complex signal power is given by:

$$P_{x,NHS} = \frac{1}{N}\{\sum_{n=0}^{N-1}|x_R(n)|^2 + \sum_{n=0}^{N-1}|x_I(n)|^2\} = 2\sigma_{x,NHS}^2 \tag{3.31}$$

Correspondingly, the complex power noise is expressed as follows:

$$P_{\mu,NHS} = \frac{1}{N}\{\sum_{n=0}^{N-1}|\mu_R(n)|^2 + \sum_{n=0}^{N-1}|\mu_I(n)|^2\} = 2\sigma_{\mu,NHS}^2 \tag{3.32}$$

When recovering the complex transmitted signal by combining the two signal components, real and imaginary, both signal and noise power are doubled. This is because the two portions of the signal are merged to reconstruct the complex signal, increasing the needed and the noise power. Consequently, the SNR of NHS-F-OFDM mathmattically expressed as:

$$SNR_{NHS-F-OFDM} = \frac{\sigma_{x,NHS}^2}{\sigma_{\mu,NHS}^2} = \frac{2\sigma_x^2}{2\sigma_\mu^2} = SNR_{F-OFDM} \tag{3.33}$$

3.5.3 Bit-Error-Rate Performance (BER)

This subsection conducts a comparative analysis of the bit error rate metric performance between NHS-F-OFDM and legacy F-OFDM systems over an AWGN channel. The simulation framework employs a DC-bias index of 7 dB to align with practical intensity-modulation constraints and utilizes MATLAB® R2023a for computational modeling. A 1024-point FFT is implemented to emulate the orthogonal subcarrier modulation and demodulation processes. BER values are evaluated for quadrature amplitude modulation schemes of orders 4, 16, 64, and 256, spanning a range of SNR conditions. The theoretical BER for each QAM constellation in AWGN is derived from the well-established analytical expression:

$$P_{b.e} = \left(\frac{2}{log_2 M} - \frac{2}{log_2 M\sqrt{M}}\right) error\ fc\left(\sqrt{\frac{3}{2}.\frac{SNR}{M-1}}\right) \tag{3.34}$$

M signifies the QAM order, and *error fc* (.) is the complementary error function. Due to the error probability delivered by (3.35) depending only on SNR [98], NHS-F-OFDM and established F-OFDM show the similar error rate performance as validated theoretically in the previous section 3.5.2. Figure 3.11 compares the BER functioning of NHS-F-OFDM and conventional F-OFDM. Based on the model results, both NHS-F-OFDM and traditional F-OFDM exhibit comparable performance of BER, which aligns with the mathematical assumptions.

3.5.4 Peak-to-Average-Power Ratio (PAPR)

OFDM procedures have some important pros, such as immunity to ISI which stems from the orthogonal nature of their constituent subcarriers. However, their practical implementation is constrained by their elevated PAPR. The raised PAPR indicates to serious signal falsification in systems implementing nonlinear elements, as these devices are driven by high-power signal peaks to regions outside their linear dynamic range. These nonlinear distortions originate mainly from: Nonlinearities in power amplifiers (PAs) and data conversion (D/A and A/D), causing high-amplitude OFDM symbols to compress or clip.

Moreover, under large PAPR scenarios [113], [114], intensity-modulated responses with a curve, can be observed for Light-emitting diodes, optical fibers, and photodiodes. The OFDM signal PAPR, $x(n)$, is extracted as,

$$PAPR = \frac{max\{|x(n)|)^2\}}{E\{|x(n)|)^2\}} \tag{3.35}$$

In OFDM procedures, the scale of the OFDM signal varies randomly. In practical scenarios, when N is large ($N \geq 64$), the scale of the complicated OFDM signal can be approximated as a Gaussian arbitrary process with a mean of zero and a variance σ^2, corresponding to the total power of the complicated time-domain signal.

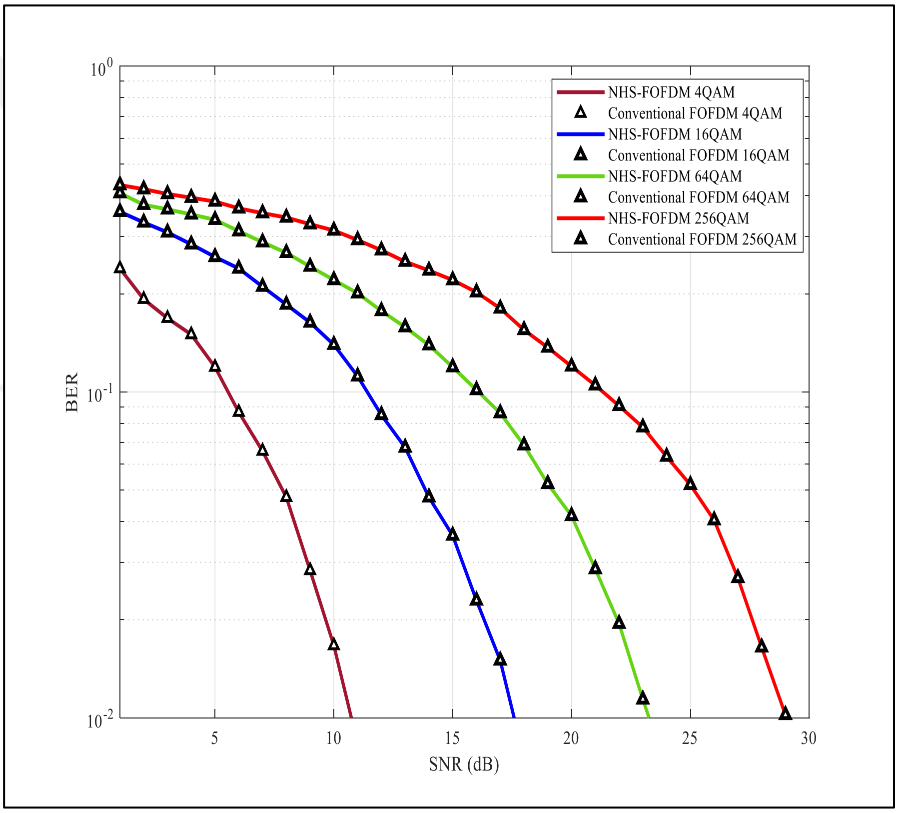

Figure 3.11: Comparison of BER Performance between NHS-F-OFDM and Traditional F-OFDM for 4, 16, 64, and 256 QAM Orders.

The complex OFDM signal, $x(n)$, probability density function (PDF) is described as follows:

$$p(x) = \frac{1}{\sqrt{2\pi}\,.\sigma}\, e^{\frac{-x^2}{2\sigma^2}} \tag{3.36}$$

The magnitudes of the two components of $x(n)$, (real and imaginary), can be approached as Gaussian distributions, each with a mean of zero and a variance of $\sigma^2/2$. As a result, the variance of the $2N$-point real signal, denoted as σ_{2N}^2, is expressed as follows:

$$\sigma_{2N}^2 = E\{|x_{2N}(n)|)^2\} = \frac{1}{2N}\sum_{n=0}^{2N-1}|x_{2N}(n)|^2$$

$$= \frac{1}{2}\left\{\frac{1}{N}\sum_{n=0}^{N-1}|x_R(n)|^2 + \frac{1}{N}\sum_{n=N}^{2N-1}|x_I(n-N)|^2\right\} \tag{3.37}$$

where $E\{.\}$ is the expectation operator. For simplicity, let's assume $n' = n - N$, Substituting in (3.38) will get,

$$\sigma_{2N}^2 = \frac{1}{2}\left\{\frac{1}{N}\sum_{n=0}^{N-1}|x_R(n)|^2 + \frac{1}{N}\sum_{n'=0}^{N-1}|x_I(n')|^2\right\} = \frac{1}{2}\left\{\frac{\sigma^2}{2} + \frac{\sigma^2}{2}\right\} = \frac{\sigma^2}{2} \tag{3.38}$$

Alternatively, the maximum power of $x(n)$ can determine using the following representation:

$$max\{|x(n)|)^2\} = max\{x_R(n)^2 + x_I(n)^2\} \tag{3.39}$$

To clarify the analysis, let us suppose,

$$max\{x_R(n)^2\} = max\{x_I(n)^2\} = K^2 \tag{3.40}$$

Then we get,

$$max\{|x(n)|)^2\} = 2K^2 \tag{3.41}$$

So, the maximum power of $x_{2N}(n)$ can be expressed as,

$$max\{x_{2N}(n)^2\} = max\{max\{x_R(n)^2\}, max\{x_I(n)^2\}\} = K^2 = \frac{max\{|x(n)|)^2\}}{2} \tag{3.42}$$

Conversely, the peak powers oscillate around a specific average value. The N-point complex signal PAPR, $x(n)$, is provided by,

$$PAPR_{x(n)} = \frac{max\{|x(n)|)^2\}}{E\{|x(n)|)^2\}} = \frac{2K^2}{\sigma^2} \tag{3.43}$$

Therefore, the PAPR of the 2N-point noncomplex signal mathmatically expressed as,

$$PAPR_{x_{2N}(n)} = \frac{max\{|x_{2N}(n)|)^2\}}{E\{|x_{2N}(n)|)^2\}} = \frac{K^2}{\sigma^2/_2} = \frac{2K^2}{\sigma^2} = PAPR_{x(n)} \quad (3.44)$$

The key analysis demonstrates that the average and peak powers of transmitted F-OFDM signals can be decreased by half by employing the NHS-F-OFDM technique compared to traditional F-OFDM implementations. In the sense that this reduction keeps PAPR unchanged, our approach avoids the classical trade-off between power consumption and increased PAPR. Thus, NHS-F-OFDM can provide unipolar F-OFDM waveforms in a way to keeps the original PAPR performance as same as that of the conventional unipolar F-OFDM system.

It is critical to emphasize that the analytical framework underpinning these findings, as detailed in [115], is rigorously derived and tailored to DC-biased Optical OFDM (DCO-OFDM) signaling. However, F-OFDM adopts a methodology analogous to conventional OFDM but incurs an elevated PAPR. This degradation arises from the spectral shaping filter integrated into the transmitter, which induces a broader temporal redistribution of signal energy across samples compared to the inherent rectangular windowing of unfiltered OFDM systems.

F-OFDM namely produces a stochastic variation of the amplitude, which may result in arbitrary high-power spikes in the transmitted signal. The Complementary Cumulative Distribution Function (CCDF) is a canonical metric to statistically quantify PAPR in these procedures. The CCDF is the formal definition indicating the probability (Pr) of the instantaneous PAPR of the signal surpassing a defined limit $PAPR_0$, thus expressed mathematically as:

$$CCDF = P_r\ (PAPR > PAPR_0) \quad (3.45)$$

This probabilistic metric is essential for assessing the robustness of the F-OFDM against nonlinear distortions introduced by practical hardware, such as power amplifier saturation or clipping effects. The CCDF helps system designers forecast the probability of observing the worst-case power excursions, enabling them to minimize the dynamic range specifications of both transmitters and receivers.

Figure 3.12 compares the CCDF curves of F-OFDM signals generated via the NHS-F-OFDM technique and conventional F-OFDM. The analysis used a 16-QAM constellation for signals of lengths N = 512 and N = 1024. In the figure, it can also be seen that the CCDF curves of both methods are statistically indistinguishable as they completely overlap for all the signal lengths that are tested. The simulation result illustrates that the PAPR of the F-OFDM signal is independent of the modulation scheme used. With PAPR being only related to the signal length parameter N, this underscores the robustness of PAPR as a signal-length-dependent metric in F-OFDM architectures, irrespective of advanced modulation techniques.

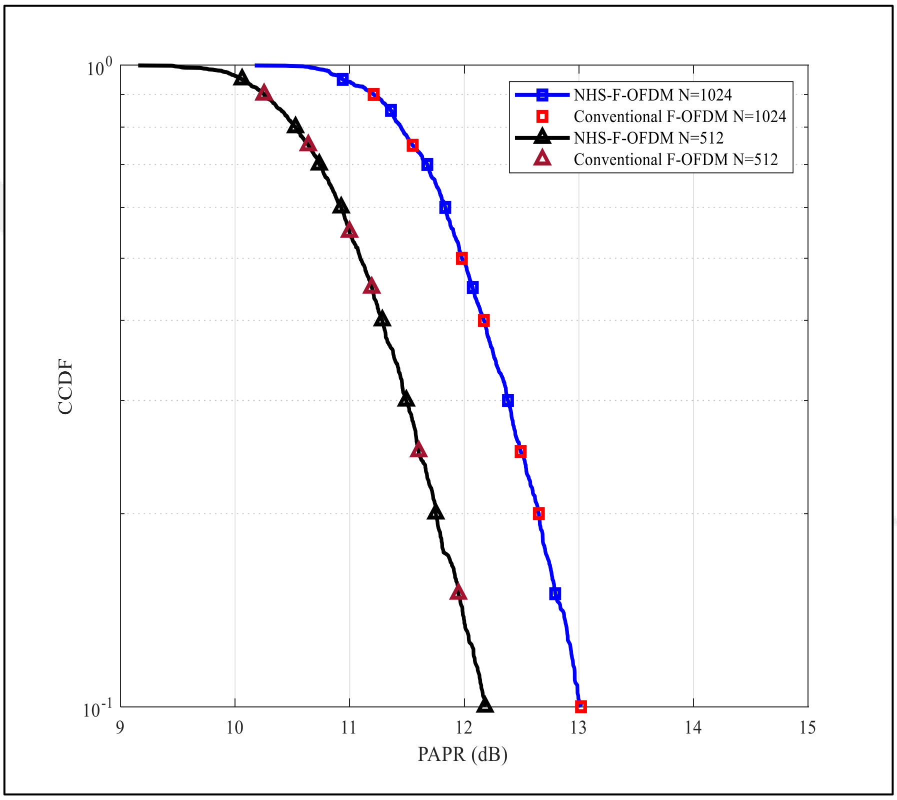

Figure 3.12: The CCDF Curves of the Proposed and Traditional F-OFDM Using Signal Length N=512, and N=1024.

3.6 SUMMARY

In this chapter, a new procedure was introduced to supply real-amounted signals suitable for feeding into intensity modulation/direct detection systems in DCO-F-OFDM architectures. Departing from conventional approaches that enforce Hermitian symmetry (HS) to ensure signal reality, the proposed HS-free framework achieves IM/DD compatibility while eliminating the structural constraints of HS. The proposed method utilizes an N/2-point IFFT to synthesize an N-point fast Fourier transform (FFT) output, thereby reducing the computational burden by around 50%, and improving operational efficiency greatly. This computational simplification consequently means lower power usage and a smaller silicon footprint making the method suitable for hardware implementation for extremely constrained devices. It is found that the proposed scheme achieves BER robustness and retains SNR success at similar levels compared to traditional HS-based F-OFDM, thus verifying no performance loss was incurred with reduced complexity. Furthermore, results from the simulation confirm that Non-Hermitian Symmetry-based F-OFDM (NHS-F-OFDM) exhibits PAPR performance that is equivalent to conventional unipolar F-OFDM, yielding no statistical increase in peak power excursions.

The NHS-F-OFDM method enables the creation of spectrally efficient, unipolar waveforms essential for VLC systems, while circumventing the traditional trade-offs between computational complexity, power efficiency, and PAPR resilience. This innovation positions NHS-F-OFDM as a scalable solution for next-generation IM/DD-based networks, particularly in applications demanding low-latency, high-throughput, and energy-efficient signal processing.

4. EXPERIMENTAL OF NON-HERMITIAN FLIP-FILTERED-OFDM TO REDUCE COMPLEXITY AND BOOST SYSTEM PERFORMANCE

4.1 INTRODUCTION

Flip-OFDM is a unipolar procedure that solves the issue of negative signal values arising during the modulation phase by inverting the polarity of any sample with a negative value, which achieves much of the spectral efficacy restriction in ACO-OFDM systems [116]–[118]. This procedure decomposes a real dipolar OFDM signal to its nonpositive and nonnegative components while maintaining the Hermitian symmetry condition, which is a fundamental constraint to get real-valued signal transmission. The negative parts are phase-inverted to enable unipolar transmission, then both segments are sequentially transmitted as two consecutive OFDM frames with their original positive parts. With a nonnegative transmitted signal, Flip-OFDM is a unipolar modulation schematic and thus can be used conveniently in communication techniques that facilitate unipolar signaling, such as optical wireless applications [117], [119].

Conversely, the spectral efficacy of ACO-OFDM procedures is diminished because only fifty percent (50%) of subcarriers are actively benefited, in contrast to DCO-OFDM. To mitigate this limitation, ADO-OFDM proposed an effective hybrid framework, which integrates the benefits of DCO-OFDM and ACO-OFDM [120]. However, one major challenge faced by many OFDM-based approaches is the unwanted OOBE causing interference in neighbouring frequency spectra. Modified configurations of Flip-OFDM that aim to use Hermitian symmetry have been suggested in recent works for increasing spectral efficiency. However, as previously noted, the fundamental limitations of HS only allow information to be transmitted across half of the subcarriers. Not only does this create a bottleneck and spoil the bandwidth utilization but it also doubles the size of the IFFT block at the transmitter leading to computational overhead.

An alternative method to ACO-OFDM, Flip-OFDM which offers analogous functioning but with different hardware complexity, was introduced in [63]. In this study, the functioning of Flip-OFDM was contrasted to ACO-OFDM, revealing that Flip-OFDM reduces receiver equipment complexity by 50% while maintaining comparable performance. Additionally, researchers in [121] identified Flip-OFDM configurations as time-compressed variations of conventional Flip-OFDM. Their findings demonstrated that the time-compression notably improves both bandwidth efficacy and DC electrical power. Furthermore, the authors in [122] introduced a Flip-OFDM approach incorporating channel coding to enhance the signal-to-noise ratio. The study in [123] demonstrated improved system performance by employing an iterative receiver within the Flip-OFDM framework. Conversely, [124] explored Flip-WPM (flip-wavelet packet modulation) as an alternate to Flip-OFDM for generating unipolar signals. Their findings indicated Flip-WPM offered reduced computational complexity while maintaining comparable power efficiency.

Recent advancements in [125]–[128] have advanced the paradigm of filtered OFDM (F-OFDM), a framework that segments the OFDM waveform into multiple subbands, each tailored with distinct parameterizations, and implements adaptive filtering to optimize spectral containment [129]. Relative to conventional OFDM, F-OFDM offers superior out-of-band (OOB) emission suppression, enhanced compatibility with asynchronous multi-user environments, lower peak--average power ratio, heightened spectral utilization efficacy, and a streamlined system architecture [125]. To further mitigate computational complexity in non-Hermitian symmetric F-OFDM (NHS-F-OFDM) and improve the energy efficiency of non-bipolar F-OFDM approaches, this work proposes a novel methodology that synthesizes a low-complexity NHS-F-OFDM architecture with Flip-F-OFDM principles, enabling the production of real-valued F-OFDM signals with optimized performance metrics.

This chapter examines the execution of the proposed Flip-F-OFDM approach and measures its performance in comparison to conventional frameworks to quantify improvements in system efficiency. The chapter starts with the implementation and validation of a baseline Hermitian Symmetry (HS)-based Flip-F-OFDM system — by nature an output real-valued signal; Then, the novel Flip-F-OFDM architecture is presented, discussing in detail its operational principles, algorithmic workflow, and design innovations. Accordingly, a comparative study of both methods is performed addressing the notable performance metrics including computational complexity, SNR, BER, and PAPR.

4.2 FLIP-FILTERED-ORTHOGONAL FREQUENCY DIVISION MULTIPLEXING (FLIP-F-OFDM) BASED ON HERMITIAN PROPERTY

4.2.1 System Model

A typical Flip-F-OFDM transmitter architecture, as illustrated in Figure 4.1, operates by digitally mapping an input data stream onto frequency-domain symbol vectors. This transformation necessitates the imposition of Hermitian symmetry constraints on the frequency-domain symbols input to the IFFT block, ensuring the resultant time-domain baseband waveform retains real-valued properties. Specifically, adherence to Hermitian symmetry in the subcarrier allocation serves as a prerequisite for generating real-valued F-OFDM signals, eliminating quadrature components that would otherwise necessitate complex-domain signal processing. This limitation, as we mathematically formalize in previous references [128] and [129], creates a mirroring pattern that couples symmetric subcarriers, ensuring the time-domain signal is real-valued following its IFFT treatment as shown mathematically:

$$X_H = (X_0, X_1, X_2, \dots X_{N-1}, X_{N-1}^*, X_2^*, X_1^*) \quad (4.1)$$

The real-valued time-domain signal, denoted as X_H, is synthesized from complex frequency-domain symbols through the imposition of HS. This symmetry constraint enforces a conjugate mirroring operation, appending X^* to the original frequency-domain sequence. Additionally, nullifying the DC ($X_0 = X_N = 0$) subcarriers ensures the elimination of residual complex artifacts in the resultant time-domain signal, preserving strict real-valued orthogonality [98].

The complex QAM symbols (X_1 to $X_{(N-1)}$) provide the basis for the real-valued signal synthesis. The first half of the subcarriers receive one set of values, and the latter half receives their complex conjugate so as to comply with the HS constraint. This conjugate mirroring certifies the IFFT output is strictly real-valued. There is, however, an intrinsic limitation in this structural symmetry: half of the subcarriers would carry no information, which results in spectral waste [130].

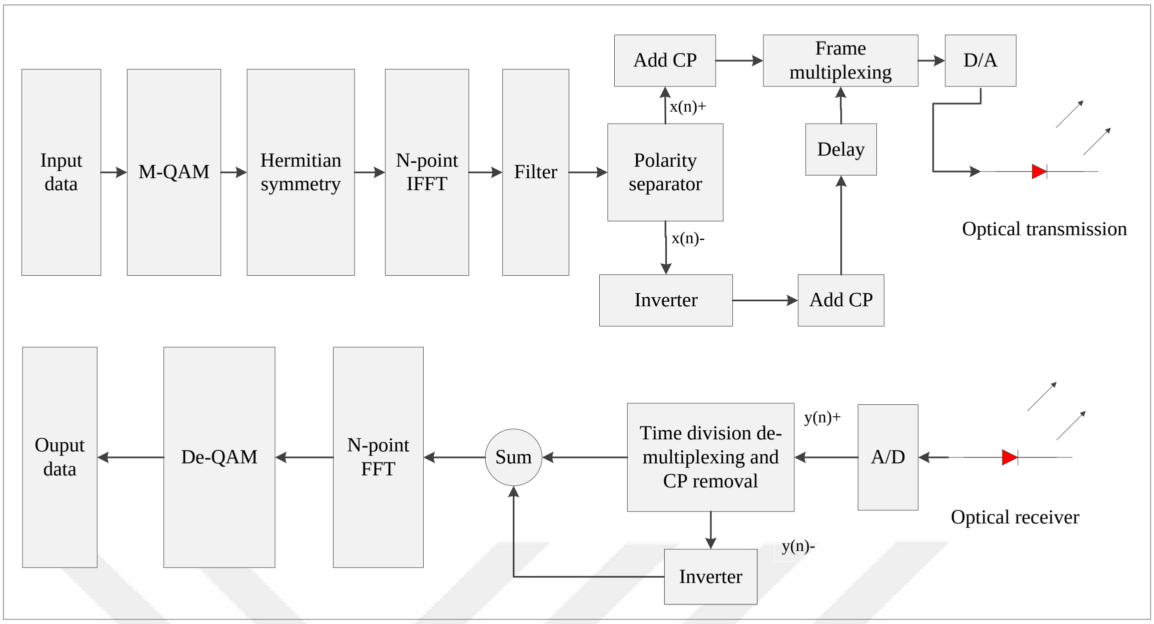

Figure 4.1: Conventional Flip F-OFDM Transmitter and Receiver.

Mathematically, the signal $x(n)$ in discrete time-domain is obtained by acting the frequency-domain symbols $X(k)$ with the IFFT, expressed by:

$$x(n) = \frac{1}{N}\sum_{k=0}^{N-1} X_k e^{\frac{2\pi jkn}{N}}, \quad n = 0,1,\ldots,N-1 \tag{4.2}$$

Here, N implies the FFT/IFFT operational length, and $X(k)$ implies the sub-carrier symbols k^{th}. However, the enforcement of Hermitian symmetry constraints on the signals to the IFFT necessitates doubling the transform size to $2N$ points. This modification arises from the requirement to maintain conjugate symmetry across subcarriers, ensuring the resultant time-domain signal remains real-valued. Consequently, the mathematical formulation in equation 4.2 must be restructured to account for the expanded IFFT dimensionality, as derived below:

$$x(n) = \frac{1}{2N}\sum_{k=0}^{2N-1} X_H e^{\frac{j\pi kn}{N}}, \quad n = 0,1,\ldots\ldots,2N-1 \tag{4.3}$$

The Hermitian limitation is employed to nullify the signal imaginary part of the IFFT output led toward a real-amounted F-OFDM waveform. This removes complex- amounted, but the signal remains bipolar (i.e., positive and negative amplitudes) [130]. A polarity separator is used to decompose a bipolar signal into pair-wise non-negative components, which is specified as follows for unipolar transmission:

$$x(n) = x(n)^+ + x(n)^- \tag{4.4}$$

The positive $x(n)^+$, and negative $x(n)^-$, polarity components are defined through a piecewise decomposition of the bipolar time-domain signal $x(n)$, ensuring strict non-negativity for unipolar transmission. These components are expressed as:

$$x(n)^+ = \begin{cases} x(n), & \rightarrow \quad x(n) \geq 0 \\ 0, & \rightarrow \quad x(n) < 0 \end{cases} \tag{4.5}$$

$$x(n)^- = \begin{cases} x(n), & \rightarrow \quad x(n) < 0 \\ 0, & \rightarrow \quad x(n) \geq 0 \end{cases} \tag{4.6}$$

In the time-domain multiplexing technique, bipolar signal x(n) is converted into a unipolar signal for systems relying on intensity-based transmission. In particular, a non-negative portion $x(n)^+$, which corresponds to the positive amplitudes of $x(n)$, will be assigned to the first F-OFDM subframe. Simultaneously, its inverted negative component $x(n)^-$, which is calculated by mirroring the negative amplitudes of $x(n)$ to the non-negative region, is sent in the second frame of the F-OFDM subframe. Mathematically, this dual-subframe decomposition can be written as:

$$x_{2N}(n) = \begin{cases} x^+(n), & n = 0, 1, .., N-1 \\ -x^-(n-N), & n = N, ..., 2N-1 \end{cases} \tag{4.7}$$

Upon the receiver part pointed in Figure 4.1, the bipolar real F-OFDM signal, $y(n)$, is reconstructed as shown in 4.8:

$$y(n) = y(n)^+ - y(n)^- \tag{4.8}$$

Here, $y(n)^+$,and $y(n)^-$ denote the first and second received F-OFDM subframes, respectively, which correspond to the transmitted non-negative components $x(n)^+$, and $-x^-(n)$. This operation inverts the polarity separation applied at the transmitter, restoring the bipolar signal $y(n)$, which approximates $x(n)$ under ideal channel conditions. Subsequently, the transmitted frequency-domain vector $X(k)$ is retrieved via standard OFDM demodulation.

4.3 NON-HERMITIAN SYMMETRY FLIP FILTERED-OFDM (NHS-FLIP-F-OFDM)

4.3.1 System Model

To mitigate the inherent spectral and computational inefficiencies imposed by Hermitian symmetry limitations in conventional real-valued signal production architectures. we propose a new approach to enable the faster generation of complex-valued signals while reducing transmitter hardware complexity by avoiding an HS constraint on frequency-domain symbols. Thus, at the modulation level of the signal, it reduces computational overhead and provides more spectrum flexibility by eliminating the symmetric distribution allocation of symbols. This scheme is also called the Juxtaposition Method (JM) or Non-Hermitian Symmetry (NHS). The architecture of the proposed Flip-F-OFDM is schematically depicted in Figure 4.2. This approach sidesteps Hermitian symmetry constraints that are intrinsic to standard real-valued signal generation by directly performing IFFT on the unconstrained frequency-domain symbols.

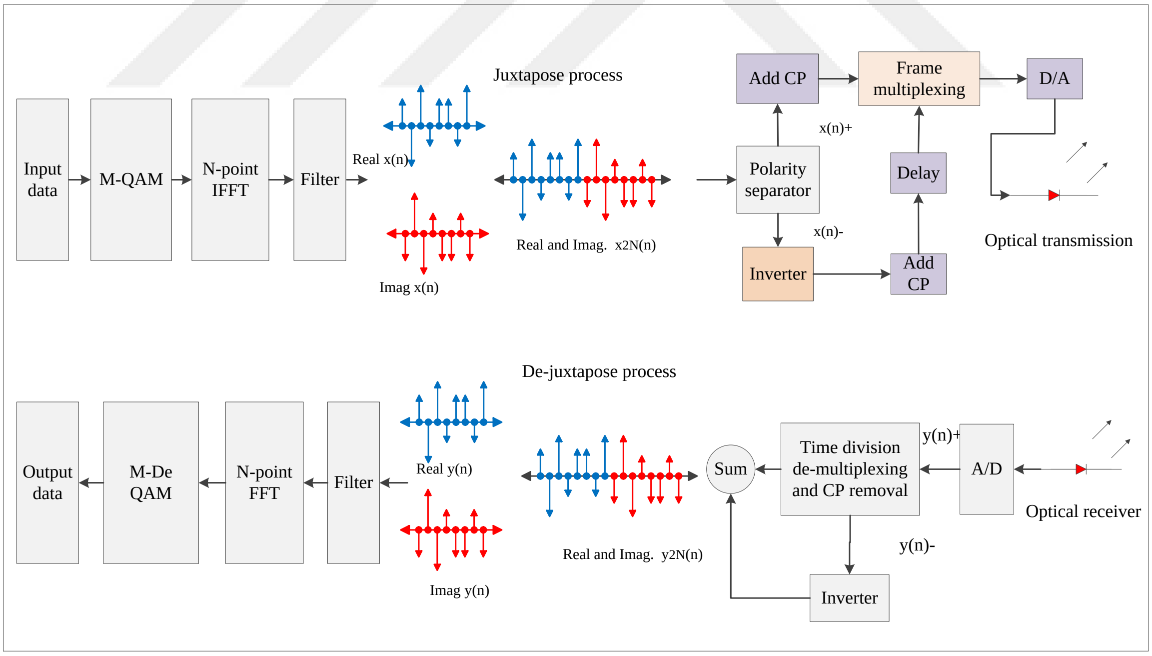

Figure 4.2: The Proposed System of NHS-Flip-F-OFDM.

Accordingly, the IFFT output produces a complicated time-domain signal rather than a real-amounted F-OFDM signal. To exploit the noise resilience and spectral efficiency of quadrature amplitude modulation—critical for mitigating channel impairments and enabling high-speed data transmission—this framework integrates QAM symbol mapping [98], [129]. Next, a dedicated signal processing stage converts the complicated IFFT output to a non-complex (real-amounted) signal to be used in DD/IM procedures.

At the transmitter (Figure 4.2), the input data stream is initially modulated into QAM symbols. These symbols are subsequently processed through an N-point IFFT without imposing HS constraints. Due to the absence of HS requirements, the IFFT operates on unconstrained frequency-domain symbols, producing a complex-amounted time-domain signal. This output can be mathematically extracted as [98]:

$$x(n) = \sum_{k=0}^{N-1}[X_R(k) + jX_I(k)]e^{\frac{2\pi jkn}{N}} \tag{4.9}$$

$X_R(k)$, and $X_I(k)$ are denoted the two components of the QAM-mapped frequency-domain symbols $X(k)$ separately. The complex F-OFDM signal generated at the IFFT output is subsequently refined using a windowing function and a spectrally localized sub-band filter, as detailed in Chapter 3, to suppress out-of-band emissions and optimize spectral containment [87], [130]. To synthesize a real-amounted F-OFDM signal meet for intensity modulation, the real and imaginary parts of the processed complex waveform are strategically combined in the time domain. This is achieved by concatenating the real part and the imaginary part of the N-point complicated signal $x(n)$, resulting in a double-length $x_{2N}(n)$:

$$x_{2N}(n) = \begin{cases} x_R(n), & n = 0, 1, .., N-1 \\ x_I(n-N), & n = N,\ 2N-1 \end{cases} \tag{4.10}$$

This temporal juxtaposition effectively doubles the sampling rate while preserving the signal's real-valued nature, ensuring compatibility with DD/IM approaches. The elimination of HS constraints simplifies frequency-domain symbol allocation and enhances spectral adaptability, as the sub-carriers are no longer restricted to symmetric pairings.

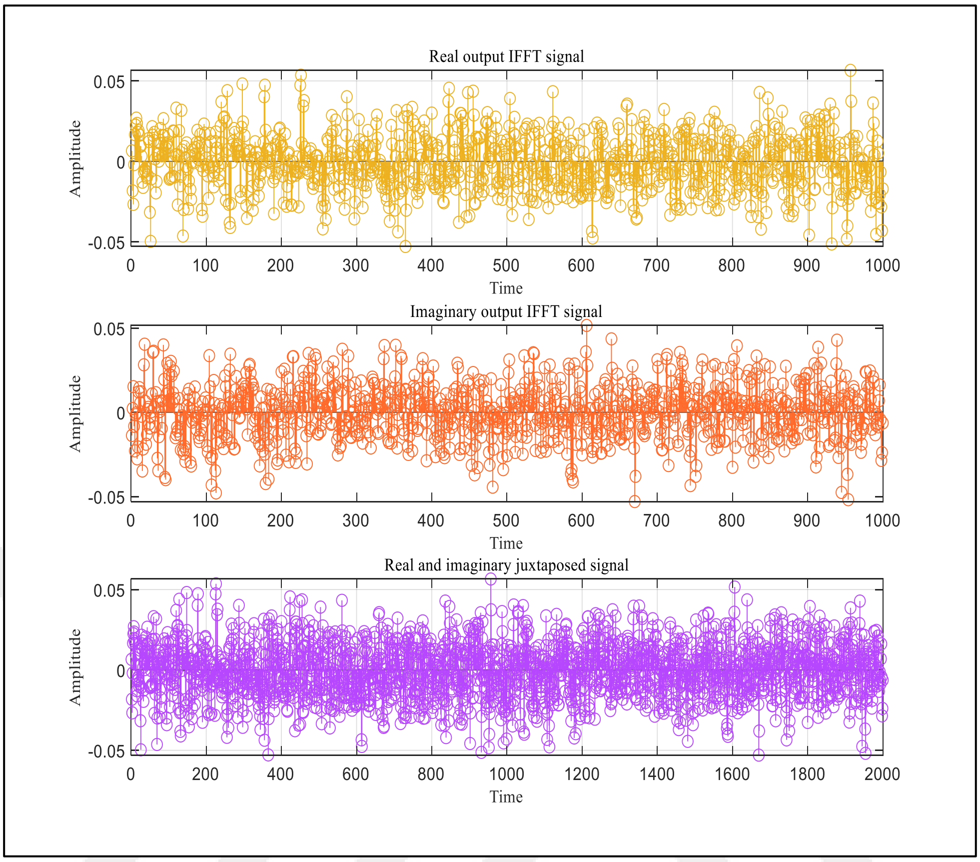

Figure 4.3: Real, Imaginary, and Juxtaposed Signal.

The resultant 2N-point bipolar time-domain signal is subsequently fed into a polarity separation module. This separator deals with the dipolar signal as a pattern of a positive component $x_{2N}^{+}(n)$, and a negative component $x_{2N}^{-}(n)$ which can be squeezed out as:

$$x_{2N}^{+}(n) = \begin{cases} x_{2N}(n) & \rightarrow \quad x(n) \geq 0 \\ 0, & \rightarrow \quad x(n) < 0 \end{cases} \tag{4.11}$$

$$x_{2N}^{-}(n) = \begin{cases} x_{2N}(n) & \rightarrow \quad x(n) < 0 \\ 0, & \rightarrow \quad x(n) \geq 0 \end{cases} \tag{4.12}$$

The generated unipolar signal then can be represented as:

$$x_{4N}(n) = \begin{cases} x_{2N}^{+}(n), & n = 0, 1, \ldots, 2\,N - 1 \\ -x_{2N}^{-}(n - N), & n = 2N, \ldots, 4N - 1 \end{cases} \tag{4.13}$$

As mentioned earlier, within the Flip-F-OFDM system, the first subframe transmits the positive signal $x_{2N}^{+}(n)$, whereas the later subframe is employed to hold the flipped (inverted polarity) signal $-x_{2N}^{-}(n)$ as displayed in Figure 4.4.

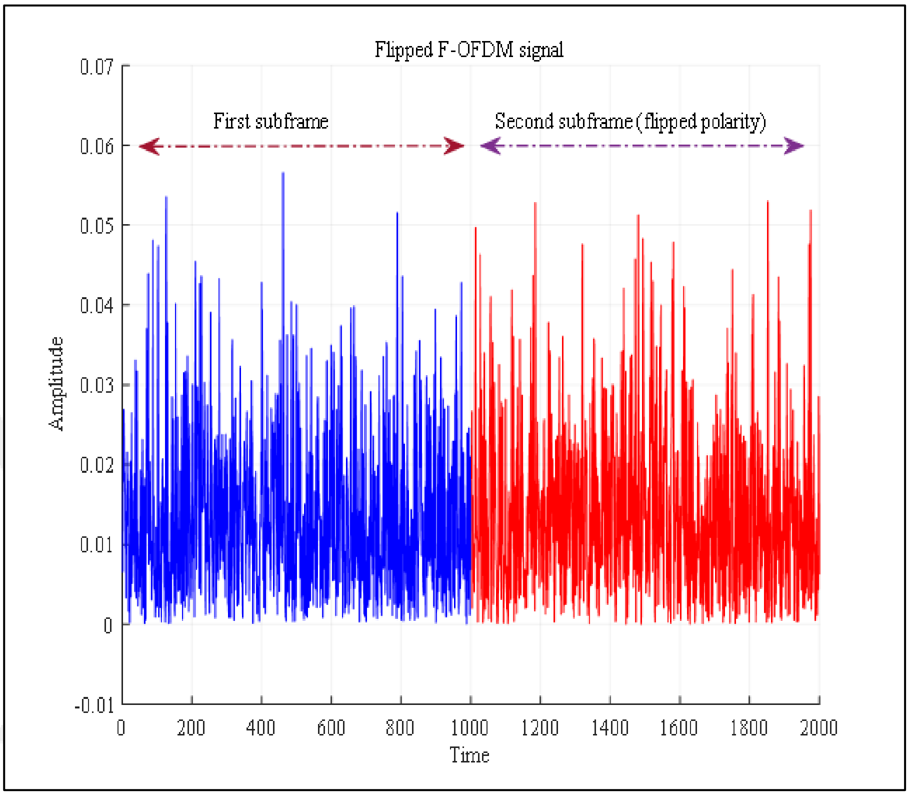

Figure 4.4: Unipolar (Flipped) Filtered-OFDM Signal.

To counterbalance ISI owing to chromatic dispersion on the optical channel, we add cyclic prefixes (CPs) to every F-OFDM sub-frame. This is implemented by prefixing a new duplicate of the last CP copies of the N-point time-domain subframe to its head, increasing the sub-frame duration to N+CP. The produced nonbipolar signal will then facilitate IM and is appropriate to be transmitted over the optical channel.

The Flip-F-OFDM receiver architecture, shown in Figure 4.2, operates on the assumption of AWGN optical channel and perfect equalization to give a received optical signal $y(n)$. This signal is initially translated into the electrical domain using a photodetector and then discretized by analog-to-digital conversion to generate the waveform. Then, going to remove the CP which is attached to every F-OFDM sub-frame, and restore the sub-frame period. Given the oversampled unipolar received signal $y_{4N}(n)$, the following time-domain operation is employed to reconstruct the bipolar signal $y_{2N}(n)$:

$$y_{2N}(n) = {y_{4N}}^{+}(n) - {y_{4N}}^{-}(2N+n) \tag{4.14}$$

Consequently, the non-complex signal, $y_{2N}(n)$, is reassembled to the complex-signal, as extracted in the following:

$$\begin{cases} y_R(n) = y_{2N}(n), & n = 0, 1, \ldots N-1 \\ y_I(n) = y_{2N}(N+n), & n = 0, 1, \ldots, N-1 \end{cases} \tag{4.15}$$

Where $y_R(n)$, and $y_I(n)$ denote the two components of the complex baseband signal, real and imaginary, $y(n)$ respectively. Next, the composite complex signal undergoes subband filtering which focuses the spectral energy of the signal in the frequency band allocated to it and suppresses emissions outside of the band and inter-carrier interference. The filtered signal is then demodulated, following a frequency-domain transformation similar to the one used in standard complex F-OFDM architectures. An N-point FFT is applied to the time-domain samples after subband processing. The recovered frequency-domain symbols $Y(k)$ is then expressed as follows:

$$Y(k) = \sum_{n=0}^{N-1} y_n e^{\frac{-2\pi jk}{N}} \tag{4.16}$$

$$Y(k) = \sum_{n=0}^{N-1} [y_R(k) + j y_I(k)] e^{\frac{-2\pi jk}{N}} \rightarrow Y(k) = Y_R(k) + jY_I(k) \tag{4.17}$$

Here $y_R(k)$ and $y_I(k)$ signify the two components, real and imaginary, of the received frequency symbols respectively. The transmitted signal, $x(n)$, propagates through a dispersive optical channel characterized by the impulse response $h(n)$, as detailed in Chapter 3. The channel output is subsequently corrupted by AWGN $\mu(n)$, which is statistically impartial of $x(n)$ and exhibits zero mean and variance σ_μ^2. The resultant received signal $y(n)$ at the receiver is mathematically modelled as [130], [131]:

$$y(n) = (x(n) * h(n)) + \mu(n) \tag{4.18}$$

Here $*$ is the linear convolution, $x(n)$ is denoted the signal transmitted, and $\mu(n)$ implies the noise factor. In the frequency domain, the received frequency-symbol $Y(k)$ is derived by converting the time-domain convolution into a multiplicative operation via the discrete Fourier transform. Specifically, the frequency-domain received signal is expressed as:

$$Y(k) = X(k).H(k) + M(k) \tag{4.19}$$

4.4 SIMULATION RESULTS AND DISCUSSION

In this division, we thoroughly assess the execution of the proposed NHS-Flip-F-OFDM framework as contrasted with the established Flip-F-OFDM architecture. The evaluation methodology comprises four critical metrics: computational complexity, SNR, BER performance, and PAPR features. The analysis combines numerical simulations, which are designed to capture the reality of the channel and the system behavior, with analytical modeling that helps derive theoretical performance bounds, thus providing methodological rigor. Keeping these two approaches side-by-side confirms the possible gains of the suggested NHS-Flip-F-OFDM system with respect to the trade-offs between spectral efficiency, power utilization, and error resilience for conventional multicarrier setups.

4.4.1 Computational Complexity

Computational complexity is a key performance index, where it measures the arithmetic computations needed to implement the system. In this analysis, the propositioned NHS-Flip-F-OFDM architecture is contrasted to the established Flip-F-OFDM scheme in terms of computational cost, with clear statistics on the number of required complex multiplications and additions during transmission and reception chains. The NHS-Flip-F-OFDM framework, makes use of these symmetry properties of non-Hermitian signal constellations to optimize algorithmic efficiency. The proposed system utilizes N-point IFFT blocks that synthesize the real-valued F-OFDM signals to transmit coherent demodulation of 2N-point real F-OFDM signals [109]. Indeed, it cuts the multiplicative complexity in half relative to more traditional 2N-point complex IFFT/FFT methods for generating the same amount of equivalent real signal. This simplification is done without loss of waveform orthogonality or spectral containment, which allows to keep the functionality of a system while adding computational tractability features, that are like on-edge devices that are in many cases resource constrained.

Contrasted to the conventional Flip-F-OFDM system, the suggested framework leads to a great reduction in hardware complexity, namely, about 50% reduction of arithmetic operations. This efficiency gain is attributed to the integration of HS and the radix-2 FFT algorithm. So, the utilization of HS enables real-valued Flip-F-OFDM signal synthesis through N/2-point FFT/IFFT computing rather than the traditional N-point transformations in regular implementations. The analysis of the mainstream computational load characterized by complex multiplication and addition for an N/2-point real signal is as follows [109], [110]:

$$O_{FFT\ Add} = \frac{3N}{2} log_2\left(\frac{N}{2}\right) - \frac{3N}{2} + 4 \tag{4.20}$$

$$O_{FFT\ Multip.} = \frac{N}{2} log_2\left(\frac{N}{2}\right) - \frac{3N}{2} + 4 + \frac{N}{2}(L-1) \tag{4.21}$$

Within this formulation, N denotes the FFT size, while L corresponds to the finite impulse response filter length. The computational complexity—quantified by the total arithmetic operations (additions and multiplications)—inherent to the FFT transformation within the Flip F-OFDM receiver architecture, which employs an N/4-point inverse FFT (IFFT), is derived from prior analyses [109], [110]. This reduction in IFFT size (from N-point to N/4-point) strategically optimizes resource allocation, aligning with the system's objective of minimizing latency and hardware footprint without compromising spectral resolution and is expressed as:

$$O_{FFT\ Add} = 3\frac{N}{4} log_2\left(\frac{N}{4}\right) - 3\frac{N}{4} + 4 \tag{4.22}$$

$$O_{FFT\ Multip.} = \frac{N}{4} log_2\left(\frac{N}{4}\right) - 3\frac{N}{4} + 4 + \frac{N}{4}(L-1) \tag{4.23}$$

Figures 4.5 and 4.6 analytically compare the computational complexity of the purported Flip F-OFDM and conventional Flip F-OFDM procedures for real-signal generation. The results demonstrate that scaling FFT/IFFT size proportionally increases hardware resource utilization (chip area, power) [132]. By employing an elevated IFFT algorithm [62], [131], the anticipated method substantially mitigates transmitter-side complexity—a critical factor for practical deployment. In contrast, the conventional approach retains high transmitter complexity due to its reliance on large subcarrier counts and full IFFT operations per subcarrier, which preclude algorithmic efficiency gains.

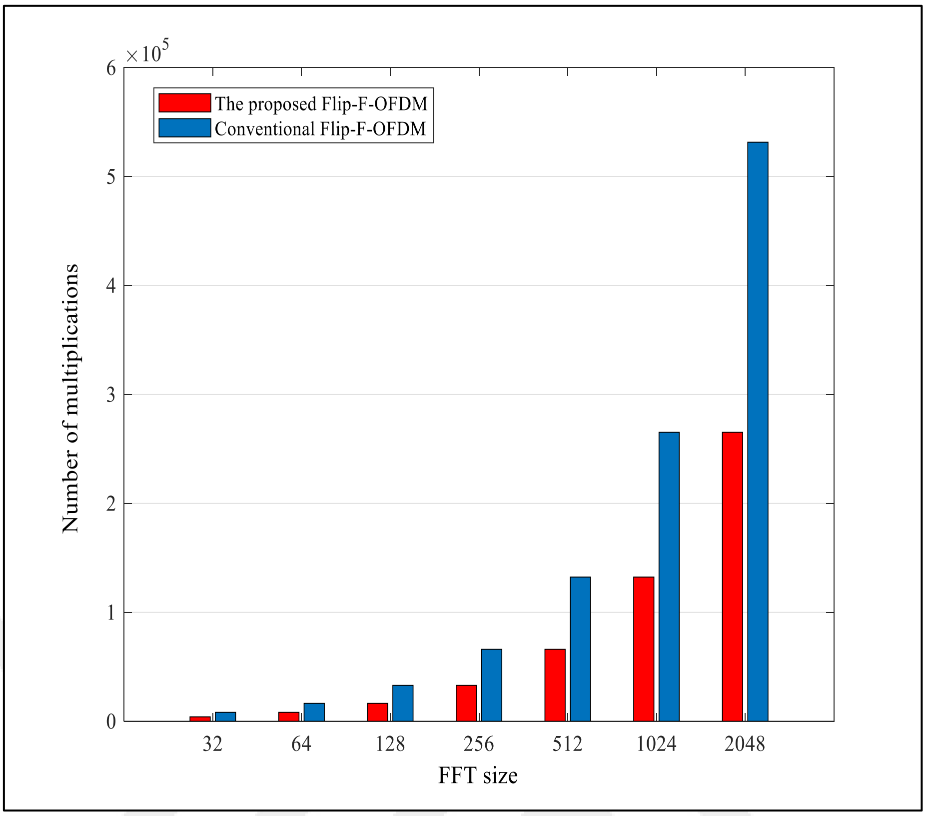

Figure 4.5: Flip-F-OFDM Multiplications Complexity.

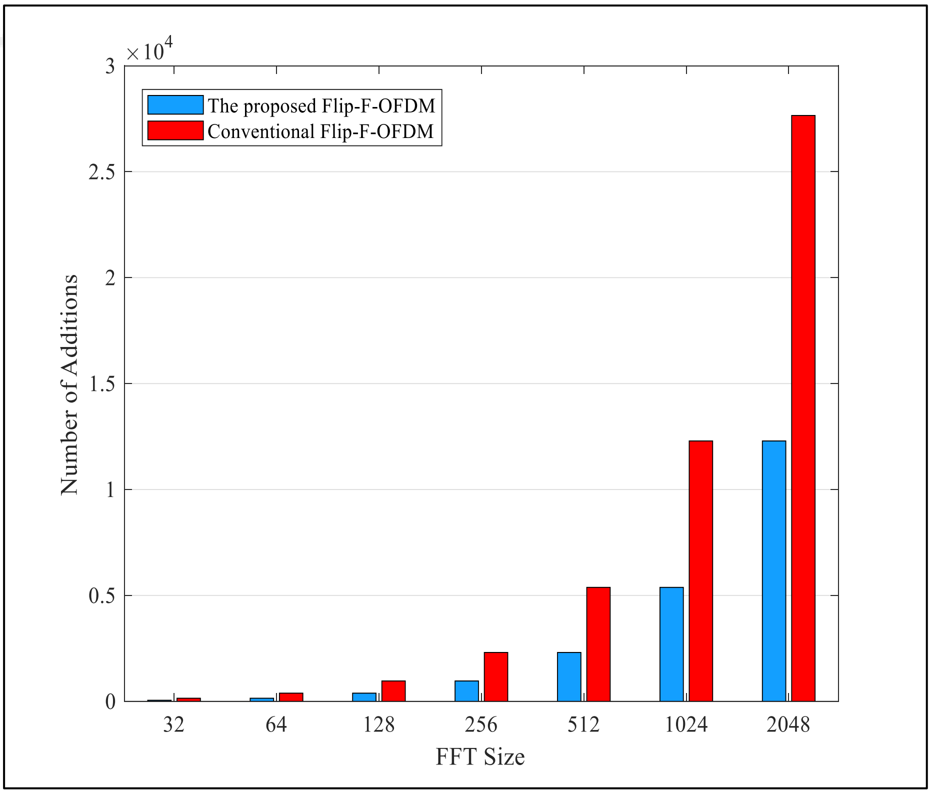

Figure 4.6: Flip-F-OFDM Additions Complexity.

4.4.2 Signal-to-Noise Ratio (SNR)

For Flip-F-OFDM, the non-nagative quantity of the F-OFDM signal is sent in the first sub-frame, whilst in the second the non-positive signal is sent inverted, resulting in a unipolar signal. Let $\mu^{+}(n)$ and $\mu^{-}(n)$ denote the additive noise introduced by the channel into the first and the subsequent F-OFDM sub-frame, correspondingly, the received signals on both sub-frames can be obtained as mathematically represented below:

$$y^{+}(n) = x^{+}(n) + \mu^{+}(n) \tag{4.24}$$

$$y^{-}(n) = -x^{-}(n) + \mu^{-}(n) \tag{4.25}$$

The transmitted signal power, $\sigma^2_{x,Flip}$ is mathematically expressed as the variance of the time-domain signal in the Flip-Filtered OFDM approach. This can be formulated as:

$$\sigma^2_{x,Flip} = \frac{1}{2N}\{\sum_{n=0}^{N-1}|x^{+}(n)|^2 + \sum_{n=N}^{2N-1}|x^{-}(n)|^2\} \tag{4.26}$$

Using an analogous methodology, the receiver noise power, denoted as $\sigma^2_{\mu,Flip}$, is defined as the variance of the aggregated noise components across the two sub-frames. This can be formulated as:

$$\sigma^2_{\mu,Flip} = \frac{1}{2N}\{\sum_{n=0}^{N-1}|\mu^{+}(n)|^2 + \sum_{n=N}^{2N-1}|\mu^{-}(n)|^2\} \tag{4.27}$$

In established Flip-Filtered-OFDM, the non-unipolar (bipolar) signal is reconstructed at the receiver through a coherent combination of the dual sub-frames transmitted over successive time intervals. Accordingly, the received bipolar signal power, corresponding to the reconstructed N-point waveform, is quantified as the statistical variance of the aggregated signal, formally defined by the following expression:

$$P_{s,Flip} = \frac{1}{N}\{\sum_{n=0}^{N-1}|x^{+}(n)|^2 + \sum_{n=0}^{N-1}|x^{-}(n)|^2\} \tag{4.28}$$

$$P_{s,Flip} = 2\sigma^2_{s,Flip} \tag{4.29}$$

Using an analogous methodology, the noise power defined by the following expression:

$$P_{\mu,Flip} = \frac{1}{N}\{\sum_{n=0}^{N-1}|\mu^{+}(n)|^2 + \sum_{n=0}^{N-1}|\mu^{-}(n)|^2\} \tag{4.30}$$

$$P_{\mu,Flip} = 2\sigma^2_{\mu,Flip} \quad (4.31)$$

Consequently, the SNR of the Flip-F-OFDM approach at the receiver is derived as the ratio of the reconstructed bipolar signal power $\sigma^2_{s,Flip}$ to the aggregated noise power $\sigma^2_{\mu,Flip}$ across the two sub-frames, formally expressed as:

$$SNR_{Flip-F-OFDM} = \frac{\sigma^2_{s,Flip}}{\sigma^2_{\mu,Flip}} = \frac{2\sigma^2_s}{2\sigma^2_\mu} = \frac{\sigma^2_s}{\sigma^2_\mu} \quad (4.32)$$

In the Flip-F-OFDM architecture, a coherent synthesis of real and imaginary components stimulates a twofold enhancement of signal and noise power, which is paramount in reconstructing the original complex transmitted waveform. As a result, the SNR at the receiver could be analytically extracted as:

$$SNR_{Porposed\ Flip-F-OFDM} = \frac{4\sigma^2_s}{4\sigma^2_\mu} = \frac{\sigma^2_s}{\sigma^2_\mu} = SNR_{Flip-F-OFDM} \quad (4.33)$$

4.4.3 Bit-Error-Rate Performance (BER)

This subdivision delineates a imitation-driven evaluation of the BER functioning for the proposed NHS-Flip-F-OFDM scheme, benchmarked against its conventional counterpart. Within the NHS-Flip-F-OFDM framework, the coherent integration of real and imaginary signal components—critical to reconstructing the transmitted complex waveform—necessitates a twofold escalation in both signal energy and noise variance, as rigorously derived in Section 4.4.2. This proportional amplification ensures that the SNR at the receiver's output remains mathematically congruent with the conventional system, formalized through the equivalence expressed in Equation (4.33).

Consequently, the proposed Flip-F-OFDM framework achieves unipolar F-OFDM signal generation while preserving identical SNR performance to conventional Flip-F-OFDM, yet with markedly lessened hardware complication. To empirically support this theoretical assertion, the bit error rate (BER) of the propositioned approach was simulated as a function of SNR across multiple modulation orders—4QAM, 16QAM, 64QAM, and 256QAM. The empirical results, illustrated in Figure 4.7, demonstrate BER performance parity between the proposed and conventional systems. This equivalence arises because the error probability, governed by Equation (3.35) in Section 3.5.3 [98], is solely dependent on SNR. Thus, NHS-

Flip-F-OFDM and standard Flip-F-OFDM exhibit indistinguishable BER characteristics, corroborating the analytical equivalence established in Section 4.4.2.

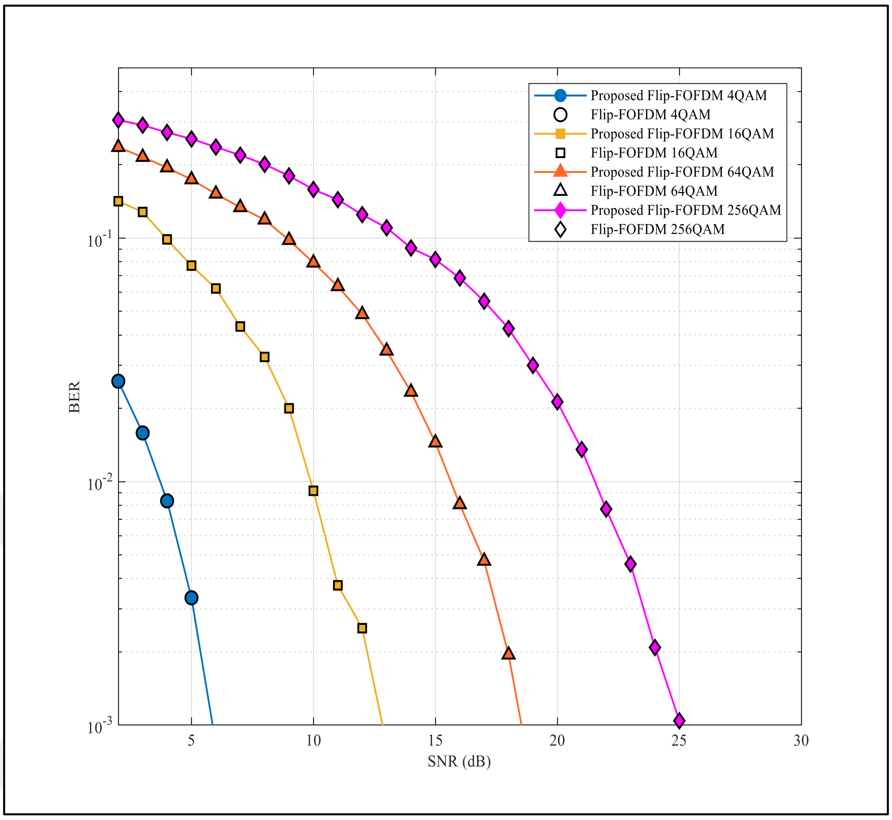

Figure 4.7: Comparison of BER Performance between NHS Flip-F-OFDM and Standard Flip-F-OFDM for 4, 16, 64, and 256QAM Orders.

4.4.4 Peak-to-Average-Power Ratio (PAPR)

The PAPR emerges as a critical design parameter governing power amplifier efficiency. Elevated PAPR levels directly precipitate nonlinear distortion in electro-optic conversion processes and stringent dynamic range requirements. This metric fundamentally constrains the operational limits of optical transmitters, as excessive peak power excursions degrade both component longevity and constellational fidelity in QAM-based schemes. The Flip-F-OFDM procedure decomposes the bipolar F-OFDM signal into two non-negative waveforms: a positive component $x^+(n)$, which retains all non-negative amplitude samples, and a flipped negative component $x^-(n)$, generated by inverting the polarity of negative amplitudes. These components are transmitted sequentially in non-overlapping temporal frames, and the receiver reconstructs the original bipolar signal through coherent superposition of the two parts. The peak power of the system is defined as the maximum instantaneous power monitored in either $x^{+}(n)$ or $x^{-}(n)$, mathematically expressed as:

$$max\left\{\left|x_{Flip}(n)\right|^{2}\right\} = \ max\{max\ |x^{+}(n)^{2}|\ ,\ max\ |x^{-}(n)^{2}|\} \tag{4.34}$$

Nonetheless since both halves are obtained from the identical signal $x(n)$, then equation (4.34) can rewrite as:

$$max\{\left|x_{Flip}(n)\right|)^{2}\} = max\{|x(n)|^{2}\} \tag{4.35}$$

This approach preserves the peak power characteristics of conventional F-OFDM, ensuring compatibility with power amplifier constraints while enabling unipolar transmission.

In contrast to its peak power behavior, the total average power in Flip-F-OFDM is characterized by the linear summation of the average powers from both the positive and flipped non-positive components. Since each unipolar segment occupies a dedicated temporal resource (i.e., transmitted in independent, non-overlapping time slots), the aggregate average power of the composite Flip-F-OFDM signal is expressed as:

$$E\{\left|x_{Flip}(n)\right|)^{2}\} = E\{|x^{+}(n)|)^{2}\} + E\{|x^{-}(n)|)^{2}\} \tag{4.36}$$

Since $x^{+}(n)$, and $x^{-}(n)$ are resulting from the identical signal, the mean power is separated uniformly between the two halves as follows:

$$E\{\left|x_{Flip}(n)\right|)^{2}\} = 2 \times \tfrac{1}{2}E\{|x(n)|)^{2}\} = E\{|x(n)|)^{2}\} \tag{4.37}$$

Using the above expressions (4.35 and 4.37) for peak and average powers, the PAPR of the Flip-OFDM can present as:

$$PAPR_{Flip-F-OFDM} = \frac{max\{|x_{Flip}(n)|)^{2}\}}{E\{|x_{Flip}(n)|)^{2}\}} \tag{4.38}$$

The purported Flip-F-OFDM retains the same peak power as established Flip-F-OFDM, as omitting Hermitian symmetry modifies the spectral configuration but leaves the time-domain signal's peak amplitude unaffected. Since both real and imaginary components equally contribute to the signal's total power, the average power aligns with conventional

Flip-OFDM, yielding an identical PAPR. Hence, the PAPR of the suggested Flip-F-OFDM is expressed as:

$$PAPR_{NHS\ Flip-F-OFDM} = \frac{max\{|x_{Flip}(n)|)^2\}}{E\{|x_{Flip}(n)|)^2\}} = PAPR_{Flip-F-OFDM} \tag{4.39}$$

The examination demonstrates that the NHS-Flip-F-OFDM technique effectively mitigates peak-average power ratio (PAPR) escalation, achieving unipolar F-OFDM signal generation with PAPR characteristics equivalent to conventional Flip-F-OFDM. This parity is empirically validated through complementary cumulative distribution function (CCDF) curves in Figure 4.8, which compare the PAPR performance of NHS-Flip-F-OFDM and established Flip-F-OFDM for 16-QAM-modulated signals with lengths N=512 and N=1024. The overlapping CCDF trajectories confirm that the novel technique preserves the PAPR advantages of legacy methods while enabling enhanced structural or computational efficiencies (e.g., reduced complexity or improved hardware compatibility).

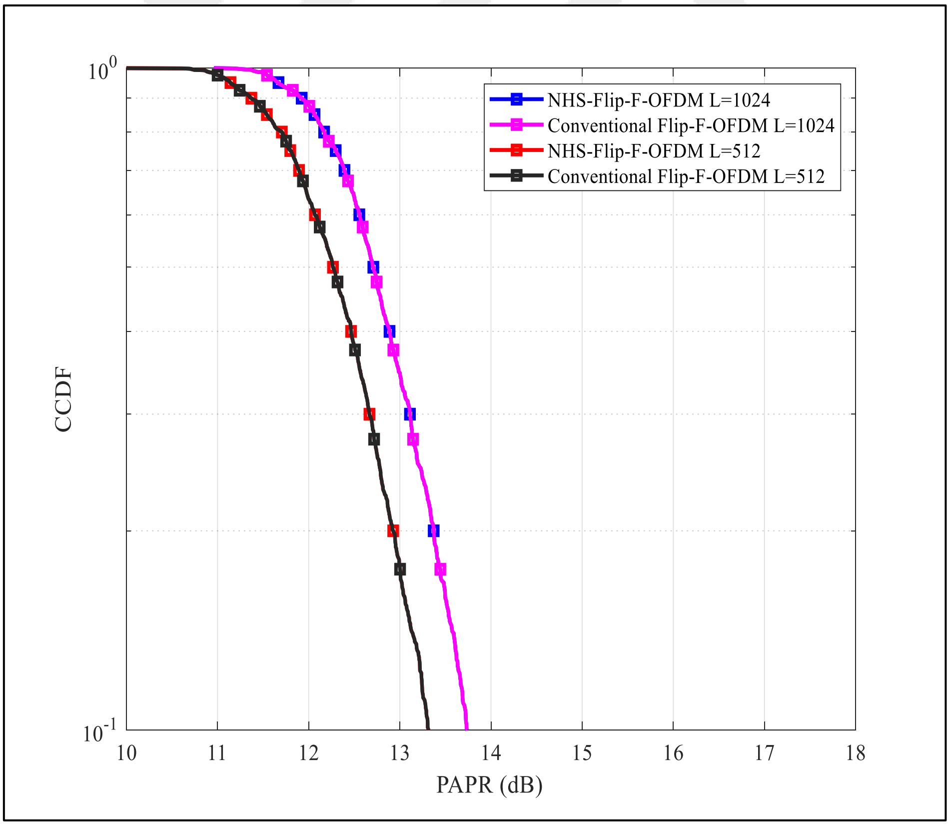

Figure 4.8: The CCDF Curves of the Proposed and Conventional Flip F-OFDM Using Signal Length N=512, and N=1024.

As illustrated in Figure 4.8, the CCDF curves of the suggested and conventional F-OFDM superposed for all tested signal lengths. This demonstrates that the PAPR of the produced F-OFDM signal remains unaffected by the applied procedure and is determined solely by the signal length.

4.5 SUMMARY

The chapter presented a different method for generating real-amounted signals within IM/DD procedures called NHS-Flip-F-OFDM. Unlike conventional HS-based methods, the proposed method does not require HS, yet employs IM/DD compatibility. The proposed method decreases the complexity of data transmission by sending $N-1$ data symbols per frame through the application of N-point IFFT/FFT operations to combine an N-point non-dipolar waveform into a 4N-point waveform, in contrast to the conventional system. The architectural simplification leads to reduced power consumption and minimized hardware footprint (e.g., minimized chip area) for no increase in error rate and SNR performance in comparison with traditional Flip-F-OFDM. Most importantly, the analytical results validate that NHS-Flip-F-OFDM does not increase the PAPR as it has the same PAPR property as conventional unipolar Flip-F-OFDM, which is again confirmed by the simulated CCDF curves. The technique, therefore, achieves efficient computational, hardware-friendly IM/DD waveform generation while maintaining spectral and power efficiency.

5. PROPOSED WORK RESULTS ANALYSIS AND DISCUSSIONS

5.1 INTRODUCTION

In this chapter, a comparison is made between the proposed NHS-Filtered-OFDM system to conventional HS-based F-OFDM and other benchmark architectures. The evaluation framework quantifies the extent to which the NHS paradigm delivers quantifiable advancements in key performance indicators, such as computational efficiency, spectral utilization, error resilience, and power fluctuations. Through the establishment of a comprehensive performance profile by systematically evaluating computational complexity, BER, PAPR, and spectral efficiency characteristics, the research presents a holistic analysis. The findings confirm that NHS-Filtered-OFDM can simultaneously optimize over multiple dimensions: compromises hardware implementation (via lowered algorithmic overhead) and communication robustness (by maintaining the BER and PAPR) in addition to improving spectral use.

5.2 COMPUTATIONAL COMPLEXITY ANALYSIS

A systematic computational intricacy analysis is conducted to quantify the operational productivity of the suggested NHS-F-OFDM relative to conventional F-OFDM. This study theoretically evaluates the reduction in computational overhead by comparing the requisite number of complex multiplications and additive operations, with FFT and inverse FFT stages identified as the dominant computational modules in the F-OFDM transceiver chain. By eliminating Hermitian restrictions, the proposed NHS-F-OFDM architecture inherently streamlines spectral processing while retaining FFT/IFFT core operations, thereby enabling direct computational benchmarking of algorithmic enhancements. In particular, increasing the FFT/IFFT block size results in additive increases in power dissipation and required chip area for transceiver implementations, which is an important constraint in resource-limited hardware. In traditional optical F-OFDM frameworks, the application of Hermitian symmetry on frequency-domain symbols—necessary to obtain output signals matching with intensity modulation/direct detection—results in a twofold increase of the transform size. This requires 2~N-point IFFT/FFT operations to modulate N frequency symbols, leading to increased algorithmic overhead and hardware resource costs.

Earlier works [133], [134] systematically analyzed how FFT/IFFT block sizes affect the operational performance of optical OFDM transceivers. Empirically demonstrated as shown in Figure 5.1, which measures the error-vector magnitude (EVM) in both FFT/IFFT frequencies ranging from 32 to 1024 points, scaling the transform size is an important trade-off. The dimensional scaling of FFT/IFFT operations, driven by an increased subcarrier count, achieves finer spectral resolution (granularity) in the frequency domain. Nonetheless, this advantage is offset by a larger energetic span of the OFDM signal [133]. The broadening of the signal (both transmitted and received) bandwidth forces the arithmetic to perform better leading to an increased requirement on ADC and DAC resolution which can result in quantization error effects.

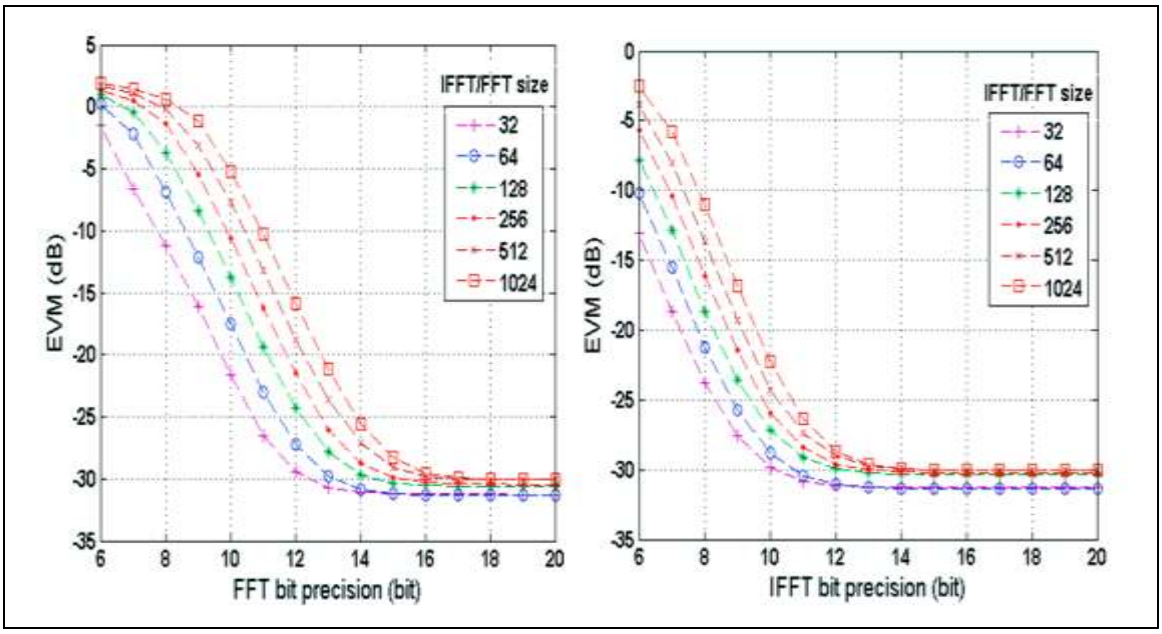

Figure 5.1: EVM as a Behavior of FFT/IFFT Bit Precision [133].

This observed interdependence exerts a deterministic influence on the transceiver's error vector magnitude (EVM) characteristics. As analytically corroborated in Figure 5.1, the requisite quantization bit-depth for FFT/IFFT computational units scales monotonically with transform dimensionality to sustain a target EVM performance threshold. For example, with an FFT bit accuracy of 8, doubling the size of the FFT/IFFT leads to an EVM punishment of nearly 2 dB. It is also noteworthy that at higher FFT/IFFT bit accuracies, an EVM floor emerges owing to the resolution limitations of the DAC/ADC, as reported in [133], [134].

The analysis further confirmed that enlarging FFT/IFFT block sizes directly escalates power dissipation and on-chip area occupancy. This growth becomes particularly significant for transform sizes of N ≥ 512. As reported in [133], Empirical results quantified that downscaling the FFT/IFFT transform length from N=1024 to N=512 yielded correlated reductions in on-chip area (~40%) and dynamic power dissipation (~38%), demonstrating substantial computational resource efficiency gains for the implemented system. Under the radix-2 FFT algorithm framework [109], the computational complexity associated with real-valued FFT of an OFDM signal differ slightly from that of an F-OFDM signal.

The F-OFDM architecture exhibits escalation in time-domain computational complexity relative to conventional OFDM systems, attributable to the convolution-based filtering operations at transmit nodes. This complexity is governed by the composite interaction of the prime OFDM symbol duration and the filter's impulse response length, as convolving the two signals imposes a computational burden proportional to the product of their respective lengths. While arithmetic operations in additive domains remain analogous between F-OFDM and OFDM, multiplicative operations in F-OFDM scale in direct proportion to the filter's temporal span—a critical distinction formalized in [111].

The proposed NHS-Filtered-OFDM method aims to simplify the complexities associated with transmission and reception components. This approach generates a real F-OFDM signal using N-point IFFT blocks. It facilitates the transmission and demodulation of 2N-point real F-OFDM signals via NHS-DCO-F-OFDM and 4N-point real F-OFDM signals via NHS-Flip-F-OFDM. Based on mathematical analysis in equations (3.21 and 3.22), (4.22 and 4.23), Figures 5.2 and 5.3 conduct a comparative analysis of arithmetic operation counts (multiplications and additions) across four real-valued signal synthesis architectures: novel NHS-Flip-F-OFDM, legacy Flip-F-OFDM, NHS-DCO-F-OFDM, and conventional DCO-F-OFDM. The data delineate a positive correlation between transform dimensionality (FFT/IFFT size) and hardware resource utilization metrics—specifically, chip size and dynamic power dissipation—as empirically validated in [133].

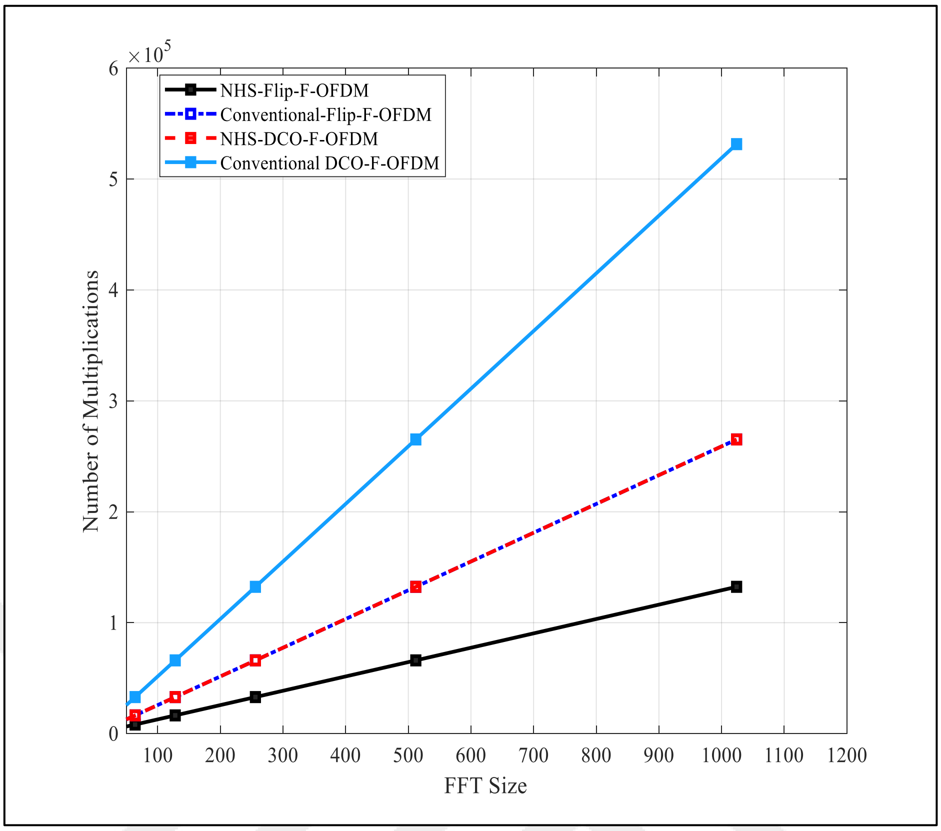

Figure 5.2: Multiplications Complexity.

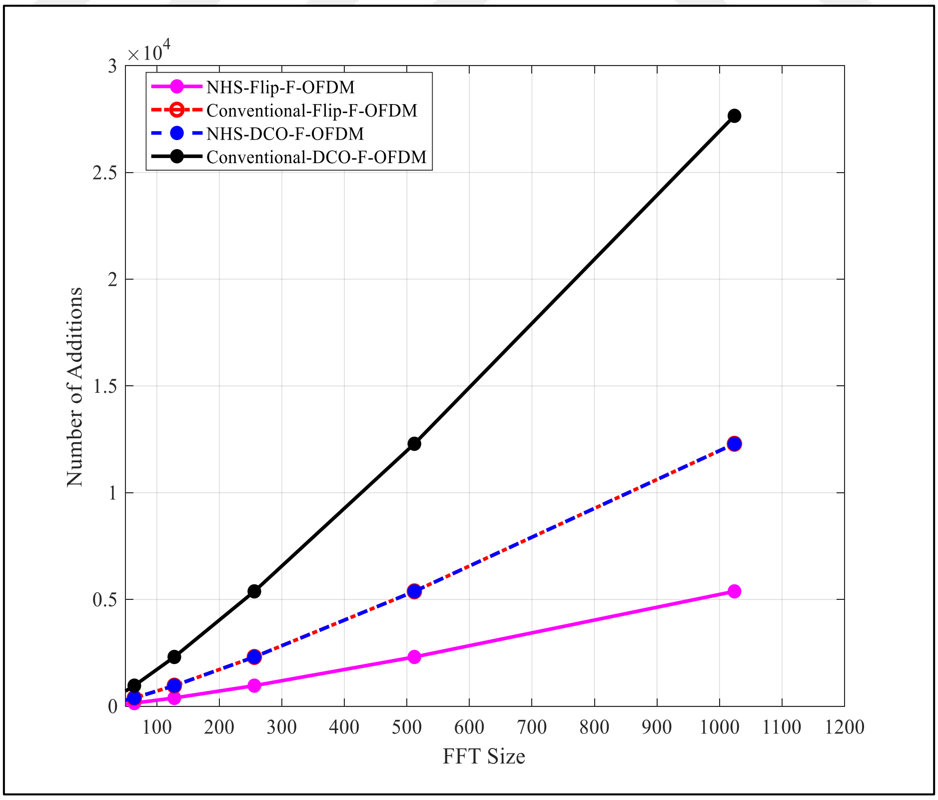

Figure 5.3: Additions Complexity.

Table 5.1 compares the computational complexity profiles for eight real-domain OFDM variants: the propositioned NHS-Flip-F-OFDM, legacy Flip-F-OFDM, NHS-DCO-F-OFDM, conventional DCO-F-OFDM, HSF Flip-OFDM, Flip-OFDM, ACO-OFDM, and DCO-OFDM; a fixed transmitted signal dimension of 128 was used. As shown, NHS-Flip-F-OFDM, symmetric in its transmitter-receiver design, realizes significant diminishing in the arithmetic loads on the chip, with multiplicative and additive operation decreases of 66.5% and about 57%, respectively, contrasted to benchmark Flip-F-OFDM. The NHS-DCO-F-OFDM architecture achieves a computational complexity reduction of ~59% in multiplicative operations and ~61% in additive operations bidirectionally (transmitter/receiver) relative to the legacy DCO-F-OFDM framework, attributable to its optimized signal-processing design.

Table 5.1: Systematic Computational Intricacy Evaluation Among the Propositioned NHS-Flip-F-OFDM, Conventional Flip-F-OFDM, NHS-DCO-F-OFDM, Conventional DCO-F-OFDM, HSF Flip-OFDM, Flip-OFDM, ACO-OFDM, and DCO-OFDM.

Scheme	**Additions**	**Multiplications**
Proposed NHS-Flip-F-OFDM	388	16,452
Conventional Flip-F-OFDM	964	32,964
Proposed NHS-DCO-F-OFDM	964	32,964
Conventional DCO-F-OFDM	2308	66052
HSF Flip-OFDM	964	196
Conventional Flip-OFDM	2308	516
ACO-OFDM	2308	516
DCO-OFDM	2308	516

Comparative simulations indicate that the propositioned NHS-Flip-F-OFDM architecture realizes a substantial saving in calculational complication relative to the baseline NHS-DCO-F-OFDM tactic. Nonetheless, NHS-F-OFDM incurs a notably higher multiplicative operational load compared to HSF-Flip-OFDM, Flip-OFDM, ACO-OFDM, and DCO-OFDM, as a consequence of the intrinsic computational demands imposed by its spectral shaping filter. This results in a parametric scaling relationship, where the arithmetic complexity of NHS-Flip-F-OFDM scales proportionally with the temporal duration of the filter kernel when evaluated against these reference methodologies.

5.3 SPECTRAL EFFICIENCY AND DATA RATE ANALYSIS

Filtered-OFDM exhibits significant improvements in spectral efficiency through enhanced spectral confinement and adaptive filtering mechanisms, thereby addressing the critical need for high-throughput data transmission in contemporary wireless communication systems. The sub-band spectral confinement achieved through F-OFDM's optimized filter design suppresses OOBEs, thereby minimizing safeguard intervals between neighbouring subbands and enabling near-optimal spectral resource allocation. The novel NHS-F-OFDM methodology innovatively eliminates the Hermitian symmetry constraint, permitting full utilization of all N orthogonal subcarriers for data modulation. This represents a marked departure from conventional F-OFDM architectures, which enforce HS to maintain real-valued signal outputs, inherently limiting active data carriers to N/2 and halving achievable throughput. By circumventing this redundancy, NHS-F-OFDM achieves a doubling of spectral efficiency while retaining compatibility with intensity-modulation-based optical wireless communication frameworks.

DCO-OFDM inherently limits the number of active subcarriers in use to N/2 by imposing Hermitian symmetry at the IFFT stage, effectively halving its data-carrying capacity. This restriction is compounded by ACO-OFDM, where modulation is allowed just on odd-indexed subcarriers under HS, with usable subcarriers N/4, leading to a fourfold penalty on spectral throughput. Meanwhile, Flip-OFDM can overcome the parity-based subcarrier exclusion by involving both subcarriers (odd and even) but demands two consecutive subframes to recover the nonunipolar waveform and decode symbols. Consequently, this entails a compensation in the time-domain, which not only remains nearly identical as the ACO-OFDM system in terms of time-domain samples required; however, its transmitted data symbols per frame are twice higher. Thus, notwithstanding considerably different techniques, Flip-OFDM and ACO-OFDM yield equal net transmission rates as a result of this trade-off counterbalance. In contrast, HSF-Flip-OFDM eliminates HS constraints achieving spectral efficiency and data rate parity with the proposed NHS-F-OFDM framework. Table 5.2 synthesizes these dynamics, quantifying transmitted data rates, rate ratios, and spectral efficiencies across methodologies to delineate their throughput trade-offs.

Table 5.2: Comparative Analysis of Transmitted Data Rate, Transmitted Data Rate Ratio, and Spectral Efficiency for the Purported NHS-F-OFDM, Established F-OFDM, HSF-Flip-OFDM, Flip-OFDM, ACO-OFDM, and DCO-OFDM.

Techniques	**Transmitted Rate (Symbols/Frame)**	**Transmitted Rate Ratio (TRR)**	**Spectral Efficiency (SE)**
Purported NHS-F-OFDM	N	100%	$\frac{log_2 M}{1+(2/N)}$
Established F-OFDM	N/2	50%	$\frac{log_2 M}{1+(2/N)}$
HSF-Flip-OFDM	N	100%	$\frac{log_2 M}{1+(2/N)}$
Flip-OFDM	N/4	25%	$\frac{log_2 M/2}{1+(2/N)}$
ACO-OFDM	N/4	25%	$\frac{log_2 M/2}{1+(2/N)}$
DCO-OFDM	N/2	50%	$\frac{log_2 M}{1+(2/N)}$

5.4 BIT-ERROR-RATE PERFORMANCE (BER)

The section presents a simulation-based performing analysis of the propositioned NHS-F-OFDM variants (i.e., NHS-Flip-F-OFDM and NHS-DCO-F-OFDM) against their corresponding standard-based counterparts: conventional F-OFDM, HSF-Flip-OFDM, ACO-OFDM, and DCO-OFDM. The simulations were conducted with MATLAB R2023a simulations, corresponding to an AWGN channel conditioned on the 1024 IFFT point framework rise through each modulation order (4-QAM-256-QAM). The filter architecture in F-OFDM acts a energetic function in shaping the procedure performance due to its inherent capability of spectral confinement and thus helps in minimizing the out-of-band emissions and hence minimizes the required guard-band requirements between the adjacent sub-channels and accordingly maximizes its spectral efficiency. Table 5.3 specifies the complete simulation parameters such as modulation schemes, subcarrier allocation, and filters. The results presented in Figures 5.4 and 5.5 compare the resultant BER properties of NHS-Flip-F-OFDM and NHS-DCO-F-OFDM against previously developed techniques and confirm their robustness with higher-order modulation systems.

Table 5.3: Simulation Setup Parameters.

Parameter	**Values**
IFFT/FFT volume	1024
No. of F-OFDM symbol	1000
No. of subcarriers	600
Filter kind	Raised cosine
Modulation method	QAM
Cyclic prefix	72
Constellation sequence	4, 16, 64, 256
Channel prototype	AWGN

Simulation outcomes validate the significant error resilience of the suggested methodologies (NHS-Flip-F-OFDM and NHS-DCO-F-OFDM) relative to conventional benchmarks across all evaluated QAM modulation orders. This performance enhancement is attributable to the adaptive windowing mechanism integrated into the filter design, which preserves time-based localization within the trimmed filter response. Such temporal precision ensures that the F-OFDM signal adheres to stringent ISI thresholds, thereby maintaining waveform integrity under high spectral efficiency demands. Furthermore, NHS-Flip-F-OFDM achieves marginally improved BER performance contrasted to NHS-DCO-F-OFDM, as it removes the necessity for DC bias insertion, circumventing associated signal distortion and power inefficiencies inherent to DCO-based approaches.

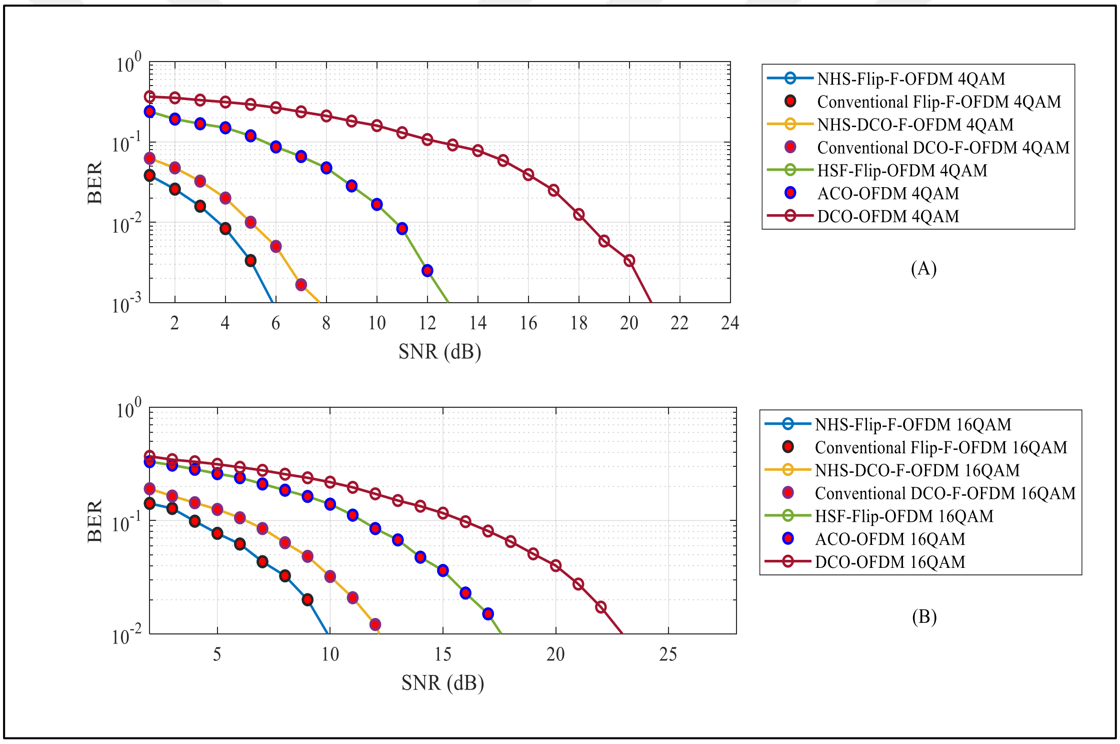

Figure 5.4: Valuation of BER Among the Propositioned NHS-Flip-F-OFDM, Established Flip-F-OFDM, NHS-DCO-F-OFDM, Conventional DCO-F-OFDM, HSF-Flip-OFDM, ACO-OFDM, and DCO-OFDM: (A) 4QAM, (B) 16QAM.

According to the comprehensive analytical frameworks of [98], and [115], ACO-OFDM attains equivalent order of BER functioning as HSF-Flip-OFDM for different orders of QAM modulation. The equivalence, in theory, is confirmed by the imitation outcomes proven in Figures 5.4 (A, B) and 5.5 (A, B), which show the two methods display similar behaviour in terms of the BER under the same modulation scheme. Proving the alignment between analytical derivations and simulated outcomes indicates the robustness of these models in estimating the error tolerance behavior of the assessed QAM constellation.

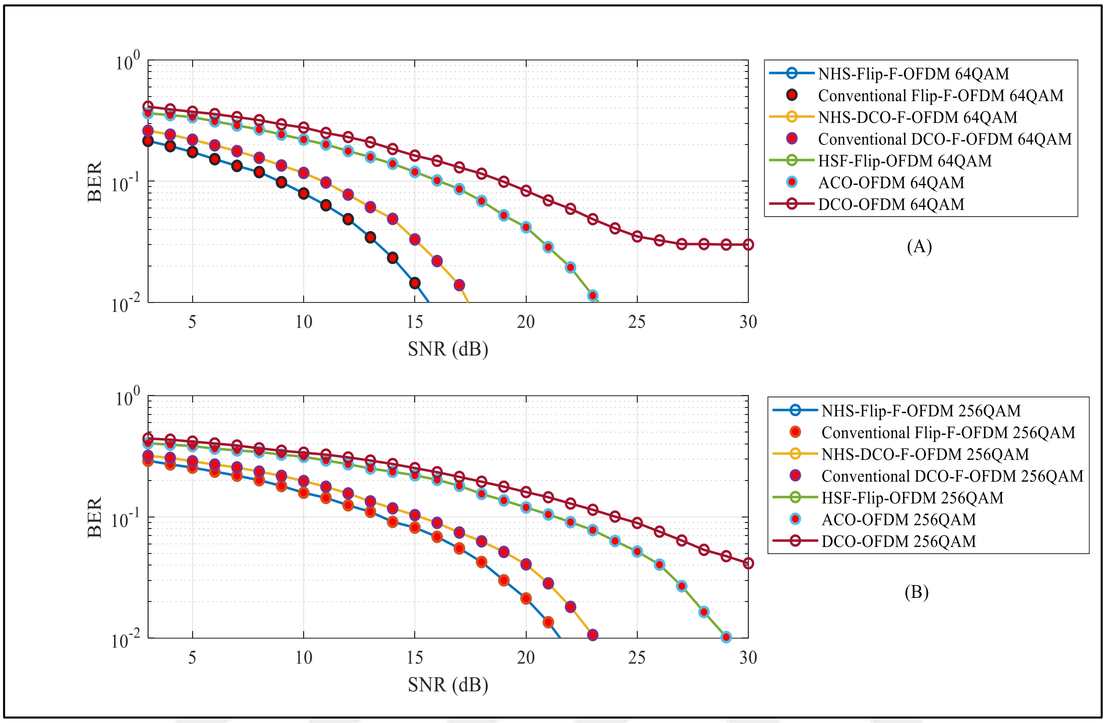

Figure 5.5: Valuation of BER among the Propositioned NHS-Flip-F-OFDM, Established Flip-F-OFDM, NHS-DCO-F-OFDM, Conventional DCO-F-OFDM, HSF-Flip-OFDM, ACO-OFDM, and DCO-OFDM: (A) 64QAM, (B) 256QAM.

5.5 PEAK-TO-AVERAGE-POWER RATIO (PAPR)

As previously established, the peak-average power ratio (PAPR) constitutes a pivotal metric in optical OFDM systems, exerting a pronounced influence on power efficiency during optical signal transmission. Elevated PAPR values signify a pronounced disparity between the average and peak power amplitudes, which exacerbates nonlinear distortions within optoelectronic subsystems and induces signal degradation. Conversely, diminished PAPR correlates with a more uniform temporal energy distribution, mitigating such impairments. While filtered OFDM architectures offer distinct advantages—notably inherent resilience against ISI—their practical deployment is constrained by elevated PAPR characteristics. This limitation arises from the nonlinear transfer characteristics of critical system components, including power amplifiers, data converters, and optoelectronic appliances like LEDs, photodiodes, and optical fibers.

It has been concluded from the mathematical analysis in sections (3.5.4) and (4.4.4) that the proposed NHS-F-OFDM approach efficiently avoids any growth in the PAPR. This means that the NHS-F-OFDM strategy can be used to realize unipolar F-OFDM waveforms while maintaining equivalent PAPR properties to the original unipolar F-OFDM schemes, and so will be backward compatible with power-efficient optoelectronic interfaces. Remarkably, this performance parity between the two PAPR measures illustrates a remarkable property: The robustness against distortion and spectral efficiency of traditional techniques is preserved with the framework, without the introduction of new nonlinear penalties or relaxation of transmitter dynamic range requirements.

The CCDF curves of the F-OFDM waveforms synthesized by the propositioned NHS-F-OFDM, as well as the propositioned Flip-F-OFDM, legacy Flip-F-OFDM, and both the propositioned and legacy DCO-F-OFDM architectures are given in Figure 5.6. The obtained PAPR curves (generated under a 16-QAM modulation with signaling lengths of L=512 and L=1024), confirm the invariance of PAPR characteristics with respect to cross-methodological variability. Among our schemes, the proposed and conventional Flip-F-OFDM schemes statistically match CCDF shapes, indicating that PAPR seemed to be independent of the modulation method and only governed by the temporal signal length, L, as a whole, wherein a directly proportional relationship between L and PAPR is found (i.e., longer signals lead to a higher peak power excursion, as seen in the rightward motion of CCDF lines in the case of L=1024).

Due to the unique manner in which the signal in the time-domain is constructed and the overarching amplitude modulation paradigm, the Flip-F-OFDM architecture would present a statistically significant reduction in PAPR as compared to a DC-biased optical F-OFDM. Furthermore, Flip-F-OFDM temporally balances the surrounding amplitudes between symbol intervals by flipping it with time symmetry by incorporating the phase-inversion (flipping) mechanism during the time-domain signal generation. This redistribution of power suppresses transients at the peak (in time) power, via interference cancellation (constructive-destructive), facilitating a more planar power envelope. Furthermore, the Flip-F-OFDM system uses systematic algorithms such as amplitude truncation and spectral shaping that minimize PAPR in terms of respect to linear dynamic range constraints of optoelectronic transmitters. On the other hand, DCO-F-OFDM utilizes a fixed DC offset to maintain unipolar signal compliance, which leads to a non-information-carrying power overhead that significantly increases PAPR. Since Flip-F-OFDM does not depend on such biasing and instead utilizes the inherent symmetry of its waveforms for its unipolarity, it, thus, avoids the PAPR increase due to biasing modulating methods.

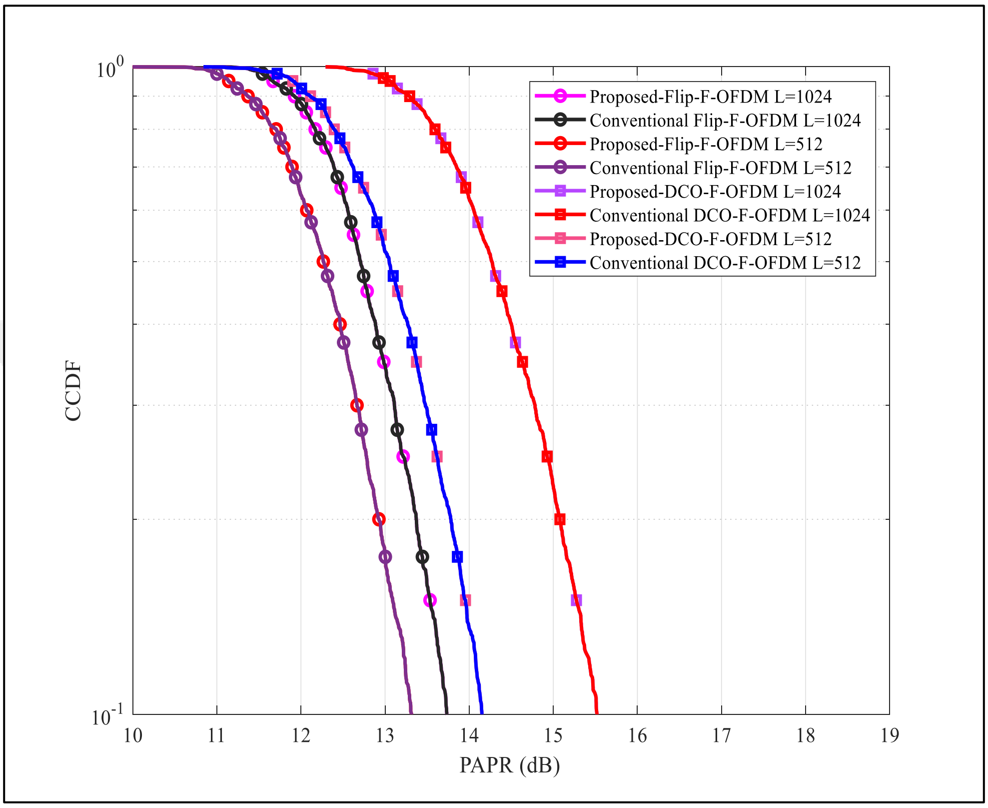

Figure 5.6: The CCDF Assessment of the Propositioned Flip−F−OFDM, Standard Flip−F−OFDM, the Propositioned DCO−F−OFDM, and Standard DCO-F-OFDM Using Signal Length: L=512, L=1024.

5.6 SUMMARY

This chapter methodologically investigated the numerically simulated outcomes of the proposed NHS-filtered OFDM framework, benchmarking its performance against conventional systems. A comparative analysis of critical metrics—computational complexity, spectral efficiency, BER, and PAPR—was conducted to systematically quantify the enhancements in system-level performance metrics achieved by the proposed techniques.

This approach significantly simplifies the system by removing the Hermitian symmetry constraints imposed on traditional benchmark systems, while maintaining its consistency with IM/DD architectures. This simplification in the structure provided smaller power utilisation and a reduced on-chip area. This framework has been significantly simplified, as it improves spectral efficiency by means of an optimized filter design, thereby reducing OOBE using spectral leakage mitigation. That allows very tight sub-band spacing, which ultimately can help to have very dense spectral packaging to meet high-throughput requirements. Moreover, a comparative analysis of PAPR highlights that Flip-F-OFDM provides improved functioning than DCO-F-OFDM which relies on advanced waveform engineering, that is, resampled time-domain signal at the output and interference-aware modulation, leading to a redistribution of peak power and preventing PAPR increase by DC-biasing process that affects classical designs.

6. CONCLUSIONS AND FUTURE WORKS

6.1 CONCLUSIONS

In this dissertation, the focus is on optimizing the computational efficiency and spectral performance of the OFDM modulation format for IM/DD-based VLC procedures. Beginning with a foundational comparative analysis of VLC and RF paradigms, an examination of the vital building blocks behind core VLC transceiver components and a critical appraisal of unipolar versions of OFDM adopted to meet IM/DD limitations as established through the initial discussions in Chapters 1 and 2. In Chapters 3 and 4, we proposed and comprehensively analyzed two new optical OFDM formats, specifically developed to accomplish a trade-off between spectral efficiency and computation tractability, whole enabling VLC systems to overcome the identified limitations, as summarized below.

Notably, the Filter-OFDM framework proved its advantages in spectral efficiency, which remains a challenge to meet future high-throughput data transmission requirements. Utilizing the advanced design of filters, the devised F-OFDM structure was able to suppress OOBE very effectively, which allowed for close in-between sub-band spacing in the spectrum diagram and overall, for even better spectral efficiency. The non-Hermitian symmetry (NHS)-F-OFDM paradigm represented a novel departure from traditional architectures by eliminating Hermitian symmetry constraints, resulting in the ability to fully utilize all N orthogonal subcarriers for payload transmission. Whereas such HS imposition is a legacy requirement towards generating real-valued signals in the intensity modulation/direct detection channel and thus conventional HS-based F-OFDM systems have always been a half subcarrier-spaced data transmission. Since HS is circumvented, the NHS-F-OFDM method essentially doubles the exploitable data rate while maintaining compatibility within IM/DD hardware absolute limitations, representing a paradigm shift in the efficiency of resource allocation for optical OFDM schemes.

In Chapter 3, the study introduced the NHS-DCO-F-OFDM scheme and showed that this scheme has considerable improvements contrasted to the established DCO-F-OFDM system. The suggested novel technique led to a 66.5% reduction in multiplicative operations and around 57% reduction in additive operations in both transmitter and receiver architectures.

They implemented methods to harness each degree-of-freedom without the constraints imposed by Hermitian symmetry whilst remaining consistent with IM/DD approaches.

The proposed approach bypasses Hermitian symmetry constraints by integrating the real and imaginary elements of the post-IFFT complex signal. Using an N/2- index IFFT to calculate an N-index FFT, the scheme significantly reduced computation requirements. This optimization also reduced power usage with integrated circuits in VLC approaches. Comparative analyses showed that the NHS-DCO-F-OFDM approach outperformed legacy OFDM-based methods (including HFS-OFDM, ACO-OFDM, and DCO-OFDM) in both spectra efficiency and BER functioning.

The new technique introduced by Chapter 4: Creation of NHS-Flip-F-OFDM, aimed to achieve higher bandwidth efficacy, lower PAPR at low computational cost. In contrast to the standard HS-based procedures, this framework removes both HS dependencies and retains compatibility with IM/DD procedures. It involves synthesizing a real-valued signal (integration of in-phase and quadrature parts of the complex F-OFDM waveform) followed by conversion into a non-bipolar format. The architecture also simplifies system design and significantly decreases resource usage by performing an N/4-index IFFT to realize an N-index FFT output.

The purported method decreases the hardware difficulty by ≈50% contrasted to the traditional Flip-F-OFDM which also minimizes power consumption while reducing the integrated circuit area in VLC systems. Additionally, the NHS-Flip-F-OFDM shows better computational complexity, spectral efficiency, and BER contrasted to the NHS-DCO-F-OFDM technique. In particular, this method does not lead to a PAPR increase over regular Flip-F-OFDM and thus more critically gives a superior performance over DCO-F-OFDM which is also suffers a PAPR increase in most cases.

Chapter 5 provides a comprehensive performance assessment of the proposed non-Hermitian symmetry (NHS) Filtered-OFDM framework with respect to its conventional and reference counterparts. It aimed to measure the ability of the propositioned method in improving the available performance metrics. A comparative analysis highlighting computational complexity, spectral efficiency, BER, and PAPR was done. These key performance indicators were exploited in order to define the gains permitted by the NHS-Filtered OFDM architecture. The findings highlighted its advantages in balancing trade-offs between efficiency on resources and integrity on signal, making it an attractive candidate for future communication systems.

The proposed techniques offer a fundamental and crucial step away from traditional and benchmark techniques in terms of system complexity, as they do not require HS, with full compatibility within IM/DD systems. This architectural simplification leads to decreased power requirements and a smaller integrated circuit footprint, yet this simplified complexity does end up with a decrease in communication performance from Filtered-OFDM (F-OFDM), which still has a strong functioning creating a significant gain on spectral efficiency for high data rates. Thanks to its filter design characteristic, F-OFDM achieves suppression of out-of-band emissions for more compact guard intervals between allocations and improved spectral utilization.

Moreover, simulations of a PAPR show that Flip-F-OFDM achieves lower PAPR than DCO-F-OFDM consistently. The upgrade arises through its unique modulation schemes and signal conditioning that correct for amplitude variations without affecting the integrity of the data transmission.

6.2 FUTURE WORKS

While this thesis advances the field through its proposed methodologies, persistent gaps and unresolved challenges warrant further investigation to fully realize the potential of non-Hermitian symmetry (NHS)-based systems. The following critical areas are identified as priorities for future research:

i. Channel Modeling and Impairment Mitigation: Develop advanced channel models for NHS-Filtered-OFDM in VLC systems, considering real-world challenges like nonlinearity, multipath propagation, and ambient light interference. Moreover, suggest adaptive equalization and pre-distortion approaches to reduce these impairments effectively.
ii. Hardware Implementation and Validation: Develop hardware prototypes to evaluate real-world performance metrics of NHS-Filtered-OFDM, including power consumption, latency, and spectral efficiency. Additionally, analyze the trade-offs

between computational complexity and deployment costs in practical visible light communication (VLC) systems.

iii. Performance in High Mobility Scenarios: Examine the performance of NHS-Filtered-OFDM in high-mobility scenarios, such as vehicular VLC systems or dynamic indoor environments, and grow strategies to mitigate doppler shift effects.

iv. Machine Learning for Adaptive Optimization: Apply machine learning models to enhance system parameters, including filter configurations and resource allocation, by adapting to real-time channel conditions and user demands.

v. Mitigate PAPR effects: Upcoming research can explore procedures such as pre-distortion, peak cancellation, and tone reservation in F-OFDM systems to effectively address peak-to-average power ratio challenges.

REFERENCES

[1] P. A. Loureiro, F. P. Guiomar, P. P. Monteiro, “Visible Light Communications: A Survey on Recent High-Capacity Demonstrations and Digital Modulation Techniques,” in *Photonics*, vol. 10, no. 9, pp. 993, 2023, doi:10.3390/photonics10090993.

[2] C. He, C Chen, “A Review of Advanced Transceiver Technologies in Visible Light Communications,” *Photonics*, vol. 10, no. 9, pp. 648, 2023, doi:10.3390/photonics10060648.

[3] W. Li, W. Zixiong, and Y Jinlong, "Performance Improvement by FRFT-OFDM for Visible Light Communication and Positioning Systems," in *Photonics*, vol. 11, no. 12, pp. 1147, 2024, doi:10.3390/photonics11121147.

[4] R. Zhang, J. Xiong, M. Li and L. Lu, "Design and Implementation of Low-Complexity Pre-Equalizer for 1.5 GHz VLC System," in *IEEE Photonics Journal*, vol. 16, no. 1, pp. 1-10, Feb. 2024, doi: 10.1109/JPHOT.2024.3351192.

[5] J. Bhattacharya *et al.*, "Implementation of OFDM modulator and demodulator subsystems using 16 point FFT/IFFT pipeline architecture in FPGA," *2017 8th IEEE Annual Information Technology, Electronics and Mobile Communication Conference (IEMCON)*, Vancouver, BC, Canada, 2017, pp. 295-300, doi: 10.1109/IEMCON.2017.8117223.

[6] P. Saengudomlert and S. Buddhacharya, "Unipolar GFDM With Dimming Support for Visible Light Communications," in *IEEE Transactions on Wireless Communications*, vol. 22, no. 12, pp. 9091-9104, Dec. 2023, doi: 10.1109/TWC.2023.3268121.

[7] Y. A. Zenhom, E. K. I. Hamad, E, M. Alghassab, & M. M. Elnabawy, “Optical-OFDM VLC System: Peak-to-Average Power Ratio Enhancement and Performance Evaluation,” in *Sensors*, vol. 24, no. 10, pp. 2965, 2024, doi:10.3390/s24102965.

[8] M. S. Ahmed, N. S. M. Shah, F. Ghawbar, Y. A. Jawhar, and A. A. Almohammedi, “Filtered-OFDM with channel coding based on T-distribution noise for underwater acoustic communication,” *J Ambient Intell Human Comput*, vol. 13, pp. 3379–3392, 2022, doi:10.1007/s12652-020-01713-9.

[9] A. J. Ramadhan, "Overview and comparison of candidate 5G waveforms: FBMC, UFMC and F-OFDM," *International Journal of Computer Network and Information Security*, vol. 14, no. 2, pp. 27-38, 2022, doi:10.5815/ijcnis.2022.02.03.

[10] S. D. Dissanayake and J. Armstrong, "Comparison of ACO-OFDM, DCO-OFDM and ADO-OFDM in IM/DD Systems," in *Journal of Lightwave Technology*, vol. 31, no. 7, pp. 1063-1072, April1, 2013, doi: 10.1109/JLT.2013.2241731.

[11] Y. Wang, Y. Wei, W. Zhang and C. -X. Wang, "Filtered-OFDM for Visible Light Communications," *2018 IEEE/CIC International Conference on Communications in China (ICCC Workshops)*, Beijing, China, 2018, pp. 227-231, doi: 10.1109/ICCChinaW.2018.8674487.

[12] K. Ramadan, B. M. ElHalawany, & M. S. Elbakry, “Performance improvement for DCO-OFDM and ACO-OFDM systems using symbol time compression,” *Telecommun Syst*, vol. 84, pp. 77–100, 2023, doi:10.1007/s11235-023-01027-z.

[13] M. F. Sanya, L. Djogbe, A. Vianou and C. Aupetit-Berthelemot, "DC-biased optical OFDM for IM/DD passive optical network systems," in *Journal of Optical Communications and Networking*, vol. 7, no. 4, pp. 205-214, April 2015, doi: 10.1364/JOCN.7.000205.

[14] C. He and J. Armstrong, "Clipping Noise Mitigation in Optical OFDM Systems," in *IEEE Communications Letters*, vol. 21, no. 3, pp. 548-551, March 2017, doi: 10.1109/LCOMM.2016.2643630.

[15] L. E. M. Matheus, A. B. Vieira, L. F. M. Vieira, M. A. M. Vieira and O. Gnawali, "Visible Light Communication: Concepts, Applications and Challenges," in *IEEE Communications Surveys & Tutorials*, vol. 21, no. 4, pp. 3204-3237, Fourthquarter 2019, doi: 10.1109/COMST.2019.2913348.

[16] J-M. Dilhac, "The telegraph of claude chappe-an optical telecommunication network for the xviiith century." *Institut National des Sciences Appliquées de Toulouse*, pp. 1-8, Jul 2001.

[17] S. Manohar, and D. Razansky, "Photoacoustics: a historical review," *Advances in optics and photonics*, vol. 8, no. 4, pp. 586-617, 2016, doi:10.1364/AOP.8.000586.

[18] F. R. Gfeller and U. Bapst, "Wireless in-house data communication via diffuse infrared radiation," in *Proceedings of the IEEE*, vol. 67, no. 11, pp. 1474-1486, Nov. 1979, doi: 10.1109/PROC.1979.11508.

[19] G. W. Marsh and J. M. Kahn, "Performance evaluation of experimental 50-Mb/s diffuse infrared wireless link using on-off keying with decision-feedback equalization," in *IEEE Transactions on Communications*, vol. 44, no. 11, pp. 1496-1504, Nov. 1996, doi: 10.1109/26.544466.

[20] Y. Tanaka, T. Komine, S. Haruyama, & M. Nakagawa, “Indoor visible light data transmission system utilizing white LED lights,” *IEICE Transactions on Communications*, vol. E86-B, no. 8, pp.2440-2454, 2003.

[21] A. Jovicic, J. Li and T. Richardson, "Visible light communication: opportunities, challenges and the path to market," in *IEEE Communications Magazine*, vol. 51, no. 12, pp. 26-32, December 2013, doi: 10.1109/MCOM.2013.6685754.

[22] E. Monteiro and S. Hranilovic, "Design and Implementation of Color-Shift Keying for Visible Light Communications," in *Journal of Lightwave Technology*, vol. 32, no. 10, pp. 2053-2060, May15, 2014, doi: 10.1109/JLT.2014.2314358.

[23] M. Ayyash *et al*., "Coexistence of WiFi and LiFi toward 5G: concepts, opportunities, and challenges," in *IEEE Communications Magazine*, vol. 54, no. 2, pp. 64-71, February 2016, doi: 10.1109/MCOM.2016.7402263.

[24] D. Svilen, and H. Haas. *Principles of LED light communications: towards networked Li-Fi*. Cambridge University Press, 2015.

[25] D. Karunatilaka, F. Zafar, V. Kalavally and R. Parthiban, "LED Based Indoor Visible Light Communications: State of the Art," in *IEEE Communications Surveys & Tutorials*, vol. 17, no. 3, pp. 1649-1678, thirdquarter 2015, doi: 10.1109/COMST.2015.2417576.

[26] H. Burchardt, N. Serafimovski, D. Tsonev, S. Videv and H. Haas, "VLC: Beyond point-to-point communication," in *IEEE Communications Magazine*, vol. 52, no. 7, pp. 98-105, July 2014, doi: 10.1109/MCOM.2014.6852089.

[27] S. Schmid, J. Ziegler, G. Corbellini, T. R. Gross, and S. Mangold, "Using consumer LED light bulbs for low-cost visible light communication systems," in *Proceedings of the 1st ACM MobiCom workshop on Visible light communication systems*, pp. 9-14, Sep. 2014.

[28] G. Blinowski, "Security of visible light communication systems—A survey," *Physical Communication*, vol. 34, pp. 246-260, 2019.

[29] C. J. Hansen, "WiGiG: Multi-gigabit wireless communications in the 60 GHz band," in *IEEE Wireless Communications*, vol. 18, no. 6, pp. 6-7, December 2011, doi: 10.1109/MWC.2011.6108325.

[30] A. H. Azhar, T. -A. Tran and D. O'Brien, "A Gigabit/s Indoor Wireless Transmission Using MIMO-OFDM Visible-Light Communications," in *IEEE Photonics Technology Letters*, vol. 25, no. 2, pp. 171-174, Jan.15, 2013, doi: 10.1109/LPT.2012.2231857.

[31] A. Gomez *et al*., "Beyond 100-Gb/s Indoor Wide Field-of-View Optical Wireless Communications," in *IEEE Photonics Technology Letters*, vol. 27, no. 4, pp. 367-370, 15 Feb.15, 2015, doi: 10.1109/LPT.2014.2374995.

[32] C. Medina, Z. Mayteé, and K. Navarro, "Led based visible light communication: Technology, applications and challenges-a survey," *International Journal of Advances in Engineering & Technology*, vol. 8, no. 4, pp. 482-495, 2015.

[33] P. H. Pathak, X. Feng, P. Hu and P. Mohapatra, "Visible Light Communication, Networking, and Sensing: A Survey, Potential and Challenges," in *IEEE Communications Surveys & Tutorials*, vol. 17, no. 4, pp. 2047-2077, Fourthquarter 2015, doi: 10.1109/COMST.2015.2476474.

[34] Q. Wang, G. Domenico, and G. Omprakash, "Low-cost, flexible and open platform for visible light communication networks," in *Proceedings of the 2nd International Workshop on Hot Topics in Wireless*, pp. 31-35, 2015, doi:10.1145/2799650.2799655.

[35] Q. Wang, G. Domenico, and D. Puccinelli, "Open VLC: Software-defined visible light embedded networks," in *Proceedings of the 1st ACM Mobi Com workshop on Visible light communication systems*, pp. 15-20, 2014.

[36] H. Z. Dhaam, F. M. Ali, "Optical GFDM for indoor visible light communication: a comprehensive review and future outlook," *Journal of Optics*, 2024, doi:10.1007/s12596-024-02061-z.

[37] S. Kumar, P. Singh, "A Comprehensive Survey of Visible Light Communication: Potential and Challenges," *Wireless Pers Commun*, vol. 109, pp. 1357–1375, 2019, doi:10.1007/s11277-019-06616-3.

[38] S. Idris, A. M. Aibinu, G. Koyunlu and J. Sanusi, "A Survey of Modulation Schemes in Visible Light Communications," *2019 3rd International Conference on Trends in Electronics and Informatics (ICOEI)*, Tirunelveli, India, 2019, pp. 1-7, doi: 10.1109/ICOEI.2019.8862538.

[39] H. Le Minh *et al*., "100-Mb/s NRZ Visible Light Communications Using a Postequalized White LED," in *IEEE Photonics Technology Letters*, vol. 21, no. 15, pp. 1063-1065, Aug.1, 2009, doi: 10.1109/LPT.2009.2022413.

[40] G. Stepniak, M. Lukasz, and S. Jerzy, "1.1 GBIT/S white lighting LED-based visible light link with pulse amplitude modulation and Volterra DFE equalization," *Microwave and Optical Technology Letters*, vol. 57, no. 7, pp. 1620-1622, 2015, doi:10.1002/mop.29182.

[41] G. Stepniak, J. Siuzdak and P. Zwierko, "Compensation of a VLC Phosphorescent White LED Nonlinearity by Means of Volterra DFE," in *IEEE Photonics Technology Letters*, vol. 25, no. 16, pp. 1597-1600, Aug.15, 2013, doi: 10.1109/LPT.2013.2272511.

[42] X. Li *et al*., "μLED-Based Single-Wavelength Bi-directional POF Link With 10 Gb/s Aggregate Data Rate," in *Journal of Lightwave Technology*, vol. 33, no. 17, pp. 3571-3576, 1 Sept.1, 2015, doi: 10.1109/JLT.2015.2443984.

[43] T. T. Ağır, M. Sönmez, “The modulation classification methods in PPM–VLC systems,” *Opt Quant Electron*, vol. 55, no. 223, 2023, doi:10.1007/s11082-022-04520-y.

[44] S. He, G. Ren, Z. Zhong and Y. Zhao, "M-ary Variable Period Modulation for Indoor Visible Light Communication System," in *IEEE Communications Letters*, vol. 17, no. 7, pp. 1325-1328, July 2013, doi: 10.1109/LCOMM.2013.060513.131046.

[45] H. Elgala, R. Mesleh and H. Haas, "Indoor optical wireless communication: potential and state-of-the-art," in *IEEE Communications Magazine*, vol. 49, no. 9, pp. 56-62, September 2011, doi: 10.1109/MCOM.2011.6011734.

[46] M. Noshad and M. Brandt-Pearce, "Application of Expurgated PPM to Indoor Visible Light Communications—Part I: Single-User Systems," in *Journal of Lightwave Technology*, vol. 32, no. 5, pp. 875-882, March1, 2014, doi: 10.1109/JLT.2013.2293341.

[47] Bo Bai, Zhengyuan Xu and Yangyu Fan, "Joint LED dimming and high capacity visible light communication by overlapping PPM," *The 19th Annual Wireless and Optical Communications Conference (WOCC 2010)*, Shanghai, 2010, pp. 1-5, doi: 10.1109/WOCC.2010.5510410.

[48] C. Quintana, V. Guerra, J. Rufo, J. Rabadan and R. Perez-Jimenez, "Reading lamp-based visible light communication system for in-flight entertainment," in *IEEE Transactions on Consumer Electronics*, vol. 59, no. 1, pp. 31-37, February 2013, doi: 10.1109/TCE.2013.6490238.

[49] D. Karunatilaka, F. Zafar, V. Kalavally and R. Parthiban, "LED Based Indoor Visible Light Communications: State of the Art," in *IEEE Communications Surveys & Tutorials*, vol. 17, no. 3, pp. 1649-1678, thirdquarter 2015, doi: 10.1109/COMST.2015.2417576.

[50] E. Monteiro and S. Hranilovic, "Design and Implementation of Color-Shift Keying for Visible Light Communications," in *Journal of Lightwave Technology*, vol. 32, no. 10, pp. 2053-2060, May15, 2014, doi: 10.1109/JLT.2014.2314358.

[51] "IEEE Standard for Local and Metropolitan Area Networks--Part 15.7: Short-Range Wireless Optical Communication Using Visible Light," in *IEEE Std 802.15.7-2011*, vol., no., pp.1-309, 6 Sept. 2011, doi: 10.1109/IEEE STD.2011.6016195.

[52] D. Tsonev, S. Videv, and H. Haas, Light fidelity (Li-Fi): towards all-optical networking." *Broadband Access Communication Technologies VIII*, vol. 9007. SPIE, pp. 900702, 2014, doi:10.1117/12.2044649.

[53] D. Tsonev and H. Haas, "Avoiding spectral efficiency loss in unipolar OFDM for optical wireless communication," *2014 IEEE International Conference on Communications (ICC)*, Sydney, NSW, Australia, 2014, pp. 3336-3341, doi: 10.1109/ICC.2014.6883836.

[54] J. Armstrong, "OFDM for Optical Communications," in *Journal of Lightwave Technology*, vol. 27, no. 3, pp. 189-204, Feb.1, 2009, doi: 10.1109/JLT.2008.2010061.

[55] M. Z. Afgani, H. Haas, H. Elgala and D. Knipp, "Visible light communication using OFDM," *2nd International Conference on Testbeds and Research Infrastructures for the Development of Networks and Communities, TRIDENTCOM 2006.*, Barcelona, Spain, 2006, pp. 6 pp.-134, doi: 10.1109/TRIDNT.2006.1649137.

[56] J. Armstrong, "OFDM for Optical Communications," in *Journal of Lightwave Technology*, vol. 27, no. 3, pp. 189-204, Feb.1, 2009, doi: 10.1109/JLT.2008.2010061.

[57] B. A. Vijayalakshmi, A. S. Kumar, V. Kavitha, *et al.*, “VLC modulation techniques in home automation system using light emitting diodes for data transmission,” *J Opt*, vol. 53, no. 3, pp. 2428–2434, 2024, doi:10.1007/s12596-023-01416-2.

[58] J. Armstrong and B. J. C. Schmidt, "Comparison of Asymmetrically Clipped Optical OFDM and DC-Biased Optical OFDM in AWGN," in *IEEE Communications Letters*, vol. 12, no. 5, pp. 343-345, May 2008, doi: 10.1109/LCOMM.2008.080193.

[59] J. M. Tang and K. A. Shore, "Maximizing the Transmission Performance of Adaptively Modulated Optical OFDM Signals in Multimode-Fiber Links by Optimizing Analog-to-Digital Converters," in *Journal of Lightwave Technology*, vol. 25, no. 3, pp. 787-798, March 2007, doi: 10.1109/JLT.2006.890457.

[60] J. Armstrong, and A. J. Lowery, "Power efficient optical OFDM," *Electronics letters*, vol. 42, no. 6, 2006.

[61] F. Barrami, Y. Le Guennec, E. Novakov and P. Busson, "An optical power efficient asymmetrically companded DCO-OFDM for IM/DD systems," *2014 23rd Wireless and Optical Communication Conference (WOCC)*, Newark, NJ, USA, 2014, pp. 1-6, doi: 10.1109/WOCC.2014.6839934.

[62] N. Fernando, Y. Hong and E. Viterbo, "Flip-OFDM for optical wireless communications," *2011 IEEE Information Theory Workshop*, Paraty, Brazil, 2011, pp. 5-9, doi: 10.1109/ITW.2011.6089566.

[63] N. Fernando, Y. Hong and E. Viterbo, "Flip-OFDM for Unipolar Communication Systems," in *IEEE Transactions on Communications*, vol. 60, no. 12, pp. 3726-3733, December 2012, doi: 10.1109/TCOMM.2012.082712.110812.

[64] S. D. Dissanayake, J. Armstrong and S. Hranilovic, "Performance analysis of noise cancellation in a diversity combined ACO-OFDM system," *2012 14th International Conference on Transparent Optical Networks (ICTON)*, Coventry, UK, 2012, pp. 1-4, doi: 10.1109/ICTON.2012.6253910.

[65] R. Islam, P. Choudhury and M. A. Islam, "Analysis of DCO-OFDM and flip-OFDM for IM/DD optical-wireless system," *8th International Conference on Electrical and Computer Engineering*, Dhaka, Bangladesh, 2014, pp. 32-35, doi: 10.1109/ICECE.2014.7026929.

[66] M. A. EA. Eltoukhi, M. Abd-Elnaby, S. A. El-Dolil, *et al.*, “Efficient coding techniques for ADO-OFDM in IM/DD systems,” *Photon Netw Commun*, vol. 36, pp. 128–139, 2018, doi:10.1007/s11107-018-0762-z.

[67] S. M. Hameed, S. M. Abdulsatar, and A. A. Sabri, "Visible light communication performance using MIMO-ADO-OFDM system," *Transactions on Emerging Telecommunications Technologies*, vol. 33, no. 7, pp. e4493, 2022, doi:10.1002/ett.4493.

[68] S. M. Hameed, S. M. Abdulsatar, and A. A. Sabri, "Performance enhancement for visible light communication based ADO-OFDM," *Optical and Quantum Electronics*, vol. 53, no. 6, pp. 339, 2021, doi:10.1007/s11082-021-02965-1.

[69] S. M. Farid, M. Z. Saleh, H. M. Elbadawy, *et al.*, "ASCO-OFDM based VLC system throughput improvement using PAPR precoding reduction techniques," *Opt Quant Electron*, vol. 55, pp. 410, 2023, doi:10.1007/s11082-023-04651-w.

[70] M. S. Baig, M. T. Alresheedi, M. A. Mahdi, *et al.*, "A spectrally efficient modified asymmetrically and symmetrically clipped optical (mASCO)-OFDM for IM/DD systems," *Opt Quant Electron*, vol. 55, pp. 411, 2023, doi:10.1007/s11082-023-04611-4.

[71] C. Gunturu, and S. Valluri, "A new complexity reduction scheme in selective mapping-based visible light communication direct current-biased optical orthogonal frequency division multiplexing systems," *IET Optoelectronics*, vol. 16, no. 5, pp. 207-217, 2022, doi: 10.1049/ote2.12074.

[72] D. W. Dawoud, F. Héliot, M. A. Imran and R. Tafazolli, "A Novel Unipolar Transmission Scheme for Visible Light Communication," in *IEEE Transactions on Communications*, vol. 68, no. 4, pp. 2426-2437, April 2020, doi: 10.1109/TCOMM.2019.2963377.

[73] W. Tong, J. Ma and P. Zhu Huawei, "Enabling technologies for 5G air-interface with emphasis on spectral efficiency in the presence of very large number of links," *2015 21st Asia-Pacific Conference on Communications (APCC)*, Kyoto, Japan, 2015, pp. 184-187, doi: 10.1109/APCC.2015.7412508.

[74] J. Abdoli, M. Jia and J. Ma, "Filtered OFDM: A new waveform for future wireless systems," *2015 IEEE 16th International Workshop on Signal Processing Advances in Wireless Communications (SPAWC)*, Stockholm, Sweden, 2015, pp. 66-70, doi: 10.1109/SPAWC.2015.7227001.

[75] M. Y. I. Afifi, E-S. S. A. Said, A. A. E-A. Ammar, "An Efficient Performance of OFDM-Shaped Symbol for 5G Green Communication Compared to FBMC," *Advances*

in Science, Technology and Engineering Systems Journal (ASTESJ), vol. 5, no. 6, pp. 1163-1170, 2020, doi:10.25046/aj0506140.

[76] S. M. Hameed, A. A. Sabri, and S. M. Abdulsatar, “Filtered OFDM for underwater wireless optical communication,” *Opt Quant Electron*, vol. 55, pp. 77, 2023, doi:10.1007/s11082-022-04359-3.

[77] K. Ramadan, B. M. ElHalawany, and M. S. Elbakry, “Performance improvement for DCO-OFDM and ACO-OFDM systems using symbol time compression,” *Telecommun Syst*, vol. 84, pp. 77–100, 2023, doi:10.1007/s11235-023-01027-z.

[78] A. Farhang, N. Marchetti, F. Figueiredo and J. P. Miranda, "Massive MIMO and waveform design for 5th generation wireless communication systems," *1st International Conference on 5G for Ubiquitous Connectivity*, Akaslompolo, Finland, 2014, pp. 70-75, doi: 10.4108/icst.5gu.2014.258195.

[79] V. Vakilian, T. Wild, F. Schaich, S. ten Brink and J. -F. Frigon, "Universal-filtered multi-carrier technique for wireless systems beyond LTE," *2013 IEEE Globecom Workshops (GC Wkshps)*, Atlanta, GA, USA, 2013, pp. 223-228, doi: 10.1109/GLOCOMW.2013.6824990.

[80] H. Kuriki, K. Mizutani, T. Matsumura and H. Harada, "Enhanced UF-OFDM for Long-Delay Multipath Fading Environment," *2017 IEEE 85th Vehicular Technology Conference (VTC Spring)*, Sydney, NSW, Australia, 2017, pp. 1-5, doi: 10.1109/VTCSpring.2017.8108398.

[81] M. Y.I. Afifi, M. S. Elbakry, E. S. S. Soliman, and A. A. Ammar, “An efficient technique for out-of-band power reduction for the eliminated CP-STC-shaped system for 5G requirements,” *International Journal of Electrical and Computer Engineering*, vol. 10, no. 5, pp. 5306-5315, 2020, doi: 10.11591/ijece.v10i5.

[82] L. Zhang, A. Ijaz, P. Xiao, M. M. Molu and R. Tafazolli, "Filtered OFDM Systems, Algorithms, and Performance Analysis for 5G and Beyond," in *IEEE Transactions on Communications*, vol. 66, no. 3, pp. 1205-1218, March 2018, doi: 10.1109/TCOMM.2017.2771242.

[83] T. Deepa, N. Bharathiraja, “Performance Evaluation of Polar Coded Filtered OFDM for Low Latency Wireless Communications,” *Wireless Pers Commun*, vol. 116, pp. 2023–2034, 2021, doi:10.1007/s11277-020-07777-2.

[84] X. Cheng, Y. He, B. Ge and C. He, "A Filtered OFDM Using FIR Filter Based on Window Function Method," *2016 IEEE 83rd Vehicular Technology Conference (VTC Spring)*, Nanjing, China, 2016, pp. 1-5, doi: 10.1109/VTCSpring.2016.7504065.

[85] S. Roy and A. Chandra, "Interpolated Band-pass Method Based Narrow-band FIR Filter: A Prospective Candidate in Filtered-OFDM Technique for the 5G Cellular Network," *TENCON 2019 - 2019 IEEE Region 10 Conference (TENCON)*, Kochi, India, 2019, pp. 311-315, doi: 10.1109/TENCON.2019.8929601.

[86] F. A. P. de Figueiredo, N. F. T. Aniceto, J. Seki, I. Moerman and G. Fraidenraich, "Comparing f-OFDM and OFDM Performance for MIMO Systems Considering a 5G Scenario," *2019 IEEE 2nd 5G World Forum (5GWF)*, Dresden, Germany, 2019, pp. 532-535, doi: 10.1109/5GWF.2019.8911702.

[87] Huawei, H. F-OFDM Scheme and Filter Design. In Proceedings of the 3GPP Contribution R1-165425, Nanjing, China, 23–27, May 2016.

[88] M. Chen *et al.*, "Real-Time Generation of NHS-OFDM Signal for Direct-Modulation and Direct-Detection PON," in *IEEE Photonics Technology Letters*, vol. 33, no. 11, pp. 533-536, 1 June1, 2021, doi: 10.1109/LPT.2021.3073971.

[89] N. Cvijetic, "OFDM for Next-Generation Optical Access Networks," in *Journal of Lightwave Technology*, vol. 30, no. 4, pp. 384-398, Feb.15, 2012, doi: 10.1109/JLT.2011.2166375.

[90] A. W. Azim, Y. Le Guennec, and G. Maury, "Hermitian symmetry free optical-single-carrier frequency division multiple access for visible light communication," *Optics Communications*, vol. 415, pp. 177-185, 2018, doi:10.1016/j.optcom.2018.01.036.

[91] R. Yang *et al.*, "Spectral and Energy Efficiency of DCO-OFDM in Visible Light Communication Systems With Finite-Alphabet Inputs," in *IEEE Transactions on*

Wireless Communications, vol. 21, no. 8, pp. 6018-6032, Aug. 2022, doi: 10.1109/TWC.2022.3145288.

[92] X. Zhang, Y. F. Zhou, Y. P. Yu, P. C. Han, and X. Wang, "Comparison and Analysis of DCO-OFDM, ACO-OFDM and ADO-OFDM in IM/DD Systems," *Applied Mechanics and Materials*, vol. 701, pp. 1059-1062, 2015.

[93] M. F. Sanya, C. Aupetit-Berthelemot, L. Djogbe and A. Vianou, "D-C ACO-OFDM and DCO-OFDM for passive optical network: Performance comparison in IM/DD fiber link," *2014 23rd Wireless and Optical Communication Conference (WOCC)*, Newark, NJ, USA, 2014, pp. 1-5, doi: 10.1109/WOCC.2014.6839940.

[94] T. Zhang, L. Sun, C. Zhao, S. Qiao and Z. Ghassemlooy, "Low-Complexity Receiver for HACO-OFDM in Optical Wireless Communications," in *IEEE Wireless Communications Letters*, vol. 10, no. 3, pp. 572-575, March 2021, doi: 10.1109/LWC.2020.3038181.

[95] S. M. Farid, M. Z. Saleh, H. M. Elbadawy and S. H. Elramly, "Novel Unipolar Optical Modulation Techniques for Enhancing Visible Light Communication Systems Performance," in *IEEE Access*, vol. 10, pp. 67925-67939, 2022, doi: 10.1109/ACCESS.2022.3186007.

[96] X. Huang, F. Yang, C. Pan and J. Song, "Pre-Distorted ADO-OFDM for Mutual Interference Eliminating with Low Complexity and Low Latency," *2020 IEEE International Conference on Communications Workshops (ICC Workshops)*, Dublin, Ireland, 2020, pp. 1-6, doi: 10.1109/ICCWorkshops49005.2020.9145474.

[97] S. Vappangi and V. V. Mani, "Performance analysis of fast optical OFDM for VLC," *2017 20th International Symposium on Wireless Personal Multimedia Communications (WPMC)*, Bali, Indonesia, 2017, pp. 206-211, doi: 10.1109/WPMC.2017.8301809.

[98] F. Barrami, Y. Le Guennec, E. Novakov, J. -M. Duchamp and P. Busson, "A novel FFT/IFFT size efficient technique to generate real time optical OFDM signals compatible with IM/DD systems," *2013 European Microwave Conference*, Nuremberg, Germany, 2013, pp. 1247-1250, doi: 10.23919/EuMC.2013.6686890.

[99] M. Chen *et al.*, "Experimental Demonstration of an IFFT/FFT Size Efficient DFT-Spread OFDM for Short Reach Optical Transmission Systems," in *Journal of Lightwave Technology*, vol. 34, no. 9, pp. 2100-2105, 1 May1, 2016, doi: 10.1109/JLT.2016.2529429.

[100] X. Deng, S. Mardanikorani, G. Zhou and J. -P. M. G. Linnartz, "DC-Bias for Optical OFDM in Visible Light Communications," in *IEEE Access*, vol. 7, pp. 98319-98330, 2019, doi: 10.1109/ACCESS.2019.2928944.

[101] A. A. Abdulkafi, M. Y. Alias and Y. S. Hussein, "Performance analysis of DCO-OFDM in VLC system," *2015 IEEE 12th Malaysia International Conference on Communications (MICC)*, Kuching, Malaysia, 2015, pp. 163-168, doi: 10.1109/MICC.2015.7725427.

[102] S. Mazahir, A. Chaaban, H. Elgala and M. -S. Alouini, "Achievable Rates of Multi-Carrier Modulation Schemes for Bandlimited IM/DD Systems," in *IEEE Transactions on Wireless Communications*, vol. 18, no. 3, pp. 1957-1973, March 2019, doi: 10.1109/TWC.2019.2901479.

[103] B. Tang, K. Qin, X. Zhang and C. Chen, "A Clipping-Noise Compression Method to Reduce PAPR of OFDM Signals," in *IEEE Communications Letters*, vol. 23, no. 8, pp. 1389-1392, Aug. 2019, doi: 10.1109/LCOMM.2019.2916052.

[104] J. Shi, et al., "Geometrically shaped 32QAM and modified binary switching coding method in underwater visible light communication," *Chinese Journal of Electronics*, vol. 31, no. 6, pp. 1106-1111, 2022, doi:10.1049/cje.2022.00.057.

[105] W. Tong, J. Ma and P. Zhu Huawei, "Enabling technologies for 5G air-interface with emphasis on spectral efficiency in the presence of very large number of links," *2015 21st Asia-Pacific Conference on Communications (APCC)*, Kyoto, Japan, 2015, pp. 184-187, doi: 10.1109/APCC.2015.7412508.

[106] M. Alhalabi, F. I. El-Nahal and N. Taşpinar, "Comparison of different modulation techniques for optical OFDM Intensity Modulation and Direct Detection IM/DD system," *2019 IEEE 7th Palestinian International Conference on Electrical and*

Computer Engineering (PICECE), Gaza, Palestine, 2019, pp. 1-4, doi: 10.1109/PICECE.2019.8747252.

[107] F. A. P. de Figueiredo, N. F. T. Aniceto, J. Seki, I. Moerman and G. Fraidenraich, "Comparing f-OFDM and OFDM Performance for MIMO Systems Considering a 5G Scenario," *2019 IEEE 2nd 5G World Forum (5GWF)*, Dresden, Germany, 2019, pp. 532-535, doi: 10.1109/5GWF.2019.8911702.

[108] H. S. R. Hujijo, M. Ilyas, A. A. Qasim and U. Ullah, "Certain Investigation of Filtered-OFDM in Visible Light Communications system," *2023 7th International Conference on Computing Methodologies and Communication (ICCMC)*, Erode, India, 2023, pp. 1455-1459, doi: 10.1109/ICCMC56507.2023.10084283.

[109] S. G. Johnson and M. Frigo, "A Modified Split-Radix FFT With Fewer Arithmetic Operations," in *IEEE Transactions on Signal Processing*, vol. 55, no. 1, pp. 111-119, Jan. 2007, doi: 10.1109/TSP.2006.882087.

[110] J. W. Cooley, and J. W. Tukey, "An algorithm for the machine calculation of complex Fourier series," *Mathematics of computation*, vol. 19, no. 90, pp. 297-301, 1965.

[111] Y. A. Al-Jawhar, et al., "Improving PAPR performance of filtered OFDM for 5G communications using PTS," *ETRI Journal*, vol. 43, no. 2, pp. 209-220, 2021.

[112] J. Wei, Y. Wang, C. Gong and N. Huang, "Noise Analysis and Modulation Optimization for Nonlinear Visible Light Communication System With Signal-Dependent Noise," in *IEEE Photonics Journal*, vol. 15, no. 6, pp. 1-11, Dec. 2023, Art no. 7304511, doi: 10.1109/JPHOT.2023.3323139.

[113] E. Vanin, "Performance evaluation of intensity modulated optical OFDM system with digital baseband distortion," *Optics Express*, vol. 19, no. 5, pp. 4280-4293, 2011.

[114] H. Elgala, R. Mesleh and H. Haas, "Practical considerations for indoor wireless optical system implementation using OFDM," *2009 10th International Conference on Telecommunications*, Zagreb, Croatia, 2009, pp. 25-29.

[115] F. Barrami, *Low-complexity direct-detection optical OFDM systems for high data rate communications*. Ph.D. dissertation, Université Grenoble Alpes, 2015.

[116] L. Wu, L. Kong, Z. Zhang, J. Dang and H. Liu, "Wide-range Dimmable Clipped Flip-OFDM For Indoor Visible Light Communications," *2018 IEEE/CIC International Conference on Communications in China (ICCC)*, Beijing, China, 2018, pp. 121-125, doi: 10.1109/ICCChina.2018.8641241.

[117] S. F. Nawaf and A. Bouallegue, "Investigation the Performance of ACO-OFDM, DCO-OFDM in Visible Light Communication System," *2023 22nd Mediterranean Microwave Symposium (MMS)*, Sousse, Tunisia, 2023, pp. 1-6, doi: 10.1109/MMS59938.2023.10421678.

[118] Z. Wang, T. Mao and Q. Wang, "Optical OFDM for visible light communications," *2017 13th International Wireless Communications and Mobile Computing Conference (IWCMC)*, Valencia, Spain, 2017, pp. 1190-1194, doi: 10.1109/IWCMC.2017.7986454.

[119] J. Koti and M. B K, "Performance Analysis of Unipolar Communication Techniques for Optical Wireless Communication," *2018 International Conference on Networking, Embedded and Wireless Systems (ICNEWS)*, Bangalore, India, 2018, pp. 1-6, doi: 10.1109/ICNEWS.2018.8903931.

[120] S. M. Hameed, A. A. Sabri, and S. M. Abdulsatar, "A novel PAPR reduction method for ADO-OFDM VLC systems," *Optical and Quantum Electronics*, vol. 53, no. 10, pp. 595, 2021, doi:10.1007/s11082-021-03251-w.

[121] U. Choudhary, and V. Janyani, "Bandwidth efficient frame structures for flip OFDM with phase conjugated sub carriers and LDPC encoding," *Optik*, vol. 204, pp. 164175, 2020.

[122] S. Temurtaş, G. Toprakcı and A. Özen, "Enhancing the Performance of Flip-OFDM Systems with Channel Coding Techniques for Visible Light Communications," *2021 International Conference on Electrical, Computer, Communications and Mechatronics Engineering (ICECCME)*, Mauritius, Mauritius, 2021, pp. 1-5, doi: 10.1109/ICECCME52200.2021.9591144.

[123] N. Huang, J. -B. Wang, C. Pan, J. -Y. Wang, Y. Pan and M. Chen, "Iterative Receiver for Flip-OFDM in Optical Wireless Communication," in *IEEE Photonics Technology*

Letters, vol. 27, no. 16, pp. 1729-1732, 15 Aug.15, 2015, doi: 10.1109/LPT.2015.2438338.

[124] P. Saengudomlert, "Flip wavelet packet modulation for visible light communications with intensity modulation and direct detection," *2017 International Electrical Engineering Congress (iEECON)*, Pattaya, Thailand, 2017, pp. 1-4, doi: 10.1109/IEECON.2017.8075841.

[125] M. S. Ahmed, N. S. M. Shah, F. Ghawbar, *et al.*, "Filtered-OFDM with channel coding based on T-distribution noise for underwater acoustic communication," *J Ambient Intell Human Comput*, vol. 13, pp. 3379–3392, 2022, doi:10.1007/s12652-020-01713-9.

[126] Q. Zheng, F. Wang, X. Chen, Y. Liu, D. Miao and Z. Zhao, "Comparison of 5G waveform candidates in high speed scenario," *2017 XXXIInd General Assembly and Scientific Symposium of the International Union of Radio Science (URSI GASS)*, Montreal, QC, Canada, 2017, pp. 1-4, doi: 10.23919/URSIGASS.2017.8105377.

[127] A. Loulou *et al*., "Multiplierless Filtered-OFDM Transmitter for Narrowband IoT Devices," in *IEEE Internet of Things Journal*, vol. 7, no. 2, pp. 846-862, Feb. 2020, doi: 10.1109/JIOT.2019.2945186.

[128] K. J. Rakhi and J. Jayakumari, "Design of flip-OFDM system for optical wireless communication," *2017 International Conference on Circuit, Power and Computing Technologies (ICCPCT)*, Kollam, India, 2017, pp. 1-4, doi: 10.1109/ICCPCT.2017.8074176.

[129] Y. -F. Huang, C. -T. Tsai, Y. -C. Chi, D. -W. Huang and G. -R. Lin, "Filtered Multicarrier OFDM Encoding on Blue Laser Diode for 14.8-Gbps Seawater Transmission," in *Journal of Lightwave Technology*, vol. 36, no. 9, pp. 1739-1745, 1 May1, 2018, doi: 10.1109/JLT.2017.2782840.

[130] H. S. R. Hujijo, and M. Ilyas, "Enhancing spectral efficiency with low complexity filtered-orthogonal frequency division multiplexing in visible light communication system," *ETRI Journal*, vol. 46, pp. 1007–1019, 2024, doi: 10.4218/etrij.2023-0300.

[131] Y. A. Zenhom, E. K. I. Hamad, and M. M. Elnabawy, “Throughput improvement in ACO-OFDM-based VLC systems using noise cancellation and precoding techniques,” *Opt Quant Electron,* vol. 56, pp. 1798, 2024, doi:10.1007/s11082-024-07592-0.

[132] R. Bouziane *et al*., "Dependence of optical OFDM transceiver ASIC complexity on FFT size," *OFC/NFOEC*, Los Angeles, CA, USA, 2012, pp. 1-3.

[133] P. Milder *et al*., "Design and simulation of 25 Gb/s optical OFDM transceiver ASICs," *2011 37th European Conference and Exhibition on Optical Communication*, Geneva, Switzerland, 2011, pp. 1-3.

[134] R. Bouziane *et al*., "Optimizing FFT Precision in Optical OFDM Transceivers," in *IEEE Photonics Technology Letters*, vol. 23, no. 20, pp. 1550-1552, Oct.15, 2011, doi: 10.1109/LPT.2011.2164059.

APPENDIX A

MATLAB CODE OF THE PROPOSED NON-HERMITIAN SYMMETRY FILTERED-OFDM

A.1 NON-HERMITIAN SYMMETRY DCO-FILTERED-OFDM TECHNIQUE

```
%% The proposed non-Hermitian symmetry (NHS)-DCO-Filtered-OFDM technique %
s = rng(211);       % Set RNG state for repeatability
for snrdB=1:30
% system parameers
numFFT = 1024;           % Number of FFT points
numRBs = 50;             % Number of resource blocks
rbSize = 12;             % Number of subcarriers per resource block
cpLen = 72;              % Cyclic prefix length in samples
bitsPerSubCarrier = 4;   % 2: QPSK, 4: 16QAM, 6: 64QAM, 8: 256QAM
toneOffset = 2.5;        % Tone offset or excess bandwidth (in subcarriers)
L = 513;                 % Filter length (=filterOrder+1), odd
% Filter Design of Filtered-OFDM
numDataCarriers = numRBs*rbSize;    % number of data subcarriers in sub-band
halfFilt = floor(L/2);
n = -halfFilt:halfFilt;
% Sinc function prototype filter
pb = sinc((numDataCarriers+2*toneOffset).*n./numFFT);
% Sinc truncation window
w = (0.5*(1+cos(2*pi.*n/(L-1)))).^0.6;
% Normalized lowpass filter coefficients
fnum = (pb.*w)/sum(pb.*w);
% Use dsp filter objects for filtering
filtTx = dsp.FIRFilter('Structure', 'Direct form symmetric', ...
    'Numerator', fnum);
filtRx = clone(filtTx); % Matched filter for the Rx
% Generate data symbols
bitsIn = randi([0 1], bitsPerSubCarrier*numDataCarriers, 1);
% QAM Symbol mapper
symbolsIn = qammod(bitsIn, 2^bitsPerSubCarrier, 'InputType', 'bit', ...
    'UnitAveragePower', true);
offset = (numFFT-numDataCarriers)/2; % for band center
symbolsInOFDM = [zeros(offset,1); symbolsIn; ...
    zeros(numFFT-offset-numDataCarriers,1)];
% Computation of IFFT operation
ifftOut = ifft(ifftshift(symbolsInOFDM));
% The Output Of IFFT for FOFDM Convert the imag to real by using Juxtaposed to
convert the imaginary signal to real
fbr=real(ifftOut);   % real output signal
fbi=imag(ifftOut);   % image output signal
fbri=[fbr;fbi];      % The new technique is the Juxtaposed
% Prepend cyclic prefix
txSigOFDM = [fbri(end-cpLen+1:end); fbri];
% Filter, with zero-padding to flush tail. Get the transmit signal
txSigFOFDM = filtTx([txSigOFDM; zeros(L-1,1)]);
%  Get the positive values
bdc =7; %DC BIAS
```

```
clip = sqrt ((10.^( bdc /10) ) -1) ; % clipping factor
bdcc = clip * sqrt ( txSigFOFDM .* txSigFOFDM ) ;%Computation of DC bias
txSig = txSigFOFDM + bdcc ; % Addition of DC bias to the cyclic prefix added
signal
% Add channal (AWGN)
rxSig = awgn(txSig, snrdB, 'measured');
% Removal of DC bias
rxSigl = rxSig - bdcc ;
% Receive matched filter
rxSigFilt = filtRx(rxSigl);
% Account for filter delay
rxSigFiltSync = rxSigFilt(L:end);
% Remove cyclic prefix
rxSymbol = rxSigFiltSync(cpLen+1:end);
% Reshape to complex real and imaginary
rx = complex(rxSymbol(1:end/2),rxSymbol(((numFFT)+1):end)) ;
% Perform FFT
RxSymbols = fftshift(fft(rx));
% Select data subcarriers
dataRxSymbols = RxSymbols(offset+(1:numDataCarriers));
% BER computation
BER = comm.ErrorRate;
% Perform hard decision and measure errors
rxBits = qamdemod(dataRxSymbols, 2^bitsPerSubCarrier, 'OutputType', 'bit', ...
    'UnitAveragePower', true);
ber = BER(bitsIn, rxBits);
disp(['F-OFDM Reception, BER = ' num2str(ber(1)) ' at SNR = ' ...
    num2str(snrdB) ' dB']);
% save data in text file
fileID = fopen('NHS-FOFDM','a');
fprintf(fileID,'%6.2f %12.8f\n',snrdB,ber(1,1));
fclose(fileID);
% Restore RNG state
rng(s);
end
```

A.2 NON-HERMITIAN SYMMETRY FLIP-FILTERED-OFDM TECHNIQUE

```
%% The proposed non-Hermitian symmetry (NHS)-Flip-Filtered-OFDM technique %
clc
clear
for snrdB=1:30
s = rng(211);           % Set RNG state for repeatability
numFFT = 1000;          % Number of FFT points
numRBs = 50;            % Number of resource blocks
rbSize = 12;            % Number of subcarriers per resource block
cpLen = 72;             % Cyclic prefix length in samples
bitsPerSubCarrier = 4;  % 2: QPSK, 4: 16QAM, 6: 64QAM, 8: 256QAM
toneOffset = 2.5;       % Tone offset or excess bandwidth (in subcarriers)
L = 513;                % Filter length (=filterOrder+1), odd

numDataCarriers = numRBs*rbSize;    % number of data subcarriers in sub-band
halfFilt = floor(L/2);
n = -halfFilt:halfFilt;
% Sinc function prototype filter
```

```
pb = sinc((numDataCarriers+2*toneOffset).*n./numFFT);
% Sinc truncation window
w = (0.5*(1+cos(2*pi.*n/(L-1)))).^0.6;
% Normalized lowpass filter coefficients
fnum = (pb.*w)/sum(pb.*w);
% Use dsp filter objects for filtering
filtTx = dsp.FIRFilter('Structure', 'Direct form symmetric', ...
    'Numerator', fnum);
filtRx = clone(filtTx); % Matched filter for the Rx

% Generate data symbols
bitsIn = randi([0 1], bitsPerSubCarrier*numDataCarriers, 1);

% QAM Symbol mapper
symbolsIn = qammod(bitsIn, 2^bitsPerSubCarrier, 'InputType', 'bit', ...
    'UnitAveragePower', true);

offset = (numFFT-numDataCarriers)/2; % for band center
symbolsInOFDM = [zeros(offset,1); symbolsIn; ...
    zeros(numFFT-offset-numDataCarriers,1)];
ifftOut = ifft(ifftshift(symbolsInOFDM));
% Prepend cyclic prefix
txSigOFDM = [ifftOut(end-cpLen+1:end); ifftOut];
% Filter, with zero-padding to flush tail. Get the transmit signal
txSigFOFDM = filtTx([txSigFOFDM; zeros(L-1,1)]);
%  New Flip-F-OFDM
    fbr=real(txSigFOFDM); % real signal x(n)
    fbi=imag(txSigFOFDM); % imaginary signal x(n)
    fbri =[fbr;fbi]; % Juxtaposed technique   x(2n)
    Xp = fbri(fbri > 0); % seperate positive sinal
    Xn = fbri(fbri < 0); % seperate negative signal
    Xn = abs(Xn);  % convert negaive to positive
    % Concatenate positive and negative parts
    Flip = [Xp; Xn];
%   Add AWGN
    rxSig = awgn(Flip, snrdB, 'measured');
%   Reshape Positive and Negative sinal, then... extract real and imaginary
parts
    rp = rxSig(1:length(Xp)); % extract Positive part
    rn = rxSig(length(Xp) + 1:end); % extract Negative part
    rn = -rn; % Invert the negative part
    RFlip = zeros(size(fbri));
    RFlip(fbri > 0) = rp; % received posiive signal
    RFlip(fbri < 0) = rn; % received negative signal
%   Reshape to complex real and imaginary
    rx = complex(RFlip(1:end/2), RFlip((end/2) + 1:end));
%   Receive matched filter
    rxSigFilt = filtRx(rx);
%   Account for filter delay
    rxSigFiltSync = rxSigFilt(L:end);
%   Remove cyclic prefix
    rxSymbol = rxSigFiltSync(cpLen+1:end);
    Rxr= real(rxSymbol);
    Rxr1=abs (Rxr);
    Rxi= imag(rxSymbol);
    Rxi1=abs(Rxi);
    Rxi1=-1*(Rxi1); %(Rxi<0);
```

```
    Rflip1=[Rxr;Rxi];
%   Perform FFT
    RxSymbols = fftshift(fft(rxSymbol));
%   Select data subcarriers
    dataRxSymbols = RxSymbols(offset+(1:numDataCarriers));
%   BER computation
    BER = comm.ErrorRate;
%   Perform hard decision and measure errors
    rxBits = qamdemod(dataRxSymbols, 2^bitsPerSubCarrier, 'OutputType', 'bit',
...
    'UnitAveragePower', true);
    ber = BER(bitsIn, rxBits);
    disp(['F-OFDM Reception, BER = ' num2str(ber(1)) ' at SNR = ' ...
    num2str(snrdB) ' dB']);
 %  Save data in text file
    fileID = fopen('Flip wihout HS','a');
    fprintf(fileID,'%6.2f %12.8f\n',snrdB,ber(1,1));
    fclose(fileID);
%   Restore RNG state
    rng(s);
end
```